IMPROVING TRANSIENT STABILITY OF THE NIGERIAN 330kV TRANSMISSION SYSTEM USING ARTIFICIAL NEURAL NETWORK BASED VOLTAGE SOURCE CONVERTER

BY

CHIDIEBERE C. OKOLO
(2015237006P)

DEPARTMENT OF ELECTRICAL ENGINEERING

FACULTY OF ENGINEERING
NNAMDI AZIKIWE UNIVERSITY, AWKA
ANAMBRA STATE, NIGERIA

MARCH, 2021

IMPROVING TRANSIENT STABILITY OF THE NIGERIAN 330kV TRANSMISSION SYSTEM USING ARTIFICIAL NEURAL NETWORK BASED VOLTAGE SOURCE CONVERTER

BY

CHIDIEBERE C. OKOLO
(2015237006P)

A

DISSERTATION SUBMITTED TO THE SCHOOL OF POST GRADUATE STUDIES IN PARTIAL FULFILMENT OF THE REQUIREMENTS FOR THE AWARD OF DOCTOR OF PHYLOSOPHY (Ph.D.) IN ELECTRICAL ENGINEERING

NNAMDI AZIKIWE UNIVERSITY, AWKA
ANAMBRA STATE

CERTIFICATION

I hereby certify that, **Okolo Chidiebere C.** with Registration No: **2015237006P** is the original author of this dissertation **(Improving Transient Stability of the Nigerian 330kV Transmission System Using ANN VSC** and that this work to the best of my knowledge has not been presented anywhere in part or in full for the award of diploma, degree or certificate. All sources of information are acknowledged.

_____

Chidiebere C. Okolo

APPROVAL PAGE

This is to certify that this dissertation has been approved and accepted having met the requirements in partial fulfillment for the award of Doctor of Philosophy (Ph.D.) in the Department of Electrical Engineering, Nnamdi Azikiwe University, Awka.

Engr. Dr. O. A. Ezechukwu, FNSE, FNEEE	_____	_____
Supervisor	Signature	Date
Engr. Prof. S. A Ike	_____	_____
External Examiner	Signature	Date
Engr. Dr. A. E. Anazia	_____	_____
H.O.D., Electrical Engineering	Signature	Date
Engr. Prof. J. T. Nwabanne	_____	_____
Dean, Faculty of Engineering	Signature	Date
Engr. Prof. P. K. Igbokwe	_____	_____
Dean, School of Postgraduate Studies	Signature	Date

DEDICATION

This dissertation is dedicated to God Almighty.

ACKNOWLEDGMENT

All praises, thanks and sincere gratitude and appreciation are to God Almighty, the Lord of the world, for helping me to accomplish this work.

First, I would like to express my profound gratitude to my supervisor, Engr. Dr. O. A. Ezechukwu. His invaluable technical advice, suggestions, discussions, and kind support were the main sources for the successful completion of the dissertation. He allowed me the opportunity to work on a highly interesting area in power system.

Secondly, I must not fail to recognize the assistance of the amiable Head of the Department, Engr. Dr. E. A. Anazia, who has been piloting the affairs of the department to a greater height. His professional advice and contributions to this work are most gratefully appreciated.

I especially want to thank Engr. Prof. F. O. Enemuoh and Engr. Dr. J. C. Onuegbu, for their kind support and wholesome initiatives towards the actualization of this work. I am also exceedingly grateful to Engr. T. F. Uketui, for his contributions and suggestions to the work throughout my study period.

I must also not fail to appreciate the love and encouragement of the Dean, Faculty of Engineering, Engr. Prof H. C. Godwin and all the lecturers in the Faculty of Engineering. I also appreciate all the lecturers in the department of Electrical Engineering, namely Engr. M. N. Eleanya, Engr. Ogbor Victor, Engr. K. C. Obute, Engr. Alex Anyalebechi, etc. and to all the staff of the department for their invaluable assistance and providing pleasant atmosphere and inspiring research environment.

Finally, I want to appreciate my family: Barr (Mrs) R. C. Okolo, Kimberly Okolo, Viva Okolo, Chidubem Okolo and Gold Okolo for their encouragement and motivation in actualizing this research work.

ABSTRACT

Enhancement of the dynamic response of generators, within a power system, when subjected to various disturbances, has been a major challenge to power system researchers and engineers for the past decades. This work presents the application of intelligent Voltage Source Converter – High Voltage Direct Current(VSC-HVDC) for improvement of the transient stability of the Nigerian 330kV transmission system. The system was modeled in Power System Analysis Toolbox (PSAT) environment and the system load flow test was done. The eigenvalue analysis of the system buses was performed to determine the critical buses. A balanced three-phase fault was then applied to some of these critical buses and lines of the transmission network in other establish the existing transient stability situation of the grid through the observation of the dynamic responses of the generators in the case network when the fault was applied. To this effect, VSC-HVDC was installed along to those critical lines. The inverter and the converter parameters of the HVDC were controlled by the conventional proportional integral (PI) method and artificial neural network. The generalized swing equations for a multi-machine power system are presented. MATLAB/PSAT software was employed as the tool for the simulations. . This shows clearly that there exist three most critical buses which are Makurdi, Ajaokuta and Benin buses and critical transmission lines (which include Jos – Makurdi Transmission line, Ajaokuta - Benin and Ikeja West – Benin Transmission line) within the network. The load flow analysis also revealed that the system loses synchronism when the balanced three-phase fault was applied to these identified critical buses and lines. This implies that the Nigeria 330-kV transmission network is on a red-alert, and requires urgent control measures with the aim of enhancing the stability margin of the network to avoid system collapse. The results obtained showed that 33.33% transient stability improvement was achieved when the HVDC was controlled with the artificial neural network when compared to the PI controllers as can be seen by observing the dynamic response of the generators in the network. Also when compared with the results of other similar works (especially Hazra, Phulpin and Ernst, 2009), there is about 20% transient stability improvement. The voltage profile result and the damping were improved when the ANN was installed.

TABLE OF CONTENTS

LIST OF FIGURES

LIST OF TABLES

LIST OF NOMENCLATURES

ACRONYMS: NAME

ANN	: Artificial Neural Network
EHV	: Extra High Voltage
EMTDC	: Electromagnetic Transients including DC
GS	: Generating Station
LLL	: Three Phase Fault
NN	: Neural Network
PI	: Proportional Integral
PNN	: Probabilistic Neural Network
PSCAD	: Power System Computer Aided Design
RBF	: Radial basis functions
VSC	: Voltage Source Converter

CHAPTER ONE

INTRODUCTION

1.1 Background of the Study

Nowadays, the demand of electricity has radically increased and a modern power system becomes a difficult network of transmission lines interconnecting the generating stations to the major load centers in the overall power system in order to support the high demand of consumers. Transmission networks being overloaded, are pushed closer to their stability limits. This is as a result of increasing demand for electricity due to growing industrialization. This could have negative effect on the power system security. The security of a power system is regarded as the ability of the network to withstand disturbances without breaking down (Khoshnaw, and Saleh, 2005).The complicated network causes the stability problem. Stability is determined by the observation of voltage frequency and rotor angle. One of the indices to assess the state of security of a power system is the transient stability and it involves the ability of power system to remain in equilibrium or return to acceptable equilibrium when subjected to large disturbances (Ayodele, Jimoh, Munda and Agee, 2012). Transient stability examines the impact of disturbance of power systems considering the operating conditions. The analysis of the dynamic behavior of power systems for the transient stability gives information about the ability of power system to sustain synchronism during and after the disturbances.

This work contributes to the enhancement of the dynamic response of generators, within a power system, when subjected to various disturbances, which has been a major challenge to power system researchers and engineers for the past decades. This work presented the application of intelligent Voltage Source Converter – High Voltage Direct Current (VSC-HVDC) for

improvement of the transient stability of the Nigerian 330kV transmission system. The Nigerian 330kV transmission system was modelled in PSAT environment and the system load flow was simulated.

Transient stability which can be defined as the ability of the power system to maintain certain parameters within limit of occurrence of the transient on power system like sudden load discharge, grid failure or any kind of fault can also be seen as the ability of a power system to regain its normal operating condition after sudden and severe disturbance in system. The ability of the Nigerian 330kV power system to maintain the synchronism after the sudden large disturbance has been a major issue. Those disturbances maybe because of the clearing of faults, switching on and off surges in EHV system. Transient stability is very much affected by the type of fault. A three-phase short circuit is the most severe fault; the fault severity decreases with 2-phase fault and single line to ground fault in that order (Masaki and Junji, 2010). If the fault is farther from the generator, the severity will be less than in the case of a fault occurring at the terminals of the generator. Power transferred during fault also plays a major role when part of the power generated is transferred to the load, the accelerating power is reduced to that extent. Theoretically an increase in the value of inertia constant M reduces the angle through which the rotor swings farther during a fault. However, this is not a practical proposition since increasing M means increasing the dimensions of the machine which is uneconomical.

Transient stability improvement is one of the important aspects in modern power system. Sahoo *et al*., 2010, have proposed many methods to improve stability of power system such as load shedding, High Voltage Direct Current (HVDC), Flexible AC Transmission system (FACTS), Numerical integration, Direct method, Probabilistic method and the artificial intelligent methods such as artificial neural networks.

Transient stability of the system can also be improved by increasing the system voltage. Increase in the voltage profile of the system implies increase in the power transfer ability. This helps in increasing the difference between initial load angle and critical clearance angle (CCT) hence increase in power allows the machine to rotate through large angle before reaching critical clearance angle. Increase in the X/R ratio in the power system increases the power limit of the line thus helps to improve the stability. High speed circuit breakers assist in clearing the fault as quickly as possible the quicker the breaker operates the faster the fault cleared and better the system restores to normal operating conditions.

The occurrence of disturbances within power networks cannot be avoided, its impact which undermines the security margin of the system could be minimized. This usually resulted to the instability in the operation of power systems. This challenge therefore poses a great concern to power system researchers recently. In resolving this issue, there is the need to evaluate the ability and response of a power network when subjected to various disturbances with the aim of maintaining the network reliability. Instability in power system networks is of various types based on the duration. When a power system is subjected to a disturbance, the network may experience loss of synchronism which could result to total voltage collapse within the network. This explains why transient stability enhancement is of paramount importance in the operation of power system. There are different techniques for enhancing transient stability of a multi-machine power system (Srinvasa and Amarnath, 2014). These techniques include: reduction in system transfer reactance, use of breaking resistor, use of bundled conductor, use of fault current limiter and the placement of FACTS devices (Rani and Arul, 2013). As the power network becomes more complex, the consequence is that the fault current increases, and transient stability problem becomes more severe.

The controllability of the HVDC power is often used to improve the operating conditions of the AC network where the converter stations are located. HVDC allows more efficient bulk power transfer over distances. However, cost is important variable in the equation. Once installed, HVDC transmission systems are integral part of the electrical power system, improving stability, reliability and transmission capacity. High Voltage Direct Current (HVDC) power transmission is employed to move large amounts of electric power. There are several possibilities to enhance the transient stability in a power system. One adequate option is by using the high controllability of the HVDC if HVDC is available in the system. The strategy controls the power through the HVDC to help make the system more transient stable during disturbances. Loss of synchronism is prevented by quickly producing sufficient decelerating energy to counteract accelerating energy gained. The power flow in the HVDC link is modulated with the addition of an auxiliary signal to the current reference of the rectifier firing angle controller.

This modulation control signal is derived from speed deviation signal of the generator utilizing a PD controller; the utilization of a PD controller is suitable because it has the property of fast response. It's has been demonstrated that the power flow in the HVDC link is modulated by the addition of an auxiliary signal to the current reference of the rectifier firing angle controller to enhance the transient stability in power system. The proportional integral derivative (PID) controller works well and damps the first swing oscillation transient so the system remains stable. Therefore, the control of HVDC has the potential for future application to power systems. The PID controllers has been used in the past for controlling HVDC, however Artificial Intelligent technique like ANN promises to be a more intelligent controller that can achieve better result in transient stability improvement of power system.

1.2 Statement of the Problem

The stability problem is concerned with the behavior of the synchronous machine after disturbances. Transient signals are one of the causes of instability. Transients occur when there is a sudden change in the voltage or the current in a power system. The Nigerian power network over the years has suffered incessant power interruptions caused by inadequacies in power generation capacity, inadequate transmission and distribution facilities and poor maintenance culture. This ugly situation has resulted in frequent transient instability on the grid network. The long time effect of this is frequent power failures long outage durations, poor availability and sustained blackouts and system collapse. The negative impact of poor availability and sustained blackouts are high on power system operators and consumers of electricity. It results in high operation costs for operators, causes drop in quality of life of electricity consumers, increases cost of living, shuts down industries, causes loss of jobs, increases production cost and in general results in down turn in national economy. Resolving the challenge of frequent transient instability on our power networks will resolve the above stated problem and its consequences.

In this research, High voltage direct Current controlled by Neural Network is proposed as a technique for improving the transient stability of the Nigerian 40 bus network. The proposed method will enhance the transient stability of the network by intelligently controlling active and reactive power balance in the network and allowing bulk power transfer of power where it is mostly needed. In recognition of these challenges, the Federal Government through its power reform, has opened up the power sector by licensing independent power producers, and expanding the Nigeria power system through National Integrated Power Projects aimed at building more power generating stations to boost generation capacity as well as reinforcing the existing power transmission and distribution facilities through building new transmission lines

across the country; and refurbishing, replacing of aging facilities, and construction of more transmission and distribution substations.

1.3 Aim and Objectives

The aim of this dissertation is to develop a model for enhancing the transient stability of Nigerian 330kV transmission grid using artificial neural network (ANN) based voltage source convertee. The Specific Objectives are to:

1. develop the PSAT model of the Nigerian 330KV transmission
2. perform load flow on the test network so as to determine the normal operating condition of the network and present transient stability of the test case network;
3. determine the transient stability of the Nigeria 330kV Network and weakest buses through the eigenvalue analysis.
4. develop the model of the controller for the HVDC system;
5. install the conventional PI controlled HVDC system and the ANN controlled VSC-HVDC system one after another to the critical buses in the test case network and then perform load flow on the entire system during occurrence of a three-phase fault;
6. Compare the results of the transient stability improvement of the 330kV transmission grid with HVDC and with ANN controlled HVDC.

1.4 Limitations

The wheeling of energy from these remotely located sites through existing transmission lines to load centers has the following limitations:

1. The power flow in ac long lines is limited by stability considerations. This implies that the lines operate at power level much below their thermal limit.
2. The lack of fast control in ac lines implies that the normal power flow in line is kept much below the peak value, which itself is limited by stability consideration. This margin is required to maintain system security even under contingency conditions.
3. The ac transmission system requires dynamic reactive power control to maintain satisfactory voltage profile under varying load conditions and transient disturbances.

1.5 Motivation for the Research

Due to the complexity and dynamic nature of the power system conditions and configurations, power system stability is always difficult to achieve. As individual, we all depend on electricity to help in our activities which includes: heating, cooling, and lightning of our homes, refrigerate and prepare our food, pump and purify our water, handle sewage and support most of our hospital, communication and entertainment. As a society also, we depend on electrical energy to light our streets, control the flow of traffic on the road, rails and in the air, operate the myriad physical and information supply chain that create, produce and distribute goods and services, maintain public safety and help to assure our national security. Unfortunately, in Nigeria these needs are not met by the 330kV grid due to its instability nature. This motivated my interest in contributing to the solution.

One of the major causes of this power system instability is the issue of power system transient disturbance, of which statistic had it that it contributes up to 70% of the total power system collapse (Ekici S. et al, 2009). This transient disturbance ranges from variation in system load demand, lack of generation and down to switching operations. This contributed to my motivation because of the fact that this transient effects, when it happened can result to frequent tripping of the system, prolonged outage duration, loss of revenue generation and even the consumers who are very sensitive to system outage. They will be forced to pay for electricity not consumed and even lack availability factor. The utility companies, commercial and business outfits will experience low profit. The government will on their own record low growth and development. Hence, the need for this research work to improve on the transient stability of the Nigeria 330KV Transmission Network using HVDC.

1.6 Scope

Transient stability improvement of power systems is to be achieved using VSC-HVDC and Artificial Neural Network to enhance the transient stability of Nigerian 330kV transmission system as the test case network using MATLAB/PSATS Software.

1.7 Significance

The improvement of transient stability of the Nigeria 330 kV transmission network using HVDC is proposed as the solution to the grid instability. VSC-HVDC limits the impact of faults on the power system. HVDC links are used within a grid to stabilize the grid against control problems with the AC energy flow. In a number of applications of HVDC, it is preferred option over AC transmission because:

- Increasing the capacity of an existing power grid in situations where additional wires are difficult or expensive to install.
- Reducing the profile of wiring and pylons for a given power transmission capacity.
- Stabilizing a predominantly AC power-grid, without increasing maximum prospective short circuit current.
- Reducing corona losses (due to higher voltage peaks) for HVAC transmission lines of same power.
- Point-to-point bulk power transmission over long distances, to overcome stability problem of ac line.
- Allows power transmission between unsynchronized AC distribution systems, it can help increase system stability, by preventing cascading failures from propagating from one part of a wider power transmission grid to another, whilst still allowing power to be imported or exported in the event of smaller failures.
- It can carry more power per conductor, because for a given power rating the constant voltage in a DC line is lower than the peak voltage in an AC line. This voltage determines the insulation thickness and conductor spacing. This allows existing transmission line corridors to he used to carry more power into an area of high power consumption, which can lower costs.

CHAPTER TWO

REVIEW OF LITERATURE

2.0 Review of Related Literature

Anazia E. A , Anionovo Ugochukwu .E, (2020), International Journal of Innovative Research in Science, Enginneerind and Technology in their work on Transient Stability Analysis of Nigerian 330kV Transmission Network using Eigenvalue analysis demonstrated the use of eigenvalue in Nigerian 330kV Transmission Network using only sectionalized 7 bus system as against expanded 40 bus Nigerian 330kV Transmission Network. In this dissertation, the 40bus are considered.

Ignatius and Emmanuel, (2017) maintained that Assessment of the dynamic response of generators, within a power system, when subjected to various disturbances, has been a major challenge to power system researchers and engineers for the past decades and their work investigated the dynamic response of the generators in the Nigeria 330-kV grid network when a balanced 3-phase fault was applied with the aim of determining the Critical Clearing Time (CCT) of the transmission network. The generalized swing equations for a multi-machine power system are presented. MATLAB software was employed as the tool for the simulations. Using the real network of Nigeria 330-kV electric grid as a case study, the result obtained clearly show that there exist critical buses such as Benin, Onitsha and Jebba Transmission Station (TS) and critical transmission lines such as Benin-Olorunshogo Generating Station (GS) and Jebba TS-Shiroro GS within the network. The results also revealed that the system losses synchronism when a balanced 3-phase fault was applied to these identified critical buses and lines which further indicate that the Nigeria 330-kV transmission network is on a red-alert and required urgent

control measures with the aim of enhancing the stability margin of the network to avoid system collapse. The authors have proved that there is the need for the stability improvement on the Nigeria 330kV transmission network through the assessment/determination of the CCT and response of the generators, within the power system, when subjected to a balanced 3-phase fault but unfortunately, they did not recommend any solution to the above mentioned problem. Hence, this dissertation has proposed the use of an ANN controlled VSC HVDC link.

Hazra, Phulpin and Ernst (2009) presented three HVDC modulation strategies to improve transient stability in an interconnected power system in their work titled "HVDC Control Strategies to Improve Transient Stability in Interconnected Power Systems". AC variables such as rotor speeds, voltage phasors, and tie line power flows were used as input to the PI controller that modified the power flow settings through the HVDC-links. The proposed techniques were tested on the IEEE 24-Bus reliability test system and critical clearing time, 0.25sec obtained for several contingencies were analyzed. The paper showed that HVDC modulation could lead to substantial improvement in transient stability. Hence, in this work efforts would be made to improve on the CCT of fault and they have used the conventional PI controller which is not smart enough compared to the intelligent controller proposed in this work.

Ali, Yehia, Abou-Hashema, El-Sayed and Amer(2019) stated that High Voltage Alternating Current (HVAC) is the most effective and efficient way for energy transmission in modern power systems around the world and the aim of the authors here is to discuss the importance of using HVDC system to link between different frequency networks and transmitting energy on a very long distance. The simulation of the fault current in their work has been performed by using MATLAB/Simulink to compare the output fault current in HVAC and HVDC system. Also their

work discussed the response of the electrical grid during fault occurrence when incorporating HVDC to link to it but failed to show that the system stability could be improved using VSC HVDC link which is the gap this work will close.

Vasudevan and Ramalakshmi presented (2019) in the work, A new management approach for the reactive-power injections of Voltage Supply Converters in High Voltage DC (VSC-HVDC) multi-terminal Systems to enhance grid transient stability whose idea was to extend (decrease) the magnetism torsion of generators close to those terminals during which the frequency is superior to (below) the weighed-average frequency used. Simulations were allotted victimization PSS/E and therefore the outcome have revealed that transient stability is enlarged victimization this approach. The issue here, is that the VSC-HVDC design was not implemented on any 330kV transmission network and secondly the authors did not use intelligent (ANN) controllers for the VSC-HVDC as proposed in this dissertation.

A novel general voltage source converter high voltage direct current (VSC HVDC) model presented by Tang, Xu, Dong & Xu,(2016) where the main donation of the new model was that it **i**s valid for every possible topology of the DC circuit. Practical implementation of the model in power system stability software was discussed in feature. The generalized DC equations can all be articulated in terms of matrices that are byproducts of the construction of the DC bus admittance matrix. Initialization, switching actions resulting in dissimilar topologies and reproduction of the loss of DC lines quantity to a simple calculation or recalculation of the DC bus admittance matrix. Again, the problem here is that the authors failed to demonstrate the performance of their VSC HVDC model on any practical transmission network. Hence, in this work the Nigerian 330kV transmission network will be emphasized.

Singaravelu and Seenivasan (2014) stated that for economic design and optimal operation, HVDC system required a detailed simulation model. Therefore, in their work a detailed Matlab simulation model of line commutated converter (LCC) based mono-polar HVDC system, feeding a strong AC network, with a fixed capacitor (FC) as a reactive power compensator was presented. Firefly algorithm based optimal proportional integral (PI) controller was proposed for the rectifier and the inverter control. The results showed the supremacy of the firefly algorithm based optimal PI controller over the conventional PI controller. The harmonic analysis was also carried out under steady state operation to assure the quality of power supply on the inverter AC side. Here, the authors have used LCC based monopolar HVDC instead of VSC based bi-polar HVDC proposed by this dissertation and also used the firefly algorithm based optimal PI controller for the control of the VSC HVDC but this dissertation has proposed to use ANN-controlled VSC-HVDC link.

In their work, Lakshminarayana, Shishir, Mukesh, and Ganga, (2014), presented a methodology for estimating the normalized transient stability margin by using the multi layered perceptron (MLP) neural network. The nonlinear mapping relation between the normalized transient stability margin and the operating conditions of the power system was established by using the MLP neural network. To obtain the training set of the neural network the potential energy boundary surface (PEBS) method along with time domain simulation method was used. The proposed method was applied on IEEE 9 bus system and the results showed that the proposed method provided fast and accurate tool to assess online transient stability. Here, the authors main

goal was to estimate the transient stability margin of the transmission network using ANN and did not work on the stability improvement of the transmission network.

2.1 Power System Stability

The ability of an electric power system to re-establish the initial state (or one practically identical) after any disturbance manifested as a deviation from the initial parameter values for the system's operation is known as system stability (Sachidananda, 2019). The electric power sources in a power system are usually synchronous generators, which are coupled together by a common electric network in such a way that the rotors of the all the generators are in synchronized rotation. This mode, called the normal, or steady state mode, should be stable; that is, the power system must return to the initial state (or one practically identical) every time after a deviation from the steady-state mode.

The deviations may be associated with a variation in load, short-circuits, disconnections of power transmission lines, and similar causes. The system's stability is usually diminished by an increase in the load (the power delivered by the generators) and a decrease in the voltage (an increase in the power consumed or a decrease in the excitation of the generators); specific limit, or critical values can be determined for each power system for theses quantities of associated quantities that characterize the stability limit (Hannan Chan, 2006). A power system can operate reliability if a specific stability margin is provided for it, that is, if the parameters of the operating mode and the system itself differ sufficiently from the critical values. Various measures are taken to ensure the stability of an electric power system, such as designing the system with an adequate stability margin, regulating the excitation of the generators automatically, and using automated counter emergency equipment.

In the analysis of the stability of an electric power system, a distribution is made between static, dynamic, and overall system stability. Static stability covers the case of small disturbances, that is those for which the system under consideration may be regarded as linear. It is analyzed with the general methods developed by A. M. Liapunov to solve stability problems (Hannan Chan, 2006). In engineering practice, the stability of an electric power system is sometimes analyzed by a simple determination of the presence or absence of stability; the approach is oriented toward practical stability criteria, with certain assumptions based on experience, for example, the impossibility of self-oscillation in the system and the frequency invariance of the system's electric current. Static stability is studied with the aid of digital and analogue computers.

Dynamic stability evaluates the behaviour of an electric power system after the occurrence of strong disturbances that arise as a result of short circuits, disconnections of power transmission lines, and the like. In the analysis of dynamic stability (the system is generally considered to be non-linear), it is necessary to integrate high-order non-linear transcendental functions; analogue computers and Ac evaluation models are used for this purpose. In the majority of cases special algorithms and programs are developed that permit the calculations to be performed on digital computers (Roberto and Charpentier, 2000). The programs are validated by comparing calculated results with experimental results on a real system or on a physical model of the system.

Overall system stability evaluates the stability of an electric power system when the synchronism of some of the working generators has been lost. The normal operating mode in this case is subsequently re-established without disconnecting major system elements (Sravani, Hari, and Basha, 2010). Calculations of the overall system stability are quite approximate because of their

complexity; they are designed to reveal inacceptable effects on equipment and to find a set of measures that will eliminate the asynchronous operating mode.

The static stability of an electric power system can be improved primarily by the use of power regulation; dynamic stability can be improved by forcing the excitation of the generators, by quickly disconnecting faulty sections, by using special braking devices on the generators, and by disconnecting some of the generators and part of the load(Ayodele, Jimoh, Munda and Agee, 2012). An improvement in the overall system stability, which is usually regarded as an improvement in the ruggedness of an electric power system, is achieved primarily by controlling the power produced by the generators that have lost synchronism and by automatically disconnecting some power consumers(Ayodele, Ogunjuyigbe and Oladele, 2016). Stability problems occur in the design of all types of electric power systems, including high-voltage ground systems, shipboard systems and aircraft systems.

2.2 Classification of Power System Stability

A typical modern power system is a high-order multivariable process whose dynamic response is influenced by a wide array of devices with different characteristics and response rates. Stability is a condition of equilibrium between opposing forces. Depending on the network topology, system operating condition and the form of disturbance, different sets of opposing forces may experience sustained imbalance leading to different forms of instability. In this section, we provide a systematic basis for classification of power system stability(Ayodele, Jimoh, Munda and Agee, 2012).

Need for Classification

Power system stability is essentially a single problem; however, the various forms of instabilities that a power system may undergo cannot be properly understood and effectively dealt with by treating it as such. Because of high dimensionality and complexity of stability problems, it helps to make simplifying assumptions to analyze specific types of problems using an appropriate degree of detail of system representation and appropriate analytical techniques (Nirupama, 2016). Analysis of stability, including identifying key factors that contribute to instability and devising methods of improving stable operation, is greatly facilitated by classification of stability into appropriate categories. Classification, therefore, is essential for meaningful practical analysis and resolution of power system stability problems (Vittal and Vijay, 2007). As discussed in Section V-C-I, such classification is entirely justified theoretically by the concept of partial stability.

The classification of power system stability proposed here is based on the following considerations (Nirupama, 2016):

- ✓ The physical nature of the resulting mode of instability as indicated by the main system variable in which instability can be observed.
- ✓ The size of the disturbance considered, which influences the method of calculation and prediction of stability.
- ✓ The devices, processes, and the time span that must be taken into consideration in order to assess stability.

Figure 2.1 gives the overall picture of the power system stability problem, identifying its categories and subcategories. The following are descriptions of the corresponding forms of stability phenomena.

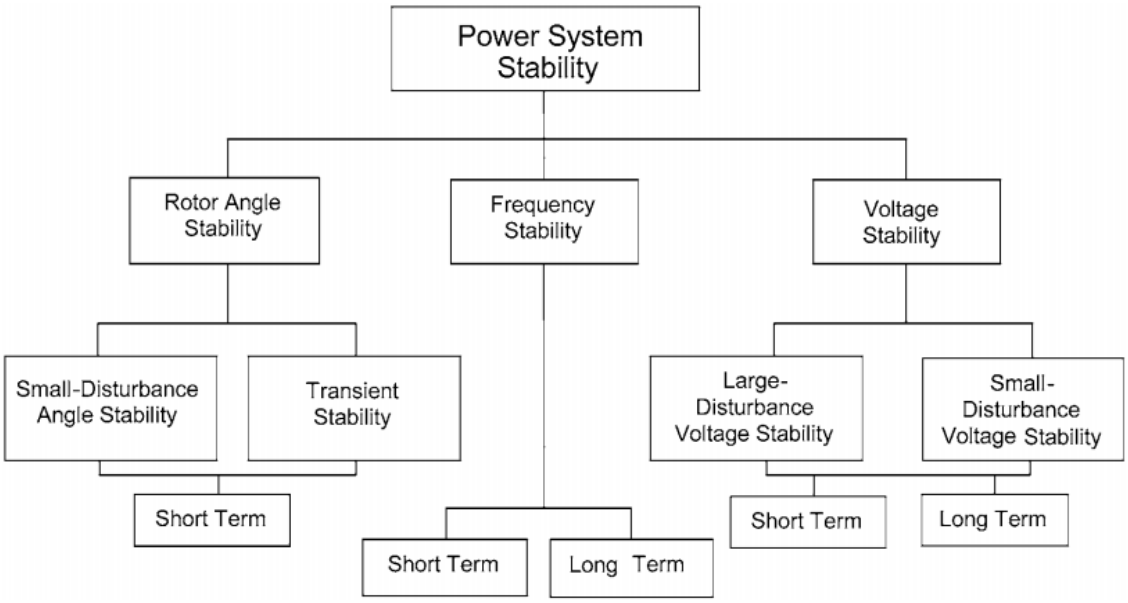

Figure 2.1: Classification of power system stability(Nirupama, 2016)

2.3 Rotor Angle Stability

Rotor angle stability refers to the ability of synchronous machine s of an interconnected power system to remain in synchronism after being subjected to a disturbance. It depends on the ability to maintain/restore equilibrium between electromagnetic torque and mechanical torque of each synchronous machine in the system. Instability that may result occurs in the form of increasing angular swings of some generators leading to their loss of synchronism with other generators (Sagar, Pavan, and Rajalakshmi, 2016). The rotor angle stability problem involves the study of the electromechanical oscillations inherent in power systems. A fundamental factor in this problem is the manner in which the power outputs of synchronous machines vary as their rotor angles change. Under steady-state conditions, there is equilibrium between the input mechanical torque and the output electromagnetic torque of each generator, and the speed remains constant. If the system is perturbed, this equilibrium is upset, resulting in acceleration or deceleration of

the rotors of the machines according to the laws of motion of a rotating body. If one generator temporarily runs faster than another, the angular position of its rotor relative to that of the slower machine will advance (Sravani, Hari, and Basha, 2010). The resulting angular difference transfers part of the load from the slow machine to the fast machine, depending on the power-angle relationship. This tends to reduce the speed difference and hence the angular separation. The power-angle relationship is highly nonlinear. Beyond a certain limit, an increase in angular separation is accompanied by a decrease in power transfer such that the angular separation is increased further. Instability results if the system cannot absorb the kinetic energy corresponding to these rotor speed differences. For any given situation, the stability of the system depends on whether or not the deviations in angular positions of the rotors result in sufficient restoring torques (Nirupama, 2016). Loss of synchronism can occur between one machine and the rest of the system, or between groups of machines, with synchronism maintained within each group after separating from each other. The change in electromagnetic torque of a synchronous machine following a perturbation can be resolved into two components:

- ✓ Synchronizing torque component, in phase with rotor angle deviation.
- ✓ Damping torque component, in phase with the speed deviation.

System stability depends on the existence of both components of torque for each of the synchronous machines. Lack of sufficient synchronizing torque results in a periodic or no oscillatory instability, whereas lack of damping torque results in oscillatory instability (Vittal and Vijay, 2007). For convenience in analysis and for gaining useful insight into the nature of stability problems, it is useful to characterize rotor angle stability in terms of the following two subcategories:

2.3.1 Small-Disturbance (Or Small-Signal) Rotor Angle Stability

This is concerned with the ability of the power system to maintain synchronism under small disturbances. The disturbances are considered to be sufficiently small that linearization of system equations is permissible for purposes of analysis (Lakshminarayana, Shishir, Mukesh and Ganga, 2014).

Small-disturbance stability depends on the initial operating state of the system. Instability that may result can be of two forms:

i) increase in rotor angle through a no oscillatory or aperiodic mode due to lack of synchronizing torque, or

ii) rotor oscillations of increasing amplitude due to lack of sufficient damping torque.

In today's power systems, small-disturbance rotor angle stability problem is usually associated with insufficient damping of oscillations. The aperiodic instability problem has been largely eliminated by use of continuously acting generator voltage regulators; however, this problem can still occur when generators operate with constant excitation when subjected to the actions of excitation limiters (field current limiters).

Small-disturbance rotor angle stability problems may be either local or global in nature. Local problems involve a small part of the power system, and are usually associated with rotor angle oscillations of a single power plant against the rest of the power system. Such oscillations are called local plant mode oscillations. Stability (damping) of these oscillations depends on the strength of the transmission system as seen by the power plant, generator excitation control systems and plant output (D´ıez-Maroto, 2013).

Global problems are caused by interactions among large groups of generators and have widespread effects. They involve oscillations of a group of generators in one area swinging against a group of generators in another area. Such oscillations are called inter-area mode oscillations. Their characteristics are very complex and significantly differ from those of local plant mode oscillations. Load characteristics, in particular, have a major effect on the stability of inter-area modes (Agha, Josiah, Dan, Augustin 2015).

The time frame of interest in small-disturbance stability studies is on the order of 10 to 20 seconds following a disturbance.

2.3.2 Transient Stability or Large-Disturbance Rotor Angle Stability

As it is commonly referred to, is concerned with the ability of the power system to maintain synchronism when subjected to a severe disturbance, such as a short circuit on a transmission line. The resulting system response involves large excursions of generator rotor angles and is influenced by the nonlinear power-angle relationship.

Transient stability depends on both the initial operating state of the system and the severity of the disturbance. Instability is usually in the form of a periodic angular separation due to insufficient synchronizing torque, manifesting as first swing instability. However, in large power systems, transient instability may not always occur as first swing instability associated with a single mode; it could be a result of superposition of a slow inter-area swing mode and a local-plant swing mode causing a large excursion of rotor angle beyond the first swing (Eriksson, 2014). It could also be a result of nonlinear effects affecting a single mode causing instability beyond the first swing. The time frame of interest in transient stability studies is usually 3 to 5 seconds following the disturbance. It may extend to 10–20 seconds for very large systems with dominant inter-area

swings. As identified in Figure 2.1, small-disturbance rotor angle stability as well as transient stability are categorized as short term phenomena.

The term dynamic stability also appears in the literature as a class of rotor angle stability. However, it has been used to denote different phenomena by different authors. In the North American literature, it has been used mostly to denote small-disturbance stability in the presence of automatic controls (particularly, the generation excitation controls) as distinct from the classical "steady-state stability" with no generator controls (Eseosa and Odiase 2012). In the European literature, it has been used to denote transient stability. Since much confusion has resulted from the use of the term dynamic stability, we recommend against its usage, as did the previous IEEE and CIGRE Task Forces (Sigrist, Echavarren, Rouco and Panciatici 2015).

2.4 Voltage Stability

Voltage stability refers to the ability of a power system to maintain steady voltages at all buses in the system after being subjected to a disturbance from a given initial operating condition. It depends on the ability to maintain/restore equilibrium between load demand and load supply from the power system. Instability that may result occurs in the form of a progressive fall or rise of voltages of some buses. A possible outcome of voltage instability is loss of load in an area, or tripping of transmission lines and other elements by their protective systems leading to cascading outages. Loss of synchronism of some generators may result from these outages or from operating conditions that violate field current limit (Sanni, Haruna, Jimoh and Aliyu, 2016). Progressive drop in bus voltages can also be associated with rotor angle instability. For example, the loss of synchronism of machines as rotor angles between two groups of machines approach 180 causes rapid drop in voltages at intermediate points in the network close to the electrical

center (Abido, 2009). Normally, protective systems operate to separate the two groups of machines and the voltages recover to levels depending on the post-separation conditions. If, however, the system is not so separated, the voltages near the electrical center rapidly oscillate between high and low values as a result of repeated "pole slips" between the two groups of machines.

In contrast, the type of sustained fall of voltage that is related to voltage instability involves loads and may occur where rotor angle stability is not an issue. The term voltage collapse is also often used. It is the process by which the sequence of events accompanying voltage instability leads to a blackout or abnormally low voltages in a significant part of the power system (Masood, Hassan and Chowohury, 2012). Stable (steady) operation at low voltage may continue after transformer tap changers reach their boost limit, with intentional and/or unintentional tripping of some load. Remaining load tends to be voltage sensitive, and the connected demand at normal voltage is not met. The driving force for voltage instability is usually the loads; in response to a disturbance, power consumed by the loads tends to be restored by the action of motor slip adjustment, distribution voltage regulators, tap-changing transformers, and thermostats. Restored loads increase the stress on the high voltage network by increasing the reactive power consumption and causing further voltage reduction. A run-down situation causing voltage instability occurs when load dynamics attempt to restore power consumption beyond the capability of the transmission network and the connected generation (Ayodele, Jimoh, Munda, and Agee, 2012).

A major factor contributing to voltage instability is the voltage drop that occurs when active and reactive power flow through inductive reactances of the transmission network; this limits the capability of the transmission network for power transfer and voltage support. The power transfer

and voltage support are further limited when some of the generators hit their field or armature current time-overload capability limits. Voltage stability is threatened when a disturbance increases the reactive power demand beyond the sustainable capacity of the available reactive power resources. While the most common form of voltage instability is the progressive drop of bus voltages, the risk of overvoltage instability also exists and has been experienced at least on one system (Haque and Kumkratug 2004). It is caused by a capacitive behavior of the network (EHV transmission lines operating below surge impedance loading) as well as by under excitation limiters preventing generators and/or synchronous compensators from absorbing the excess reactive power. In this case, the instability is associated with the inability of the combined generation and transmission system to operate below some load level. In their attempt to restore this load power, transformer tap changers cause long-term voltage instability. Voltage stability problems may also be experienced at the terminals of HVDC links used for either long distance or back-to-back applications (Nwohu, Isah, Usman and Sadiq 2016). They are usually associated with HVDC links connected to weak ac systems and may occur at rectifier or inverter stations, and are associated with the unfavorable reactive power "load" characteristics of the converters. The HVDC link control strategies have a very significant influence on such problems, since the active and reactive power at the ac/dc junction are determined by the controls. If the resulting loading on the ac transmission stresses it beyond its capability, voltage instability occurs. Such a phenomenon is relatively fast with the time frame of interest being in the order of one second or less. Voltage instability may also be associated with converter transformer tap-changer controls, which is a considerably slower phenomenon (Karthikeyan and Dhal, 2015).

Recent developments in HVDC technology (voltage source converters and capacitor commutated converters) have significantly increased the limits for stable operation of HVDC links in weak

systems as compared with the limits for line commutated converters. One form of voltage stability problem that results in uncontrolled over voltages is the self-excitation of synchronous machines. This can arise if the capacitive load of a synchronous machine is too large. Examples of excessive capacitive loads that can initiate self-excitation are open ended high voltage lines and shunt capacitors and filter banks from HVDC stations (Van and Ghandhari, 2010). The over-voltages that result when generator load changes to capacitive are characterized by an instantaneous rise at the instant of change followed by a more gradual rise. This latter rise depends on the relation between the capacitive load component and machine reactances together with the excitation system of the synchronous machine. Negative field current capability of the exciter is a feature that has a positive influence on the limits for self-excitation. As in the case of rotor angle stability, it is useful to classify voltage stability into the following subcategories:

Large-disturbance voltage stability refers to the system's ability to maintain steady voltages following large disturbances such as system faults, loss of generation, or circuit contingencies. This ability is determined by the system and load characteristics, and the interactions of both continuous and discrete controls and protections (Fuchs, Imhof, Demiray and Morari, 2014). Determination of large-disturbance voltage stability requires the examination of the nonlinear response of the power system over a period of time sufficient to capture the performance and interactions of such devices as motors, underload transformer tap changers, and generator field-current limiters. The study period of interest may extend from a few seconds to tens of minutes.

Small-disturbance voltage stability refers to the system's ability to maintain steady voltages when subjected to small perturbations such as incremental changes in system load. This form of stability is influenced by the characteristics of loads, continuous controls, and discrete controls at

a given instant of time (Vittal and Vijay, 2007). This concept is useful in determining, at any instant, how the system voltages will respond to small system changes. With appropriate assumptions, system equations can be linearized for analysis thereby allowing computation of valuable sensitivity information useful in identifying factors influencing stability. This linearization, however, cannot account for nonlinear effects such as tap changer controls (deadbands, discrete tap steps, and time delays). Therefore, a combination of linear and nonlinear analyzes is used in a complementary manner (Taylor, Mechenbier and Matthews 1993). As noted above, the time frame of interest for voltage stability problems may vary from a few seconds to tens of minutes. Therefore, voltage stability may be either a short-term or a long-term phenomenon as identified in Figure 2.2.

2.4.1 Short-Term Voltage Stability

This involves dynamics of fast acting load components such as induction motors, electronically controlled loads, and HVDC converters. The study period of interest is in the order of several seconds, and analysis requires solution of appropriate system differential equations; this is similar to analysis of rotor angle stability (Fuchs, Imhof, Demiray and Morari, 2014). Dynamic modeling of loads is often essential. In contrast to angle stability, short circuits near loads are important. It is recommended that the term transient voltage stability not be used.

2.4.2 Long-Term Voltage Stability

This involves slower acting equipment such as tap-changing transformers, thermostatically controlled loads, and generator current limiters. The study period of interest may extend to several or many minutes, and long-term simulations are required for analysis of system dynamic performance (Sharma and Hooda, 2012). Stability is usually determined by the resulting outage

of equipment, rather than the severity of the initial disturbance. Instability is due to the loss of long-term equilibrium (e.g., when loads try to restore their power beyond the capability of the transmission network and connected generation), post-disturbance steady-state operating point being small-disturbance unstable, or a lack of attraction toward the stable post-disturbance equilibrium (e.g., when a remedial action is applied too late) (Machowski, Kacejko, Nogal and Wancerz 2013). The disturbance could also be a sustained load buildup (e.g., morning load increase). In many cases, static analysis (Izuegbunem, Ubah and Akwukwaegbu 2012) can be used to estimate stability margins, identify factors influencing stability, and screen a wide range of system conditions and a large number of scenarios. Where timing of control actions is important, this should be complemented by quasi-steady-state time-domain simulations (Eleschová, Smitková and Beláň, 2010).

2.4.3 Basis for Distinction between Voltage and Rotor Angle Stability

It is important to recognize that the distinction between rotor angle stability and voltage stability is not based on weak coupling between variations in active power/angle and reactive power/voltage magnitude. In fact, coupling is strong for stressed conditions and both rotor angle stability and voltage stability are affected by pre-disturbance active power as well as reactive power flows (Izuegbunem, Ubah and Akwukwaegbu 2012). Instead, the distinction is based on the specific set of opposing forces that experience sustained imbalance and the principal system variable in which the consequent instability is apparent.

2.5 Frequency Stability

Frequency stability refers to the ability of a power system to maintain steady frequency following a severe system upset resulting in a significant imbalance between generation and load. It depends on the ability to maintain/restore equilibrium between system generation and load, with minimum unintentional loss of load(Bompard, Fulli, Ardelean and Masera, 2014). Instability that may result occurs in the form of sustained frequency swings leading to tripping of generating units and/or loads. Severe system upsets generally result in large excursions of frequency, power flows, voltage, and other system variables, thereby invoking the actions of processes, controls, and protections that are not modeled in conventional transient stability or voltage stability studies. These processes may be very slow, such as boiler dynamics, or only triggered for extreme system conditions, such as Volts/Hertz protection tripping generators. In large interconnected power systems, this type of situation is most commonly associated with conditions following splitting of systems into islands (Izuegbunem, Ubah and Akwukwaegbu 2012). Stability in this case is a question of whether or not each island will reach a state of operating equilibrium with minimal unintentional loss of load. It is determined by the overall response of the island as evidenced by its mean frequency, rather than relative motion of machines. Generally, frequency stability problems are associated with inadequacies in equipment responses, poor coordination of control and protection equipment, or insufficient generation reserve.

Examples of such problems are reported in references (Ali, Yehia, Abou-Hashema, El-Sayed and Amer, 2019) and (Bompard, Fulli, Ardelean and Masera, 2014). In isolated island systems, frequency stability could be of concern for any disturbance causing a relatively significant loss of

load or generation (Kundur, 1999). During frequency excursions, the characteristic times of the processes and devices that are activated will range from fraction of seconds, corresponding to the response of devices such as under frequency load shedding and generator controls and protections, to several minutes, corresponding to the response of devices such as prime mover energy supply systems and load voltage regulators. Therefore, as identified in Fig. 2.2, frequency stability may be a short-term phenomenon or a long-term phenomenon.

An example of short-term frequency instability is the formation of an under generated island with insufficient under frequency load shedding such that frequency decays rapidly causing blackout of the island within a few seconds. On the other hand, more complex situations in which frequency instability is caused by steam turbine over-speed controls or boiler/reactor protection and controls are longer-term phenomena with the time frame of interest ranging from tens of seconds to several minutes (Adepoju, Komolafe, Aborisade, 2011). During frequency excursions, voltage magnitudes may change significantly, especially for islanding conditions with under-frequency load shedding that unloads the system. Voltage magnitude changes, which may be higher in percentage than frequency changes, affect the load-generation imbalance. High voltage may cause undesirable generator tripping by poorly designed or coordinated loss of excitation relays or volts/Hertz relays. In an overloaded system, low voltage may cause undesirable operation of impedance relays.

2.6 Causes of Transient Instability in Power System

The most common disturbances that produce instability in industrial power systems are (not necessarily in order of probability): - Short circuits - Loss of a tie circuit to a public utility - Loss of a portion of on-site generation - Starting a motor that is large relative to a system generating

capacity - Switching operations - Impact loading on motors - Abrupt decrease in electrical load on generators (Ali, Yehia, Abou-Hashema, El-Sayed and Amer, 2019).

2.7 Improving Transient Stability

Transient stability can be improved either by using machines of higher inertia or by connecting the synchronous motors to heavy flywheels. This method, however, cannot be used in practice because of economic reasons and reasons of excessive rotor weight (Parry and Gangatharan, 2005).

On contrary, the modern trend in generator design is to achieve more power from smaller machines and hence lighter rotors. Improved methods of generator cooling have helped in this process. However, this trend is undesirable from the point of view of stability. A salient-pole generator operates at lower load angles and is, therefore, preferred over cylindrical rotor generators for consideration of stability.

Now more emphasis and reliance is placed on controls to provide the required compensating effects with which we may be able to offset the reduction in stability margins inherent from above trends in generator design. With the advent of high-speed circuit breakers, high-speed excitation systems and fast valving the loss in stability margin has been made up(Aouini, Marinescu, Kilani and Elleuch, 2015).

Note that when the maximum power limit of various power-angle curves is raised, the accelerating area decreases and decelerating area increases for a given clearing angle. Consequently, Initial Rotor Angle δ_0 is decreased and maximum clearing angle δm is increased.

This means that by increasing P_{max} the rotor can swing through a larger P_{max} increases the critical clearing time and improves stability.

The steady-state power limit is given by

$$\boldsymbol{P_{max} = \frac{E\,V}{X}} \qquad 2.1$$

$\boldsymbol{P_{max}}$ - Maximum transferable power into the network

E – Oscillation voltage

V – Busbar voltage

X – Reactance of the lime (transfer reactance)

It can be seen from this expression of (2.1) that $\boldsymbol{P_{max}}$can be increased by increasing either or both V and E and reducing the transfer reactance.

2.7.1 Methods often employed in practice to improve system transient stability

1. Increasing System Voltage:

Transient stability is improved by raising the system voltage profile, (i.e., raising E and V). Increase in system voltage means the higher value of maximum power, P_{max} that can be transferred over the lines. Since shaft power, $P_s = P_{max} \sin\delta$, therefore, for a given shaft power initial load angle $\delta_0$reduces with the increase in P_{max} and thereby increasing difference between the critical clearing angle and initial load angle(Vasudevan and Ramalakshmi, 2019). Thus machine is allowed to rotate through large angle before it reaches the critical clearing angle which results in greater critical clearing time and the probability of maintaining stability.

2. Reduction in Transfer Reactance:

Transient stability can also be improved by reducing the transfer reactance. The effect of reducing the transfer reactance means increase of P_{max} resulting in increase in transient stability. The following methods are available for reducing the transfer reactanceAnshika, 2016):

3. Operate Transmission Lines in Parallel

By operating transmission lines in parallel reactance decreases and power increases. The line reactance can be reduced by using more lines in parallel instead of a single line. In general, more power is transferred during a fault on one of the lines if there are two lines in parallel, than that would be transferred over a single faulted lineLatorre and Ghandhari (2010).

Increased power transfer means less available accelerating power, because the accelerating power is the difference between power input and power transfer. Lower accelerating power reduces the risk of instability.

4. Use of Bundled Conductors

Bundling of conductors reduces to a considerable extent the line reactance and so increases the power limit of the line and thereby improving stability.

5. Series Compensation of the Lines

The compensation of line reactance by series capacitors is another method of improving stability. The inductive reactance of a line can be reduced by connecting static capacitors in series with the line. It is to be noted that any measure to increase the steady-state limit P_{max} will improve the transient stability limit. The use of generators of high inertia and low reactance improves the transient stability, but generators with these characteristics are costly. In practice, only those methods are used which are economical(Nnachi, Munda, Nicolae and Mabwe, 2013).

For lines longer than 325 km series compensation method has proved economical as a means of increasing stability.The use of shunt reactors will reduce the danger of instability on lightly loaded lines. If saturable reactors are used, the regulation can be maintained steady over a wide range of loads.

Increasing the X/R ratio increases the power limit of the line itself, which in turn aids stability.

6. High-Speed Excitation Systems

High-Speed excitation helps to maintain synchronism during a fault by quickly increasing the excitation voltage. High-speed governors help by quickly adjusting the generator inputs.

7. Using High Speed Circuit Breaker

The best method of improving transient stability is the use of high-speed circuit breakers. The quicker a breaker operates, the faster the fault is removed from the system and better is the tendency of the system to restore to normal operating conditions(Nnachi, Munda, Nicolae and Mabwe, 2013).

The use of high-speed breakers has materially improved the transient stability of the power systems and does not require any other method for the purpose.

Use of high-speed breakers increases the decelerating area A_2 and decreases the accelerating area $A_1$and so improves the stability.

8. Automatic Reclosing

As the majority of faults on the transmission lines are transient in nature and are self-clearing, rapid switching and isolation of faulty lines followed by reclosing are quite helpful in

maintaining stability. The modern circuit breaker technology has made it possible for line clearing to be done as fast as in 2 cyclesNnachi, Munda, Nicolae and Mabwe (2013).

On occurrence of a fault on a transmission line, the faulted line is de-energized to suppress the arc in the fault and then the circuit breaker recloses, after a suitable time interval. Automatic reclosing increases the decelerating area A_2 and thus helps in improving stability.

9. Using Lightning Arresters

Transient Stability can be improved by reducing the severity of faults which can be achieved by using lightning arresters for protection of the lines.

10. High Neutral Grounding Impedance

In systems where the stability is of prime importance, high neutral grounding impedance may be used.The grounding is effective only for unbalanced faults. Zero-sequence impedance comes into picture to restrict the fault current only in case of faults like line-generator to-ground or line-to-line-to-groundHazra, Phulpin and Ernst (2009). For an electrical system depicted in Fig. 2.3 (a), the equivalent impedance diagram is shown in Fig. 2.3 (b).

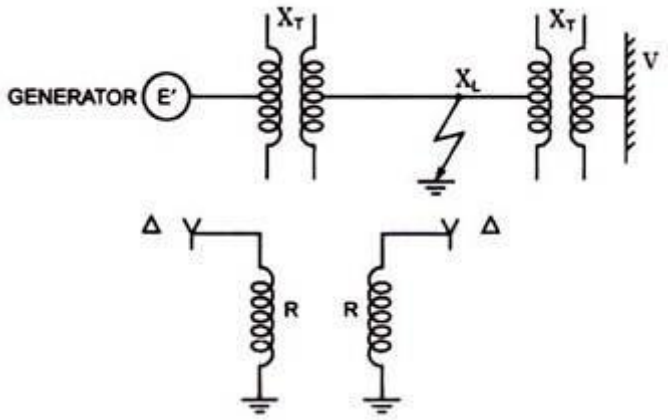

Figure 2.3 (a): Electrical System (Hazra, Phulpin and Ernst, 2009)

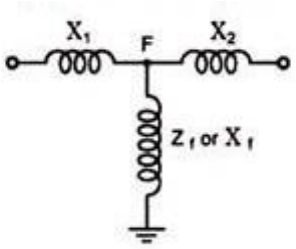

Figure 2.3 (b): Equivalent Circuit of System shown in (a). Reprinted from (Hazra, Phulpin and Ernst, 2009)

The power transfer is given by the expression:

$$P = \left[\frac{EV}{X_1 + X_2 + \frac{X_1 X_2}{X_f}}\right] \sin \delta \qquad 2.2$$

Where X_f is equivalent fault-shunt reactance.

Physically the resistance in the neutral of the transformer represents an absorption of electrical energy which in turn reduces the accelerating energy and thus improves the transient stability.

The grounding resistor consumes power during a ground fault and thus exerts braking effect on the synchronous machine which is greater, the closer the fault is to the resistor and closer the machine is to the fault. A grounding resistor located near a generator is, therefore, beneficial (Hazra, Phulpin and Ernst, 2009).

However, a grounding resistor should neither be employed near an actual or equivalent synchronous motor nor it should be employed near a synchronous condenser, as such machines already are retarded by faults. In a two machine system, it is, therefore, advisable to have resistance grounding at the sending end and reactance grounding at the receiving end.

11. Turbine Fast Valving

One reason for power system instability is the excess energy supplied by the turbine during the disturbance period. Fast valving is a means of reducing turbine mechanical input power when a unit is under acceleration due to a transmission system fault. This can be initiated by load impedance relays, acceleration transducers or by relays that recognize only severe transmission system faults (Tang, Xu, Dong & Xu, 2016).

For maximum stability gains with fast valving, the turbine input power should be reduced as fast as possible. During a fast valving operation, the interceptor valves are rapidly shut (in 0.1 to 0.2 second) and immediately re-opened. This procedure increases the critical switching time long enough so that in most of the cases the unit will remain stable for faults with stuck-breaker clearing times. Presently some stations in USA have been put to use fast valving schemes (Van & Ghandhari,2010).

12. Application of Braking Resistors

An alternative or supplement to fast turbine valving action is the application of braking resistors. Braking resistors, as employed in the context of electric power system stability, is the concept of applying an artificial electric load to a portion of the generator-transmission load complex to correct a temporary imbalance between power generated and power delivered (Fuchs, Imhof, Demiray & Morari 2014).

During a fault the resistors are connected to the terminals of the generator through circuit breakers by means of an elaborate control scheme. The control scheme determines the amount of resistance to be connected and its duration. The braking resistors remain on for a matter of cycles both during fault clearing and after system are restored to normal operation.

A few cycles after the clearance of fault, the same control scheme disconnects the braking resistors. However, the control schemes available are not very reliable(Ali, Yehia, Abou-Hashema, El-Sayed and Amer, 2019). Control schemes using thyristors have recently been suggested. The noteworthy point is that a possible failure or mal-operation of control scheme can make the matter still worse.

13. Single Pole Switching

Single pole switching or independent pole operation of a circuit breaker refers to the mechanism with which the three phases of the breaker are closed or opened independently of each other. The failure of any one phase does not automatically prevent any of the two remaining phases from proper operation (Sigrist, Echavarren, Rouco & Panciatici, 2015).

However, for a three-phase fault, the three phases are simultaneously activated for operation by the same relaying scheme. The three phases are mechanically independent, such that the mechanical failure of any one pole is not propagated for the remaining poles.

Single pole switching is used at locations where the design criterion is to guard against a three-phase fault compounded with breaker failure. The successful independent pole operation of the failed breaker will reduce a three-phase fault to a single L-G fault (if one pole of the breaker is stuck), or to L-L-G fault (if two poles of the breaker are stuck). This criterion can be applied to the substation of a generating plant with multiple transmission outlets (Machowski, Kacejko, Nogal & Wancerz, 2013).

The advantages of single poles switching under three phase fault breaker failure contingency are twofold. First, they are among the cheapest stability aids. Single pole switching operation is most efficient at high transmission voltages where equipment's are costlier.

Successful single pole switching may allow the critical clearing time of a plant circuit breaker to increase by as much as 2 to 5 cycles. Second, it is relatively easy to install. Most EHV circuit breakers are equipped with separate pole mechanism due to the large component size and wide phase space requirements at high working voltages (Adepoju, Komolafe, Aborisade, 2011). The only additional complexity is to provide separate trip coils to activate each pole.

14. Use of Quick-Acting Automatic Voltage Regulators

The satisfactory operation of synchronous generators of a complex power system at high power (or load) angles and during transient condition is very much dependent on the source of excitation for the generators and on the automatic voltage regulator (Agha, Josiah, Dan, Augustin, 2015).

The power output of a generator is proportional to internal voltage, E. Under fault conditions the terminal voltage V falls. A quick-acting voltage regulator causes increase in E so that the terminal voltage V remains constant. A higher value of E means a higher generator output.

It has already been shown that the maximum value of a power angle curve is proportional to the per unit excitation. Field forcing can, therefore, cause the machine to operate on a higher power-angle curve thereby allowing it to swing through a larger angle from its original position before it reaches the critical clearing angle (Agha, Josiah, Dan, Augustin, 2015).

As an example of the effectiveness of modern high-speed automatic voltage regulators, consider Figure 2.2. Two power-angle curves (a and b) have been drawn representing two different excitations. Curves of terminal voltage V against rotor angle for the same excitations have also been drawn. Consider working at point B on power angle curve a, where the voltage rotor angle relation is normal.

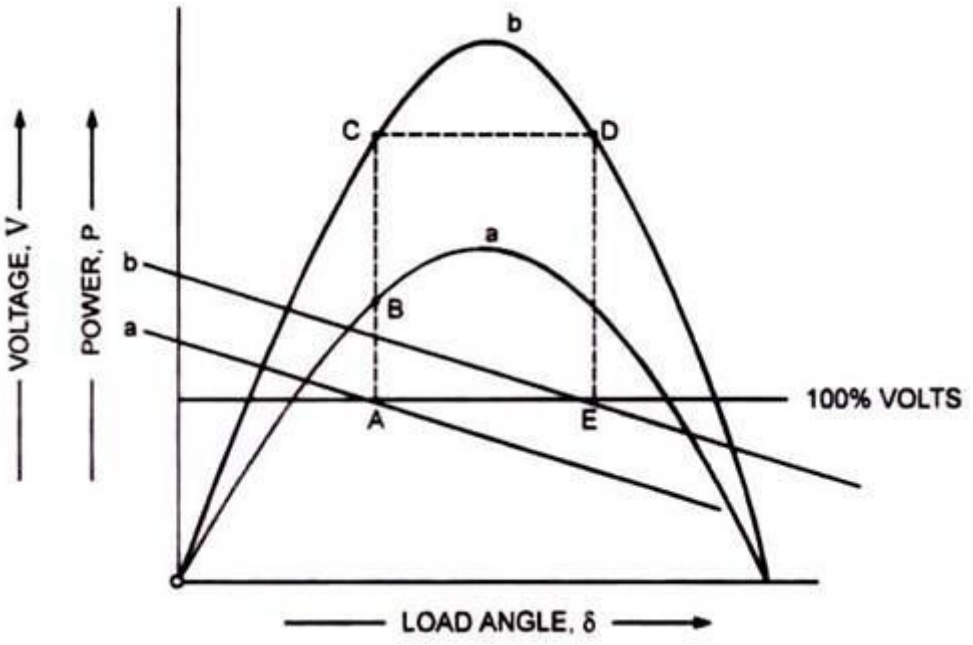

Figure 2.2: Effectiveness of High Speed Automatic Voltage Regulators (Agha, Josiah, Dan, Augustin, 2015)

If we now wish to increase the power input and maintain the same rotor angle, we can do so by increasing excitation, i.e., by working on power angle curve b at point C. Although C is in the static stability limit, the terminal voltage is above normal. However, the same power can be supplied by working at point D, in the inherently unstable region.

If the field current is constant, the slightest difference would cause instability (Ali, Yehia, Abou-Hashema, El-Sayed and Amer,2019). However, because of the high inertia, the swings are slow,

and if an automatic voltage regulator is fitted, it can sense the drop in terminal voltage as the rotor angle is increased. Before the generator has swung an appreciable amount, sufficient boost is given to the field to make the power output greater than the input, thereby arresting the swing and maintaining stability.

15. HVDC Links

High voltage direct current (HVDC) links are helpful in maintaining stability through the following advantages Anshika, 2016).

- A dc. tie line provides a loose coupling between two ac. systems to be interconnected.
- A d.c link may be interconnecting two a.c systems at different frequencies.
- There is no transfer of fault energy from one a.c. system to another if they are interconnected by a d.c. tie line.

16. Use of Double-Circuit Lines

The impedance of a double-circuit line is less than that of a single-circuit line. A double-circuit line doubles the transmission capability. An additional advantage is that the continuity of supply is maintained over one line with reduced capacity when the other line is out of service for maintenance or repair. But the provision of additional line can hardly be justified by stability consideration alone.

17. Load Shedding

If there is insufficient generation to maintain system frequency, some of the generators are disconnected immediately or during after a fault. the stability of the remaining generators is

improved. The unit to be disconnected is provided with a large steam bypass system(Singaravelu and Seenivasan, 2014). When the system recovers from the shock of the fault, the disconnected unit is resynchronized and reloaded. Extra cost of a large steam bypass system is the limitation of this method.

2.8 Methods of Evaluating Transient Stability in Electric Power Systems

The electric power system instability can be interpreted using various methods depending on system configuration and operational status. Traditionally the question of stability has been connected to maintaining synchronous operations. The production of electricity is secured primarily using synchronous generators and for this reason it is important to secure their synchronism and parallel operation and therefore the question of stability has mainly hinged on the transient stability of synchronous machinery and on the relationship between active power and the rotor angle of the generator (Ignatius and Emmanuel,2017).

Electric power system instability of course can also appear even if synchronous operation of the generators is not interrupted. Here the problem is more related to voltage control and the ability to maintain appropriate voltage within individual system circuits. Voltage instability mainly appears in extremely overloaded systems with lengthy transmission lines and weak system. The results of analysis completed for large system outages (blackouts) have led to conclusions and recommendations that should be followed for transmission system operations. In particular, these include (Haque, 2004):

−It is important to preventing such an outage from causing a chain reaction of outages with regards to the fact that it is not completely possible to avoid the occurrence of a failure in the system,

− It is absolutely necessary to secure valid N-1 safety criteria,

− The transient stability of the synchronous generator must be secured,

− Voltage stability in the electric power system must be secured (sufficient reactive power in the system), − Monitoring and control of overloads on transmission elements in the transmission system.

There are several methods to study and evaluate the transient stability of Electric Power Systems. These methods can be gathered in five groups:

1. Numerical Integration Methods,
2. Direct Methods,
3. Simulation methods,
4. Hybrid Methods and
5. Artificial Intelligence Techniques.

2.8.1 Numerical Integration Methods

An Electric Power System can be described by two sets of equations: a differential set related to the generators and an algebraic set related to the others components (Singaravelu and Seenivasan, 2014). The way these methods study the transient stability of the system is solving, in the time, the two sets of equations mentioned above. These methods offer very good modelling capabilities.

2.8.2 Direct Methods

Direct methods for analyzing transient stability allow the direct calculation of the reserve or the limit of transient stability. As opposed to simulation methods, during their application it is not necessary to explicitly calculate a system solution using a differential equation to describe the transient behavior of the electric power system over time; on the other hand, this can result in relatively conservative results. The most frequently used method is the method of area equality, which is useful for the model: one synchronous machine – an infinite bus (Lakshminarayana, Shishir, Mukesh, and Ganga,2014). This means that the transient stability of a single generator or an equivalent generator is evaluated (equivalent replacement for a number of generators) with respect to the other parts of the system (infinite bus).

The result from the application of this method is the critical rotor angle of the generator, i.e. the transient stability limit for the given machinery. In order to practically evaluate transient stability, it is necessary to know the critical time within the given contingency, e.g. a short-circuit fault– Critical Clearing Time (CCT), which, if exceeded, results in a permanent breach in the synchronous operation of the evaluated generator (Agha, Josiah, Dan, Augustin, 2015). In order to define CCT it is necessary to know the development of rotor angle over time and in order to do this it is necessary to know the differential swing equation for synchronous machinery.

$$\frac{d^2\delta}{dt^2} = \frac{\omega_0 \Delta P}{T_m S_n} \qquad 2.3$$

ΔP - change in power

δ - rotor angle

ω_0 - frequency

T_m - maximum torque

These methods are also called Energy Function Methods, because they are based in comparisons of energy values (Prabha, John, Venkat, Göran, Anjan, Claudio, at el, 2004). More precisely, these methods calculate the energy value at the clearing time and the critical energy value. If the energy value at the clearing time is higher than de critical energy value the system is unstable, otherwise the system is stable. These methods only require to solve the equations during the fault period, which leads to lower computation times.

2.8.3 Simulation Methods

The most frequent method for evaluation transient stability is a time simulation of a previous event, i.e. the resolution of the system using non-linear differential equations using numerical integration methods. Simulation methods as opposed to direct methods serve to verify both the stability of a single generator as well as the stability of the entire or a part of the electrical system (Lakshminarayana, Shishir, Mukesh, and Ganga, 2014).

2.8.4 Hybrid Methods

The Hybrid Methods gather the advantages from the Numerical Integration Methods with the advantages from the Direct Methods (Singaravelu and Seenivasan 2014). From the first they get the modelling capabilities, whereas from the second they get the fast analysis capabilities.

2.8.5 Artificial Intelligence Techniques

These are the newer approach to assess the transient stability of Electric Power Systems (Singaravelu and Seenivasan 2014). Unlike the previous methods, which are all deterministic, these kind on methods are probabilistic. They are characterized by being necessary to do a lot of simulations before being ready to use. However, when in use, they provide a very fast analysis.

Between all the methods presented here, the best results are obtained with the Hybrid Methods and with the Artificial Intelligence Techniques. Due to the simulations that the Artificial Intelligence Techniques require before being ready to use, the Hybrid Methods take advantage when it's necessary to choose one (Sanz, Chaudhuri and Strbac, 2016).

2.9 High Voltage Direct Current (HVDC) Link

High voltage direct current (HVDC) power systems use D.C. for transmission of bulk power over long distances. For long-distance power transmission, HVDC lines are less expensive, and losses are less as compared to AC transmission (Singaravelu and Seenivasan, 2014). It interconnects the networks that have different frequencies and characteristics.

In AC transmission, alternating waves of voltage and current travels in the line which change its direction every millisecond; due to which losses occur in the form of heat. Unlike AC lines, the voltage and current waves don't change their direction in DC. HVDC lines increase the efficiency of transmission lines due to which power is rapidly transferred.

In a combined AC and DC system, generated AC voltage is converted into DC at the sending end. Then, the DC voltage is inverted to AC at the receiving end, for distribution purposes. Thus, the conversion and inversion equipment are also needed at the two ends of the line (Agha, Josiah, Dan, Augustin, 2015). HVDC transmission is economical only for long distance transmission lines having a length more than 600kms and for underground cables of length more than 50kms.

2.9.1 Historical Perspective on HVDC Transmission

It has been widely documented in the history of the electricity industry, that the first commercial electricity generated (by Thomas Alva Edison) was direct current (DC) electrical power. The first electricity transmission systems were also direct current systems. However, DC power at low voltage could not be transmitted over long distances, thus giving rise to high voltage alternating current (AC) electrical systems. Nevertheless, with the development of high voltage valves, it was possible to once again transmit DC power at high voltages and over long distances, giving rise to HVDC transmission systems.

2.9.2 How HVDC Transmission System Works

In generating substation, AC power is generated which can be converted into DC by using a rectifier. In HVDC substation or converter substation rectifiers and inverters are placed at both the ends of a line. The rectifier terminal changes the AC to DC, while the inverter terminal converts DC to AC.

The DC is flowing with the overhead lines and at the user end again DC is converted into AC by using inverters, which are placed in converter substation. The power remains the same at the sending and receiving ends of the line. DC is transmitted over long distances because it decreases the losses and improves the efficiency.

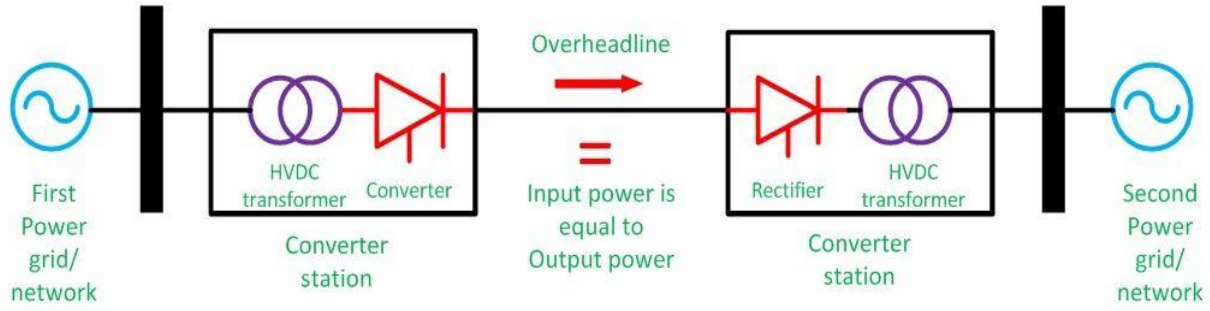

Figure 2.3: HVDC Substation Layout (Anshika, 2016).

A system having more than two converter stations and one transmission line is called a 'two terminal DC system' or a 'point-to-point system'. Similarly, if substation has more than two converter stations and interconnecting DC terminal lines, it is called multi-terminal DC substation.

2.9.3 Economic Distance for HVDC transmission lines

DC lines are cheaper than the AC lines, but the cost of DC terminal equipment is very high as compared to AC terminal cables (shown in Figure 2.4). Thus, the initial cost is high in HVDC transmission system, and it is low in the AC system.

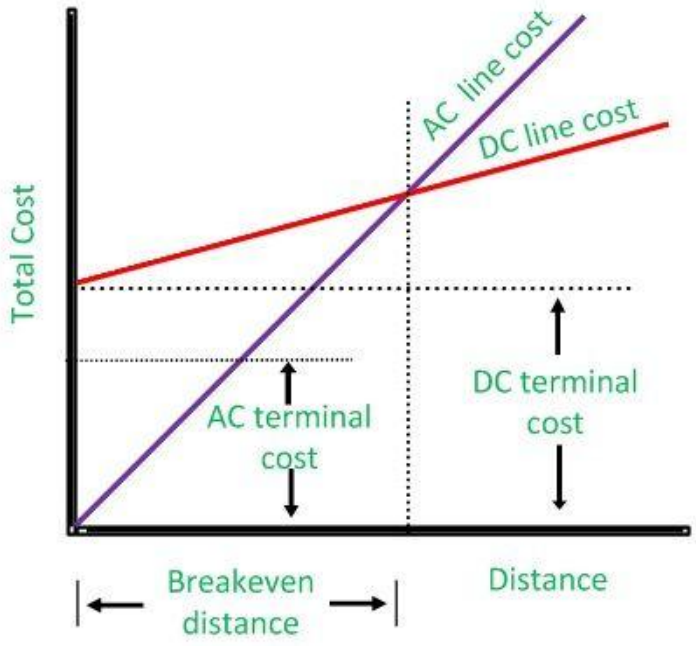

Figure 2.4: Comparison of the costs of AC and DC transmission(Anshika, 2016).

The point where two curves meet is called the breakeven distance**.** Above the breakeven distance, the HVDC system becomes cheaper. Breakeven distance changes from 500 to 900 km in overhead transmission lines.

2.9.4 Advantages of HVDC transmissions

1. A less number of conductors and insulators are required thereby reducing the cost of the overall system.
2. It requires less phase to phase and ground to ground clearance.
3. Their towers are less costly and cheaper.
4. Less corona loss as compared to HVAC transmission lines of similar power.

5. Power loss is reduced with DC because fewer numbers of lines are required for power transmission.
6. The HVDC system uses earth return. If any fault occurs in one pole, the other pole with 'earth returns' behaves like an independent circuit. This results in a more flexible system.
7. The HVDC has the asynchronous connection between two AC stations connected through an HVDC link; i.e., the transmission of power is independent of sending frequencies to receiving end frequencies. Hence, it interconnects two substations with different frequencies.
8. Due to the absence of frequency in the HVDC line, losses like skin effect and proximity effect does not occur in the system.
9. It does not generate or absorb any reactive power. So, there is no need for reactive power compensation.
10. The very accurate and lossless power flows through DC link.

2.9.5 Disadvantages of HVDC transmission

1. Converter substations are placed at both the sending and the receiving end of the transmission lines, which result in increasing the cost.
2. Inverter and rectifier terminals generate harmonics which can be reduced by using active filters which are also very expensive.
3. If a fault occurs in the AC substation, it may result in a power failure for the HVDC substation placed near to it
4. Inverter used in Converter substations have limited overload capacity.

5. Circuit breakers are used in HVDC for circuit breaking, which is also very expensive.
6. It does not have transformers for changing the voltage levels.
7. Heat loss occurs in converter substation, which has to be reduced by using the active cooling system.
8. HVDC link itself is also very complicated**.**

2.9.6 The HVDC technology

The fundamental process that occurs in an HVDC system is the conversion of electrical current from AC to DC (rectifier) at the transmitting end, and from DC to AC (inverter) at the receiving end. There are three ways of achieving conversion:

- Natural Commutated Converters.

Natural commutated converters are most used in the HVDC systems as of today. The component that enables this conversion process is the thyristor, which is a controllable semiconductor that can carry very high currents (4000A) and is able to block very high voltages (up to 10 kV) (Agha, Josiah, Dan, Augustin, 2015). By means of connecting the thyristors in series it is possible to build up a thyristor valve, which is able to operate at very high voltages (several hundred of kV).The thyristor valve is operated at net frequency (50Hz or 60Hz) and by means of a control angle it is possible to change the DC voltage level of the bridge. This ability is the way by which the transmitted power is controlled rapidly and efficiently (Singaravelu and Seenivasan, 2014).

- Capacitor Commutated Converters (CCC).

An improvement in the thyristor-based commutation, the CCC concept is characterized by the use of commutation capacitors inserted in series between the converter transformers and the

thyristor valves. The commutation capacitors improve the commutation failure performance of the converters when connected to weak networks.

- Forced Commutated Converters.

This type of converters introduces a spectrum of advantages, e.g. feed of passive networks (without generation), independent control of active and reactive power, power quality. The valves of these converters are built up with semiconductors with the ability not only to turn-on but also to turn-off (Ekici, Yildirim and Poyraz, 2009). They are known as VSC (Voltage Source Converters). Two types of semiconductors are normally used in the voltage source converters: the GTO (Gate Turn-Off Thyristor) or the IGBT (Insulated Gate Bipolar Transistor). Both of them have been in frequent use in industrial applications since early eighties.

The VSC commutates with high frequency (not with the net frequency). The operation of the converter is achieved by Pulse Width Modulation (PWM). With PWM it is possible to create any phase 3 angle and/or amplitude (up to a certain limit) by changing the PWM pattern, which can be done almost instantaneously (Anshika, 2016). Thus, PWM offers the possibility to control both active and reactive power independently. This makes the PWM Voltage Source Converter a close to ideal component in the transmission network. From a transmission network viewpoint, it acts as a motor or generator without mass that can control active and reactive power almost instantaneously.

2.10 Types of HVDC Links

The high voltage dc links may be classified broadly into three as follows:

2.10.1 Monopolar DC Link

As the name suggests, monopolar link has only one conductor and return path is provided by permanent earth or sea. The line usually operates with negative polarity with respect to ground so as to reduce corona loss and radio interference.

The earth electrodes are designed for continuous rated current operation and for any overload capacity required in the specific case. The sea or ground return is permanent and of continuous rating. The ground return path has a low resistance and, therefore, low power loss in comparison with a metallic line conductor of economical size and equal length provided the ground electrodes are of proper design (Anshika, 2016). Monopolar line is more economical than a bipolar line because the ground return saves the cost of the one metallic conductor and losses in it.

Monopolar HVDC links were used only for low power rating and mainly for cable transmission. In some cases, the monopolar lines installed earlier are converted into bipolar systems by adding additional substation pole and transmission pole.

Monopolar HVDC line has only the rating equal to half of corresponding bipolar line rating and is; therefore, not economically competitive with EHV ac schemes for submarine cables longer than 25 km and of power rating of about 250 MW. For such cable transmission high voltage ac scheme is not technically feasible due to large charging currents with ac cables beyond thermal limit. Bipolar cable is not justified for ratings up to about 500 MW. Recent HVDC cable schemes are bipolar.

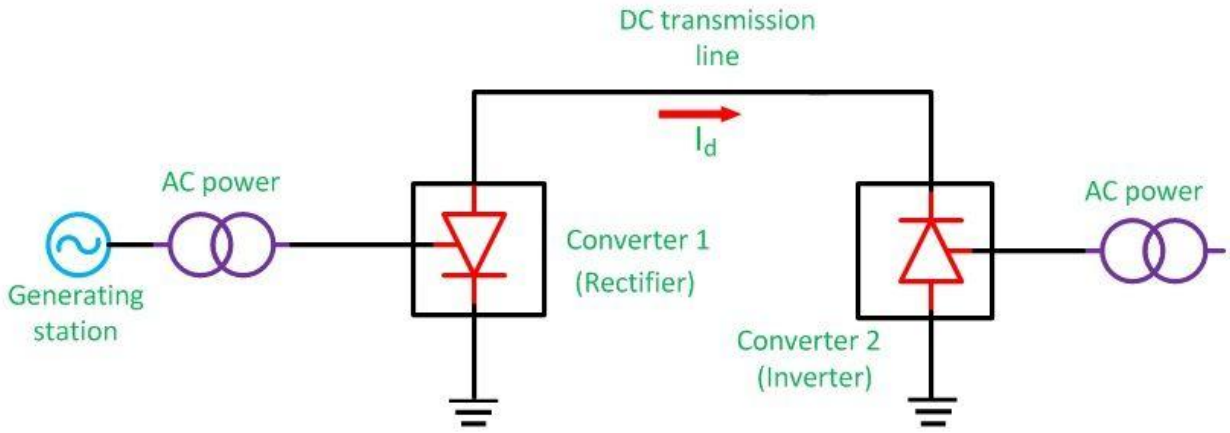

Figure 2.5: Monopolar HVDC Link (Anshika, 2016).

2.10.2 Bipolar DC Link

This is most widely used dc link for overhead long distance HVDC transmission systems and also for back-to-back HVDC system. This link has two conductors— one operating with positive polarity and the other with negative polarity with respect to the earthed tower structure.

There are two converters of equal voltage rating and connected in series at each end of the dc line. The neutral points, i.e., the junction between converters may be grounded at one end or at both the ends. If it is grounded at both ends each pole can operate independently.

The rated voltage of a bipolar link is expressed as ± 500 V. Power rating of one pole is about half of bipolar power rating. The earth carries only a small out-of-balance current during the normal operation. When the currents in the two conductors are equal, the ground current is zero.

During fault or trouble on one of the lines, the other line along with ground return can supply half of the rated load (Ekici, Yildirim and Poyraz, 2009). Thus continuity of supply is maintained.

After taking corrective measures, the system is switched over to normal bipolar operation. Thus the reliability of a bipolar line is equal to that of a double circuit 3-phase line although it has only two conductors instead of 6 for 3-phase line.

Example of bipolar HVDC link is Ranchi-Delhi single bipolar overhead line of length 810 km, capacity 1,500 MW and operating at ± 500 kV for transmission of bulk power. This line is designed to operate in bipolar mode under normal conditions, both the poles sharing the load equally with negligible current (less than 10A) in the ground return path.

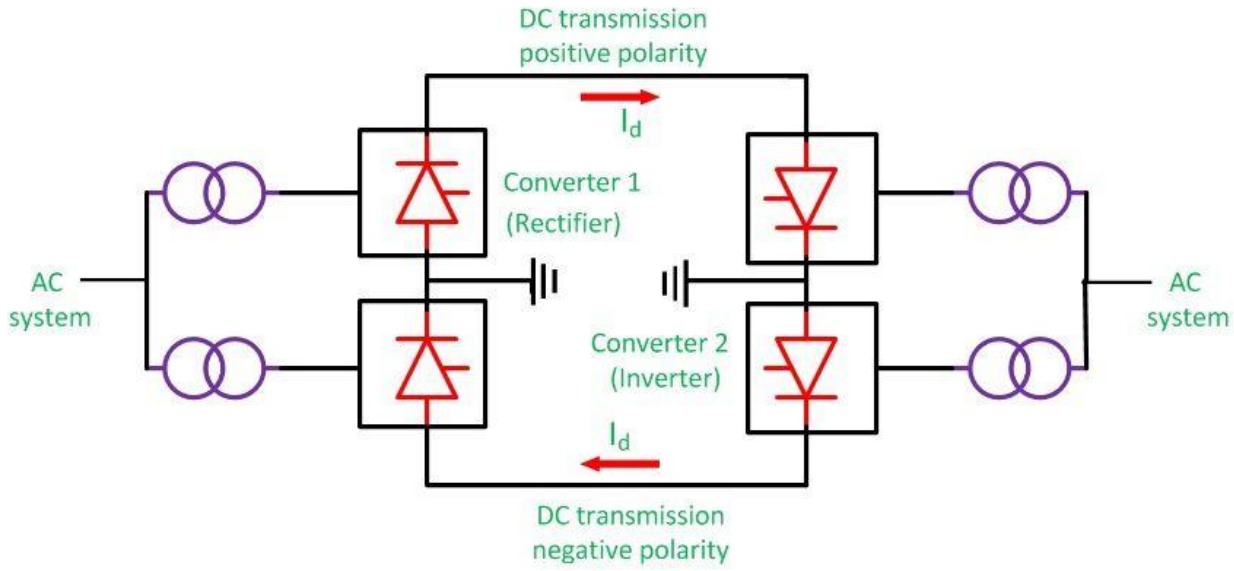

Figure 2.6: Bipolar HVDC Link (Anshika, 2016).

In case of fault on one of the poles, the system automatically switches over to monopolar ground return mode supplying 50% of the rated load. Thereafter the system may be changed over to bipolar metallic return mode when the other conductor is used as return conductor.

2.10.3 Homopolar DC Link

A homopolar link has two or more conductors having the same polarity, usually negative, and always operates with ground as the return conductor. In case of a fault on any one of the conductors, the converter equipment can be reconnected so that the healthy conductor can supply power. Such a scheme is very complicated and is preferred to a bipolar link provided continuous ground return does not pose additional problems.

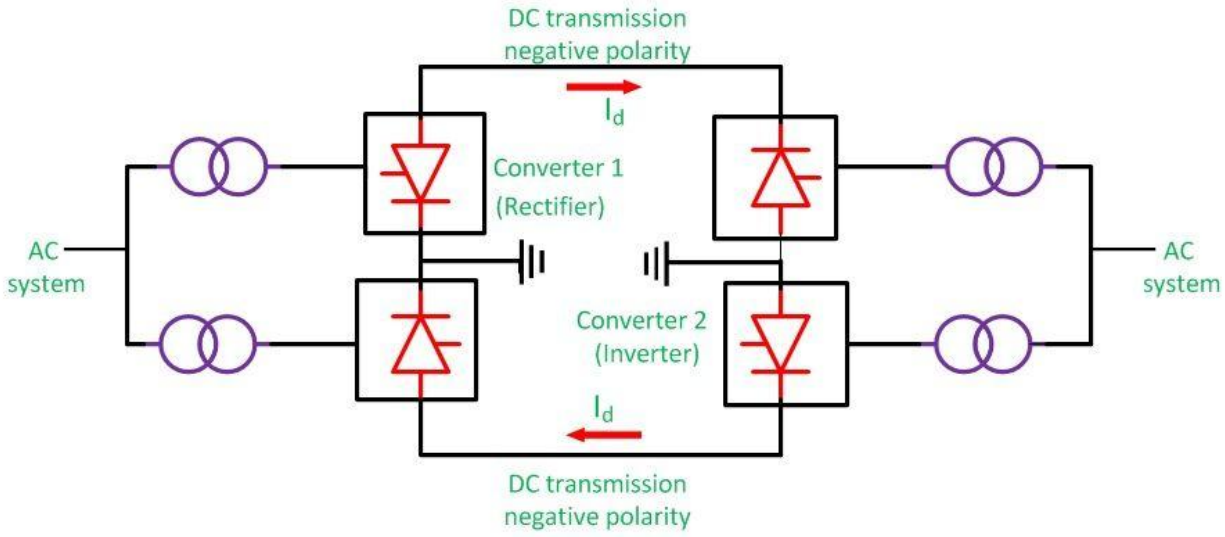

Figure 2.7: Homopolar HVDC Link (Anshika, 2016).

2.11 Application of HVDC Power System Stability Improvement

High voltage direct current (HVDC) transmission is an economic way for long distance bulk power delivery and/or interconnection of asynchronous system with different frequency (Abikhanova, Ahmetbekova, Bayat, Donbaeva, Burkitbay, 2018). HVDC system plays much more important role in power grids due to their huge capacity and capability of long distance transmission

The interconnection of AC electrical power grids has historically presented technical challenges ranging from frequency regulation, coordination of operations, and transient stability (Ekici, Yildirim and Poyraz, 2009). These challenges have gained higher interest on one hand due to the incorporation of power electronic converters in the transmission links and on the other hand, due to the integration of weak, rather than strong power systems. In a weak system a small disturbance can cause large deviations in the voltage and other variables in the network. The short circuit level at a bus is commonly used as a measure of the system strength at that particular point. Technically, a weak AC system could be evaluated following several considerations: low ratio of inductance over resistance, high impedance and low inertia Kundur, 1999). Examples of weak networks include isolated micro-grids with renewable energy (wind power, photovoltaic...). Due to network weakness, dynamics of voltage and frequency are coupled, making it difficult to simultaneously guarantee voltage stability and frequency synchronization. In response to these challenges, transmission in HVDC has been developed to mitigate these issues. The HVDC technology is able to provide to the transmission system advantages such as transfer capacity enhancement and power flow control (Leonard, Grigsby, 2012). Indeed, HVDC applications have widely increased, presenting diverse configurations: pure DC links or hybrid configurations where AC and DC circuits are parallelized. The strength of the AC system with respect to the power rating of the HVDC link is described by the ShortCircuit Ratio (SCR) (Tang, Xu, Dong and Xu 2016). The interconnected networks may be electrically strong AC systems with an SRC greater than 3, or weak networks suffering from low inertia and low SCR. Indeed, the HVDC links are increasingly used inside the same AC network in order to enhance the power transmission capacity between some zones of the grid, such as the integration of renewable energy distributed generators.

2.12 Modeling of VSC-HVDC Transmissions

This section presents three different models for VSC-HVDC transmissions, namely Injection Model, Simple Model and HVDC Light Open Model. The Injection Model and Simple Model are used for the derivation of CLF-based control strategies. The HVDC Light Open Model is used for testing control strategies and analyzing the impact of VSC-HVDC transmissions on power systems.

2.12.1 Injection Model

The Injection Model is intended for power flow and electromechanical dynamics analyses. For this reason, it is sufficient to consider the voltage and current phasors in the ac system. The Injection Model can be considered as an element, which provides adequate interaction with other elements for enhancing the dynamic performance and stability of the system as a whole. Harmonics and dc transient components are neglected, because they normally have a second order effect on the active and reactive powers. Voltages and currents are represented by phasors in the ac network, which vary with time during transients. The Injection Model is valid for symmetrical conditions, i.e., for positive sequence voltages and currents. The model is used in the derivation and test of control strategies. Figure 2.8 shows a basic structure of a VSC HVDC link connected in parallel with an ac transmission line.

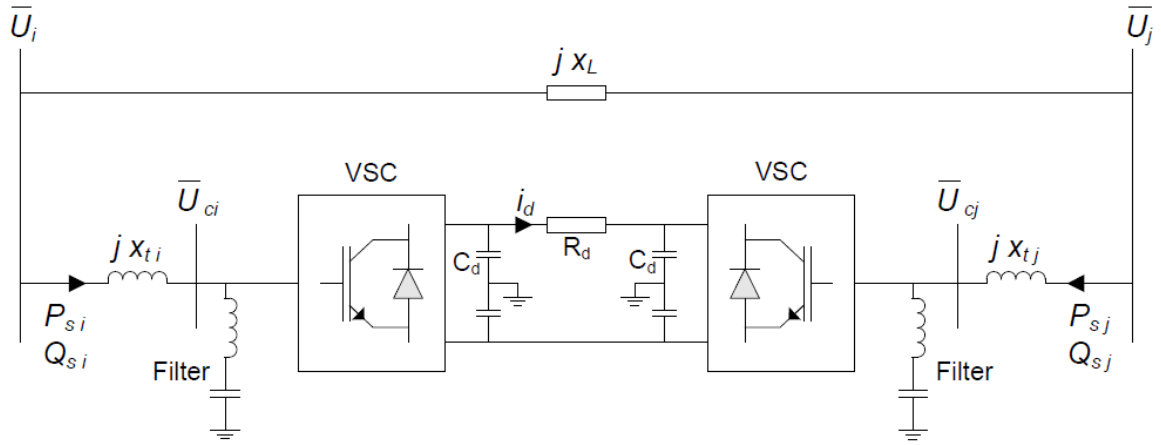

Figure 2.8: Basic Structure of a VSC-HVDC transmission(Van & Ghandhari, 2010).

From the connection nodes Bus *i* and Bus *j*, a VSC-HVDC transmission can be seen as a synchronous machine without inertia where the production or consumption of active power is independent of the production or consumption of reactive power. This interpretation leads to modeling a VSC-HVDC transmission as two controllable voltage sources in series with a reactance, which represents the impedance of the power transformer. This modeling is shown in Figure 2.9

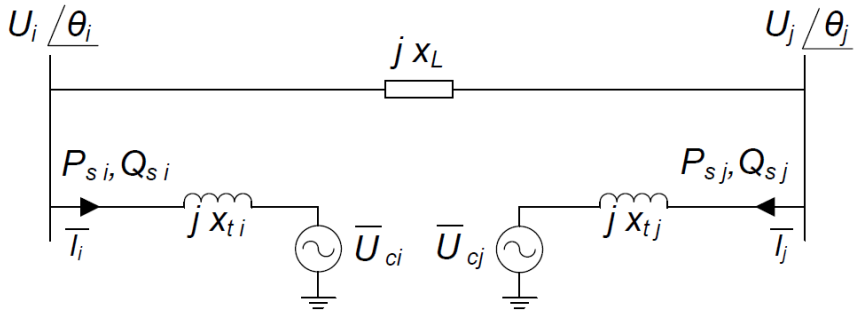

Figure 2.9: Modeling of a VSC-HVDC transmission(Van & Ghandhari, 2010).

In Figure 3.2 $\overline{U}_{ci} = U_{ci}e^{j\gamma_i}$and $\overline{U}_{cj} = U_{cj}e^{j\gamma_j}$. $P_{si}$and Q_{si}can be independentlycontrolled by $\gamma_i$and U_{ci}. Likewise,$P_{si}$and Q_{si}can be independently controlled by $\gamma_j$and U_{cj}It is assumed that dc

voltage control keeps the dc voltage magnitude close to the rated voltage. Therefore, the losses of the converters are assumed constant, regardless of the current through the converters. The losses are consequently represented as a constant active load. The losses of the dc cables are neglected. The relation between Bus *i* and Bus *j* is given by the active power: $P_{si} = -P_{si}$.

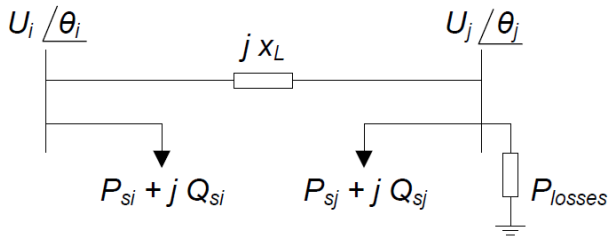

Figure 2.10: Shows the Injection Model(Van & Ghandhari, 2010).

2.12.2 Simple Model

The Simple Model is a variation of the Injection Model where the active and reactive power are controlled directly, i.e., γ_i, U_{ci}, γ_j and U_{cj} do not control the active nor the reactive power injected into the respective converter. The main assumption in the Simple Model is that the control of the VSC has a very fast PI-regulator driving the active and reactive power injected into the VSC, where ΔP_{si}, ΔQ_{si} and ΔQ_{sj} are inputs for control strategies or voltage support.

2.12.3 HVDC Light Open Model

The objective of the model is to provide the correct interaction between ac and dc systems. It interacts with ac networks through the injected currents. The node voltages of the networks are determined by the Kirchoff's current law. It defines an equation for each node, from which the node voltages can be solved, given the injected currents as function of the node voltages.

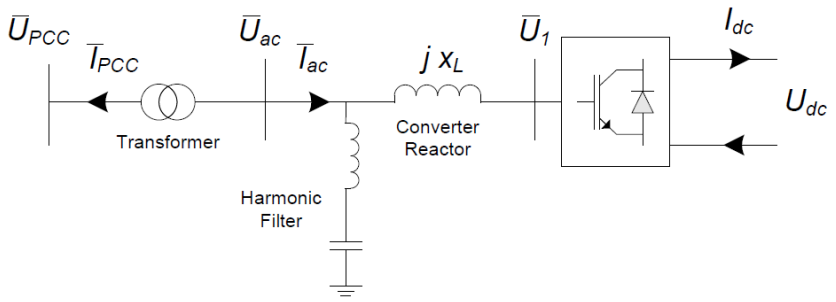

Figure 2.11: Single line diagram of one end of a VSC-HVDC transmission (Latorre and Ghandhari 2010).

Hence, the modeling objective is to provide equations of the HVDC Light, which give the phasor of the ac current injected to the ac network as function of the phasor of the voltage of the ac node. The model is written for transient conditions. The model for steady state conditions is obtained by neglecting all time derivatives.

Reference values for the different controls in the ABB HVDC Light Open Model Version 1.1.6, such as active power, reactive power and ac voltage references can be set by the user and, if necessary, modified during the simulation. However, the dc voltage reference cannot be controlled by the user and is set by the model to match the nominal dc voltage of the dc nodes.

Figure 3.4 shows the single line diagram of one end of a VSC-HVDC transmission. The Figure shows a PWM converter, a series reactor, xL, an ac filter and a transformer.

In the figure, $\bar{U}_{PCC}$ and $\bar{I}_{PCC}$ are the injected voltage and the current into the Point of Common Coupling (PCC). The active power through the converter reactor, xL, is equal to the dc power injected into the dc nodes. The losses of the PWM converter are modeled inside and are divided into no-load losses and load losses.

The PWM converter controls the internal ac voltage bus U_1, so that the real and imaginary part of the current $\bar{I}_{PCC}$ on the primary side of the converter transformer corresponds to current orders from internal controllers. For a converter in active power control mode, an internal active power PI-regulator controls the real part of the current $\bar{I}_{PCC}$ so that the active power is equal to the active power reference. For a converter in dc voltage control mode, an internal dc voltage PI-regulator controls the real part of the current $\bar{I}_{PCC}$ so that the set value for the dc node voltage, e.g. 1.0 p.u., is maintained.

For a converter in either reactive power control mode or ac voltage control mode, an internal PI-regulator controls the imaginary part of the current $\bar{I}_{PCC}$ so that either the reactive power or ac voltage is equal to the reference value. Figure 3.5 shows a block diagram of the control of the HVDC Light Open Model. In the figure, $\Delta P_c, \Delta Q_c$ and ΔU_{ac-c} are user inputs and they are intended for supplementary control. In this thesis the input $\Delta Uac{-}c$ is not used.

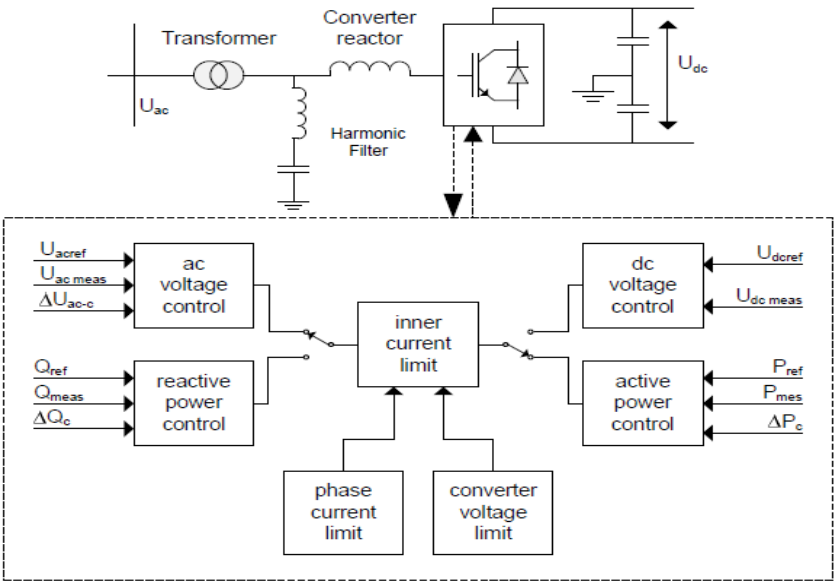

Figure 2.12: Overview control of HVDC Light Open Model (Latorre and Ghandhari 2010)

2.13 Limits Capability Converters

The limits restricting the operation of the converters are considered in the HVDC Light Open Model. Figure 2.13 shows the restricted operating area of a P-Q diagram due to the limitation on the dc cable and dc voltage.

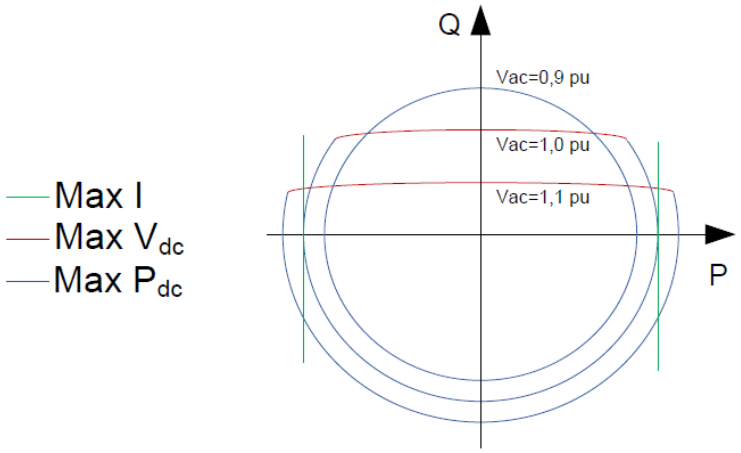

Figure 2.13: The restricted operating area of a P-Q diagram due to the limitation on the dc cable and dc voltage (Singaravelu and Seenivasan, 2014).

There are three main factors that could limit the capability of the converters seen from a power system stability perspective.

1. **Maximum current:** Maximum current that can flow through the valves. This current when multiplied by the ac voltage yields the maximum MVA circle in the power plane. If the ac voltage decreases, so does the MVA capability.
2. **Maximum dc voltage:** Reactive power is mainly dependent on the voltage difference between the ac voltage the VSC can generate from the dc voltage and the ac network. If the ac voltage is high, the difference between the maximum dc

voltage and ac voltage is low. The reactive power capability is then moderate, but increases with decreasing ac voltage.

3. **Ampacity cables:** Maximum dc current that can flow through the cables.

2.14 Artificial Neural Network (ANN)

The ANNs are very different from expert systems since they do not need a knowledge base to work. Instead, they have to be trained with numerous actual cases. An ANN is a set of elementary neurons which are connected together in different architectures organized in layers of what is biologically inspired. An elementary neuron can be seen like a processor which makes a simple non-linear operation of its inputs producing its single output. The ANN techniques are attractive because they do not require tedious knowledge acquisition, representation and writing stages and, therefore, can be successfully applied for tasks not fully described in advance. The ANNs are not programmed or supported by knowledge base as are Expert systems. Instead, they learn a response based on a given inputs and required output by adjusting the node weights and biases accordingly. The speed of processing, allowing real time applications, is also advantage.

Since ANNs can provide excellent pattern recognition, they are proposed by many researchers to perform different tasks in power system relaying for signal processing and decision making (Lukowicz, Rosolowski, 2013).

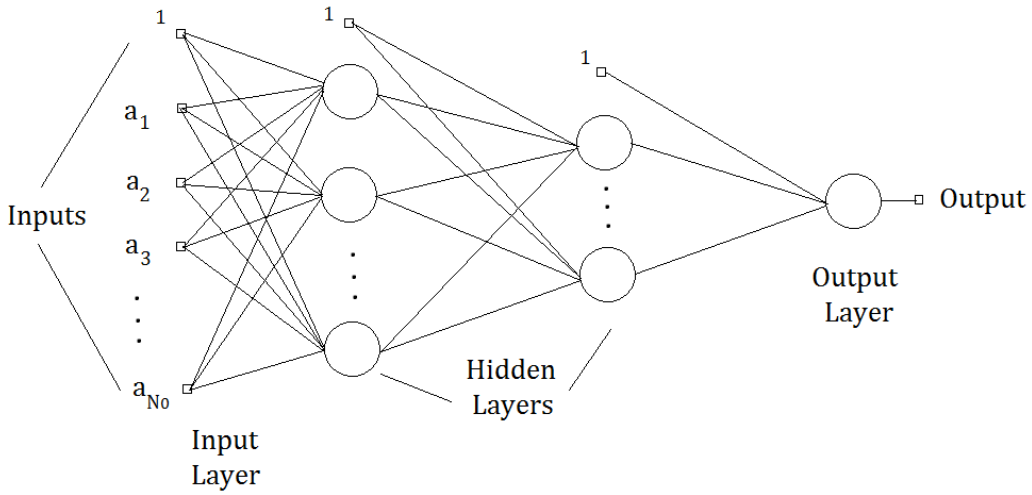

Figure 2.14: A basic three-layer architecture of a feed-forward ANN.

An Artificial Neural Network (ANN) can be described as a set of elementary neurons that are usually connected in biologically inspired architectures and organized in several layers. The structure of a feed-forward ANN, also known as the perceptron is shown in Fig 2.15. There are N_i numbers of neurons in each ith layer and the inputs to these neurons are connected to the previous layer neurons. The input layer is fed with the excitation signals. Simply put, an elementary neuron is like a processor that produces an output by performing a simple non-linear operation on its inputs (Haykin, 1994). A weight is attached to each and every neuron and training an ANN is the process of adjusting different weights tailored to the training set. An Artificial Neural Network learns to produce a response based on the inputs given by adjusting the node weights. Hence, we need a set of data referred to as the training data set, which is used to train the neural network.

In Fig. 2.11, a_1, a_2 … a_{N0} is the set of inputs to the ANN. Due to their outstanding pattern recognition abilities ANNs are used for several purposes in a wide variety of fields including

signal processing, computers and decision making. Some important notes on artificial neural networks are (Kezunovic, 1997):

- Either signal features extracted using certain measuring algorithms or even unprocessed samples of the input signals are fed into the ANN.
- The most recent along with a few older samples of the signals are fed into the ANN.
- The output provided by the neural network corresponds to the concerned decision which might be the type of fault, existence of a fault or the location of a fault.
- The most important factor that affects the functionality of the ANN is the training pattern that is employed.
- Pre-processing and post-processing techniques may be employed as well to enhance the learning process and reduce the training time of the ANN.

One of the biggest drawbacks of applications that make use of artificial neural networks is that no well-defined guide exists to help choose the ideal number of hidden layers to be used and the number of neurons per each hidden layer (Pao, 2012). From a different perspective, it is advantageous considering the wonderful ability to generalize. A vital feature of ANN is its dedication to parallel computing. Hence it can produce a correct output corresponding to any input even if the concerned input was not fed into the ANN during the training process. Another challenge in the ANN based application development was to synthesize the algorithm for the adaptive learning process. The back error-propagation algorithm is the basic algorithm in which

the neuron weights are adjusted in consecutive steps to minimize the error between the actual and the desired outputs. This process is known as supervised learning.

Neural networks have seen an explosion of interest over the last few years and are being successfully applied across an extraordinary range of problem domains, in areas as diverse as finance, medicine, engineering, geology, physics and biology. The excitement stems from the fact that these networks are attempts to model the capabilities of the human brain. From a statistical perspective neural networks are interesting because of their potential use in prediction and classification problems.

Artificial neural networks (ANNs) are non-linear data driven self-adaptive approach as opposed to the traditional model based methods. They are powerful tools for modelling, especially when the underlying data relationship is unknown. ANNs can identify and learn correlated patterns between input data sets and corresponding target values (Aggarwal and Song, 1997). After training, ANNs can be used to predict the outcome of new independent input data. ANNs imitate the learning process of the human brain and can process problems involving non-linear and complex data even if the data are imprecise and noisy. Thus they are ideally suited for the modelling of agricultural data which are known to be complex and often non-linear (Pao, 2012).

A very important feature of these networks is their adaptive nature, where "learning by example" replaces "programming" in solving problems. This feature makes such computational models very appealing in application domains where one has little or incomplete understanding of the problem to be solved but where training data is readily available.

These networks are “neural” in the sense that they may have been inspired by neuroscience but not necessarily because they are faithful models of biological neural or cognitive phenomena. In fact, majority of the network are more closely related to traditional mathematical and/or statistical models such as non-parametric pattern classifiers, clustering algorithms, nonlinear filters, and statistical regression models than they are to neurobiology models.

Neural networks (NNs) have been used for a wide variety of applications where statistical methods are traditionally employed. They have been used in classification problems, such as identifying underwater sonar currents, recognizing speech, and predicting the secondary structure of globular proteins (Sidhu, Singh, and Sachdev, 2005). In time-series applications, NNs have been used in predicting stock market performance. As statisticians or users of statistics, problems are normally solved through classical statistical methods, such as discriminant analysis, logistic regression, Bayes analysis, multiple regression, and ARIMA time-series models. It is, therefore, time to recognize neural networks as a powerful tool for data analysis.

ANN does not require a knowledge base, that is, an expertise body of coded information of any particular system under consideration before they could be applied. Hence, it is well suited to generalized and rapid deployment.

2.14.1 Characteristics of Neural Networks (NNs)

- The NNs exhibit mapping capabilities, that is, they can map input patterns to their associated output patterns.
- The NNs learn by examples. Thus, NN architectures can be ‘trained’ with known examples of a problem before they are tested for their ‘inference’ capability on

unknown instances of the problem. They can, therefore, identify new objects previously untrained.

- The NNs possess the capability to generalize. Thus, they can predict new outcomes from past trends.
- The NNs are robust systems and are fault tolerant. They can, therefore, recall full patterns from incomplete, partial or noisy patterns.
- The NNs can process information in parallel, at high speed, and in a distributed manner.

2.14.2 Basics of Artificial Neural Networks

The terminology of artificial neural networks has developed from a biological model of the brain. A neural network consists of a set of connected cells; the neurons. The neurons receive impulses from either input cells or other neurons and perform some kind of transformation of the input and transmit the outcome to other neurons or to output cells (Kumar, Raghuwanshi, Singh, Wallender and Pruitt, 2012). The neural networks are built from layers of neurons connected so that one layer receives input from the preceding layer of neurons and passes the output on to the subsequent layer.

A neuron is a real function of the input vector $(y_1, \dots, y_k)$. The output is obtained as;

$$f(x_j) = f(\alpha_j + \sum_{i=1}^{k} w_{ij}\, y_j) \qquad 2.4$$

Where;
y_j – variable input

w_{ij} - sapic weight between i and j

α_j - acceleration cost

Where; *f* is a function, typically the sigmoid (logistic or tangent hyperbolic) function.

A graphical presentation of neuron is given in Figure 2.11. Mathematically, a Multi-Layer Perceptron network is a function consisting of compositions of weighted sums of the functions corresponding to the neurons.

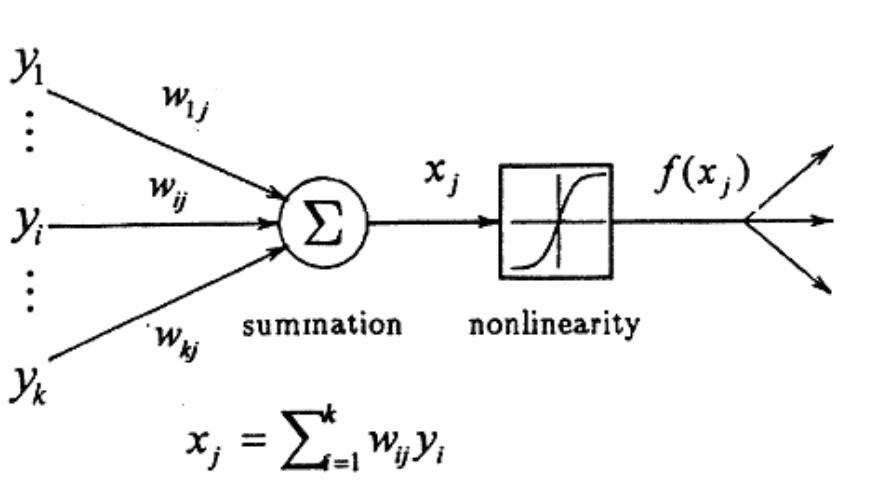

Figure 2.15: Single Neuron

2.14.3 Neural Networks Architectures

An ANN is defined as a data processing system consisting of a large number of simple highly inter connected processing elements (artificial neurons) in an architecture inspired by the structure of the cerebral cortex of the brain. There are several types of architecture of NNs. However, the two most widely used NNs are the Feed forward networks and the Recurrent networks.

In a feed forward network, information flows in one direction along connecting pathways, from the input layer via the hidden layers to the final output layer. There is no feedback (loops) i.e., the output of any layer does not affect that same or preceding layer.

Recurrent networks differ from feed forward network architectures in the sense that there is at least one feedback loop. Thus, in these networks, for example, there could exist one layer with feedback connections. There could also be neurons with self-feedback links, i.e. the output of a neuron is fed back into itself as input.

2.14.4 Learning/Training Strategies

The basic concept behind the successful application of neural networks in any field is to determine the weights to achieve the desired target and this process is called learning or training. The three different learning mechanisms usually employed are supervised and unsupervised learning (Tarafdar, Haque and Kashtiban, 2005).

Supervised Learning

In the case of supervised learning the network weights are modified with the prime objective of minimization of the error between a given set of inputs and their corresponding target values. Hence, the training data-set is known which is a set of inputs and the corresponding targets the neural network should output ideally. This is called supervised learning because both the inputs and the expected target values are known prior to the training of ANN.

Unsupervised Learning

On the other hand, in the case of unsupervised learning, we are unaware of the relationship between the inputs and the target values. We train the neural network with a training data set in which only the input values are known. Hence, it is very important to choose the right set of examples for efficient training. These examples are usually chosen using some sort of a similarity principle. The most commonly used unsupervised learning algorithms are the Self-Organizing Map (SOM) and the Adaptive Resonance Theory (ART).

Reinforced learning

In this method, a teacher though available, does not present the expected answer but only indicates if the computed output is correct or incorrect. The information provided helps the network in its learning process. A reward is given for a correct answer computed and a penalty for a wrong answer. But, reinforced learning is not one of the popular forms of learning.

The learning strategy employed depends on the structure of the neural network. Feed-forward networks are trained using the supervised learning strategy. The supervised learning strategy for a feed-forward neural network has been shown in the Fig. 2.17.

The set of input-output pairs (shown in Fig. 2.16) that are used to train the neural network are obtained prior to the training process either by using physical measurements or by performing some kind of simulations. Fig. 2.16 shows that the teacher teaches the neural network to modify its weights according to the error ‘e’ between the outputs and the targets. The weights of the neural network are then modified iteratively according to (2.5). The general idea behind supervised learning and the mathematics involved has been adopted from.

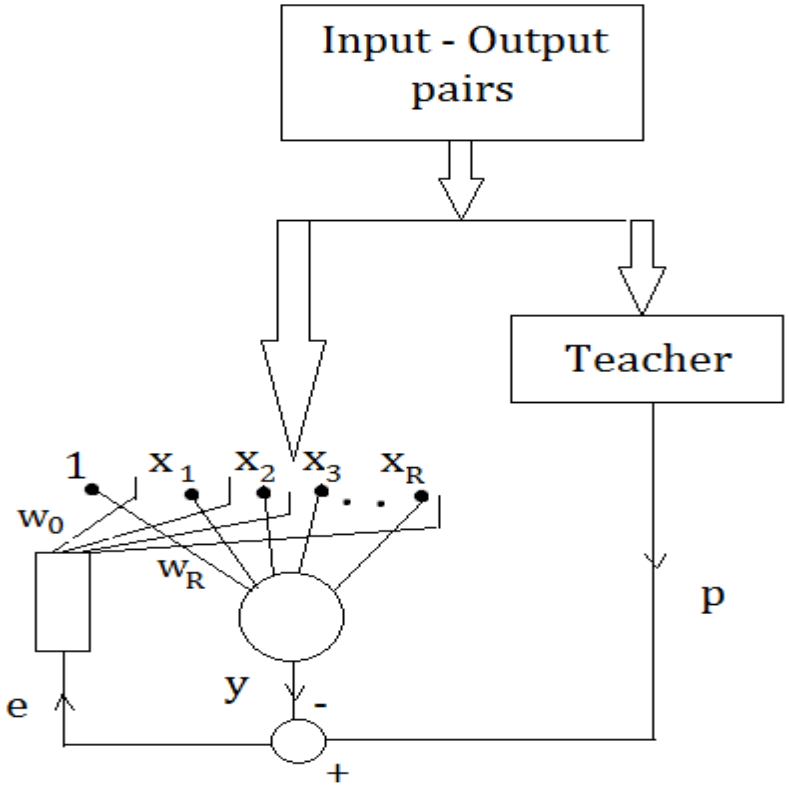

Figure 2.16: Scheme of supervised learning.

$$w_{ji}(n+1) = w_{ji}(n) + \Delta w_{ji}(n) \qquad 2.5$$

Where: $w_{ji}(n)$ and $w_{ji}(n+1)$ are the previous and the modified weights connected between the ith and the jth adjoining layers respectively. $\Delta w_{ji}(n)$stands for the correction or modification factor and n stands for the number of the iteration. If we consider the jth neuron in a single layer neural network, the training efficiency is enhanced by minimizing the error between the actual output of the jth neuron and the output that has been dictated by the teacher. Let $y_j(n)$ and $p_j(n)$be the actual and the teacher-requested outputs for the jth neuron in the nth iteration. Then the error value of that iteration is given by (2.6).

$$e_j(n) = p_j(n) - y_j(n) \qquad 2.6$$

The vector e(n) that stores the values of all the errors is also a function of the weights w(n) for the corresponding layers' inputs. The value by which the weighing coefficients change (also called the correction factor) is given by the following (2.7).

$$\Delta w_{ji}(n) = \eta e_j(n) x_i(n) \qquad 2.7$$

Where: x_i is the ith input signal and η is the rate at which the learning process takes place. As mentioned earlier, learning process aims at the minimization of the error function. The same criterion can also be achieved by the usage of a Least Squares Method (LSM). Hence, if there are L neurons in a particular network, the cost function to be ultimately minimized is given by (2.8).

$$S_2(w) = \frac{1}{2}\sum_{j=1}^{L}(p_j - y_j)^2 \qquad 2.8$$

If the number of learning pairs with an input vector x(n) and an output vector d(n) of the form (x(n), d(n)) are P in the training set, then during the nth iteration of the learning process, we have:

$$S_2\big(w(n)\big) = \frac{1}{2}\sum_{n=1}^{p}\sum_{j=1}^{L}(p_j(n) - y_j(n))^2 \qquad 2.9$$

Since the activation functions that are employed are more often non-linear, minimization of the above (2.9) is a non-linear problem. Several numerical methods that can handle non-linear functions effectively are available and are based on the steepest-decent method. The steepest-decent method is an extension to the Laplace's method of integral approximation where the contour integral in a complex plane is deformed to approach a stationary point in the direction of the steepest decent. The back-error-propagation learning technique is based on the steepest-decent method and is usually widely applied in a version known as the Levenberg-Marquardt algorithm (Vasilic, and Kezunovic, 2004).

The back-error-propagation algorithm chooses random weights for the neural network nodes, feeds in an input pair and obtains the result. Then, the error for each node is calculated starting from the last stage and by propagating the error backwards. Once this is done, the weights are updated and the process is repeated with the entire set of input output pairs available in the training data set. This process is continued till the network converges with respect to the desired targets. The back-error-propagation technique is widely used for several purposes including its application to error functions (other than the sum of squared errors) and for the evaluation of Jacobian and Hessian matrices. The correction values are calculated as functions of errors estimated from the minimization of (2.9). This process is carried out layer by layer throughout the network in the backward direction. This algorithm is pictorially depicted in Fig 2.17.

The corresponding weighing vectors are shown in blocks $\mathbf{A^{(M)}}, \mathbf{A^{(M-1)}}, \ldots, \mathbf{A^{(1)}}$ and the errors that are propagated to the lower layers are calculated and stored in the blocks $\mathbf{B^{(M-1)}}, \mathbf{B^{(M-2)}}, \ldots, \mathbf{B^{(2)}}$. The back-error-propagation algorithm has been implemented in many ways but the basic idea remains the same. The only thing that changes in each of these implementations is the method used for the calculation of the weights that are iteratively upgraded when passed backward from layer to layer in the neural network.

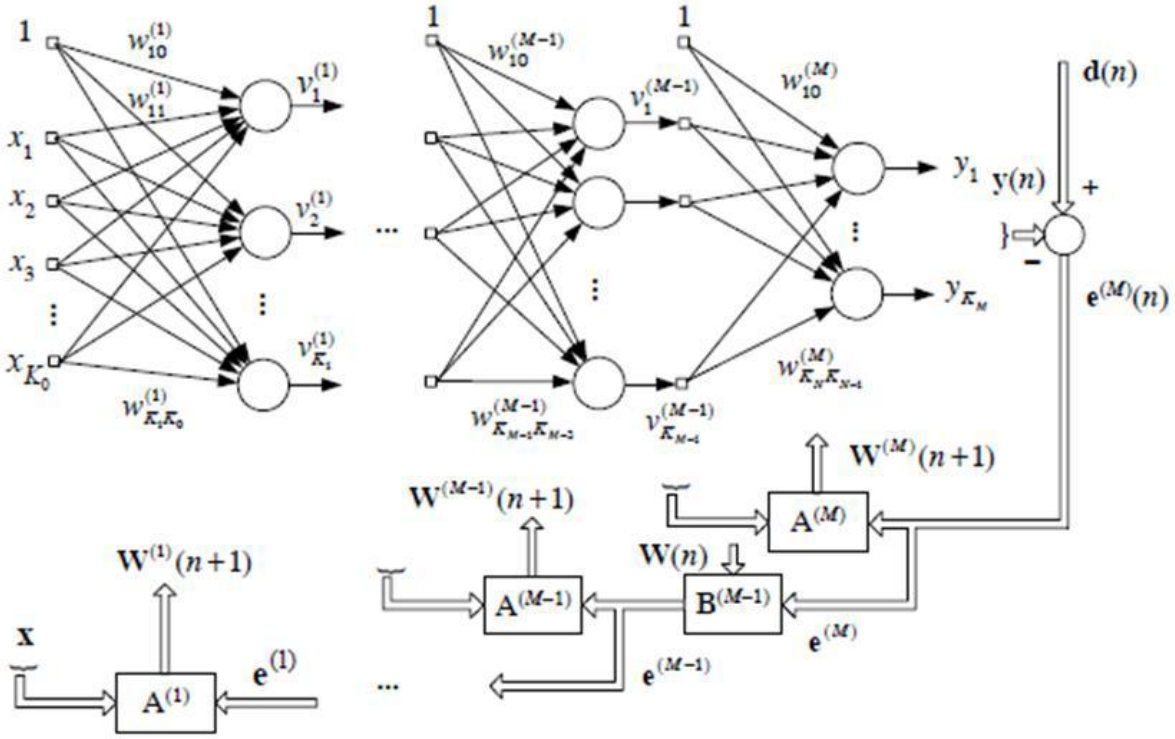

Figure 2.17: Structure of back-error-propagation algorithm [adopted from Vasilic, and Kezunovic, (2004)]

The modifications involved are also used in the training process of recurrent networks. The rate at which the learning process takes place can be estimated by keeping a check on the correction values in successive stages. The total number of iterations required to achieve satisfactory convergence rate depends on the following factors:

- Size of the neural network
- Structure of the network
- The problem being investigated
- The learning strategy employed
- Size of the training/learning set

The efficiency of a chosen ANN and the learning strategy employed can be estimated by using the trained network on some test cases with known output values. This test set is also a part of the learning set. Hence, the entire set of data consists of the training data set along with the testing data set. The former is used to train the neural network and the latter is used to evaluate the performance of the trained artificial neural network.

2.14.5 Types of Neural Networks

The most important class of neural networks for real world problems solving includes

- Multilayer Perceptron
- Radial Basis Function Networks
- Kohonen Self Organizing Feature Maps

2.14.6 Multilayer Perceptrons

The most popular form of neural network architecture is the multilayer perceptron (MLP). A multilayer perceptron:

- has any number of inputs.
- has one or more hidden layers with any number of units.
- uses linear combination functions in the input layers.
- uses generally sigmoid activation functions in the hidden layers.
- has any number of outputs with any activation function.
- has connections between the input layer and the first hidden layer, between the hidden layers, and between the last hidden layer and the output layer.

Given enough data, enough hidden units, and enough training time, an MLP with just one hidden layer can learn to approximate virtually any function to any degree of accuracy. (A statistical analogy is approximating a function with *n*th order polynomials.) For this reason, MLPs are known as universal approximators and can be used when there is little prior knowledge of the relationship between inputs and targets. Although one hidden layer is always sufficient provided there are enough data, there are situations where a network with two or more hidden layers may require fewer hidden units and weights than a network with one hidden layer, so using extra hidden layers sometimes can improve generalization (Vasilic and Kezunovic, 2004).

2.14.7 Radial Basis Function Networks

Radial basis functions (RBF) networks are also feed forward, but have only one hidden layer. An RBF network:

- has any number of inputs.
- typically has only one hidden layer with any number of units.
- uses radial combination functions in the hidden layer, based on the squared Euclidean distance between the input vector and the weight vector.
- typically uses exponential or softmax activation functions in the hidden layer, in which case the network is a Gaussian RBF network.
- has any number of outputs with any activation function.
- has connections between the input layer and the hidden layer, and between the hidden layer and the output layer.

MLPs are said to be distributed-processing networks because the effect of a hidden unit can be distributed over the entire input space. On the other hand, Gaussian RBF networks are said to be local-processing networks because the effect of a hidden unit is usually concentrated in a local area centered at the weight vector.

2.14.8 Kohonen Neural Network

Self-Organizing Feature Map (SOFM, or Kohonen) networks are used quite differently to the other networks. Whereas all the other networks are designed for supervised learning tasks, SOFM networks are designed primarily for unsupervised learning. At first glance this may seem strange. Without outputs, what can the network learn? The answer is that the SOFM network attempts to learn the structure of the data (Vasilic and Kezunovic, 2004). One possible use is therefore in exploratory data analysis. A second possible use is in novelty detection.

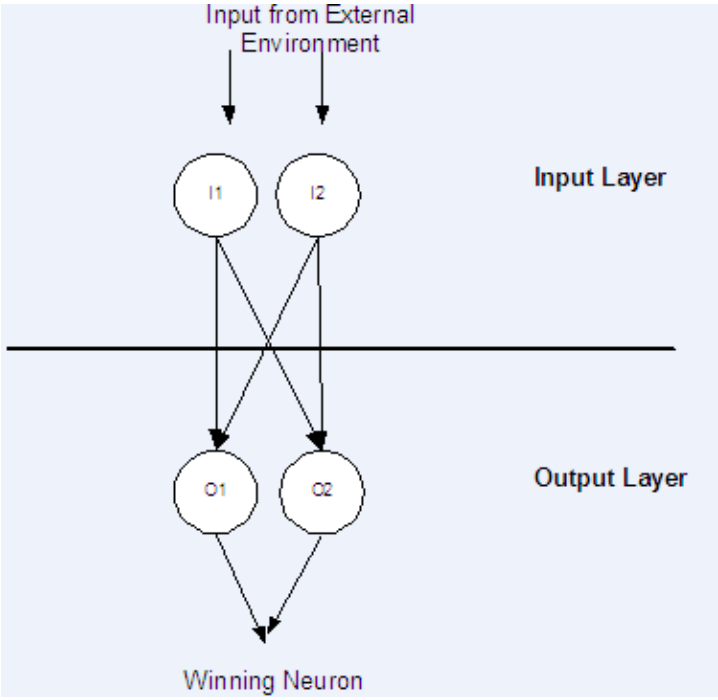

Figure 2.18: A Kohonen Neural Network Applications

SOFM networks can learn to recognize clusters in the training data, and respond to it. If new data, unlike previous cases, is encountered, the network fails to recognize it and this indicates novelty. A SOFM network has only two layers: the input layer, and an output layer of radial units (also known as the topological map layer).

Neural networks have proven to be effective mapping tools for a wide variety of problems and consequently they have been used extensively by practitioners in almost every application domain ranging from agriculture to zoology. Since neural networks are best at identifying patterns or trends in data, they are well suited for prediction or forecasting applications. A very small sample of applications has been indicated in the next paragraph. Anderson, 2003 developed neural network model for forecasting financial and economic time series.

2.15 Application of ANN Power System Stability Improvement

If the relationship between system operating conditions and system stability is reached, by training neural network, the network model should be used to assess online transient stability. For on-line transient stability assessment, CCT is chosen as an accurate indicator of transient stability margin. The fast calculation of CCT is also necessary for on-line stability assessment. Application of Artificial Neural Network (ANN) to the above-mentioned problem has attained increasing importance mainly due to the efficiency of present day computers. Moreover, real-time use of conventional methods in an energy management center can be difficult due to their significant large computational times. One of the main features, which can be attributed to ANN, is its ability to learn nonlinear problem offline with selective training, which can lead to sufficiently accurate online response (Zhou, Huang, Xu, Hua, Yang and Liu 2015). The ability of

ANN to understand and properly classify such a problem of highly non-linear relationship has been established in most of the papers and the significant consideration is that once trained effectively ANN can classify new data much faster than it would be possible with analytical model.

The neurons are assumed to be arranged in layers, and the neurons in the same layer behave in the same manner. All the neurons in a layer usually have the same activation function. The neuron in one layer can be connected to neuron in another layer. The arrangement of neurons into layers and the connection pattern within and between layers is known as network architecture The architecture of a developed network consists of input layer, one hidden layer, and one output layer. Time domain simulation method is used in this work to assess the transient stability of the power system because it is the most reliable, mature and accurate method compared to other method. The differential equations to be solved in transient stability analysis are non-linear ordinary equations with known initial values.

2.16 Control of VSC-HVDC Transmissions

2.16.1 Topology of ANN based controller

The ANN controller has two inputs, one hidden layer and one output neuron; which is the simplest architecture version since it consists of a single hidden layer. The input layer simply acts as a fan-out input to the hidden layer where two neurons are used. The outputs are transformed through a sigmoidal activation function and fed to the output layer through their weights. The output layer has only one neuron with a sigmodal activation function. The input to the suggested

ANN controller (Fig. 3.7) is the reference current I_{ref} and measured dc current I_{dc} and its output is the converter's thyristor firing angle.

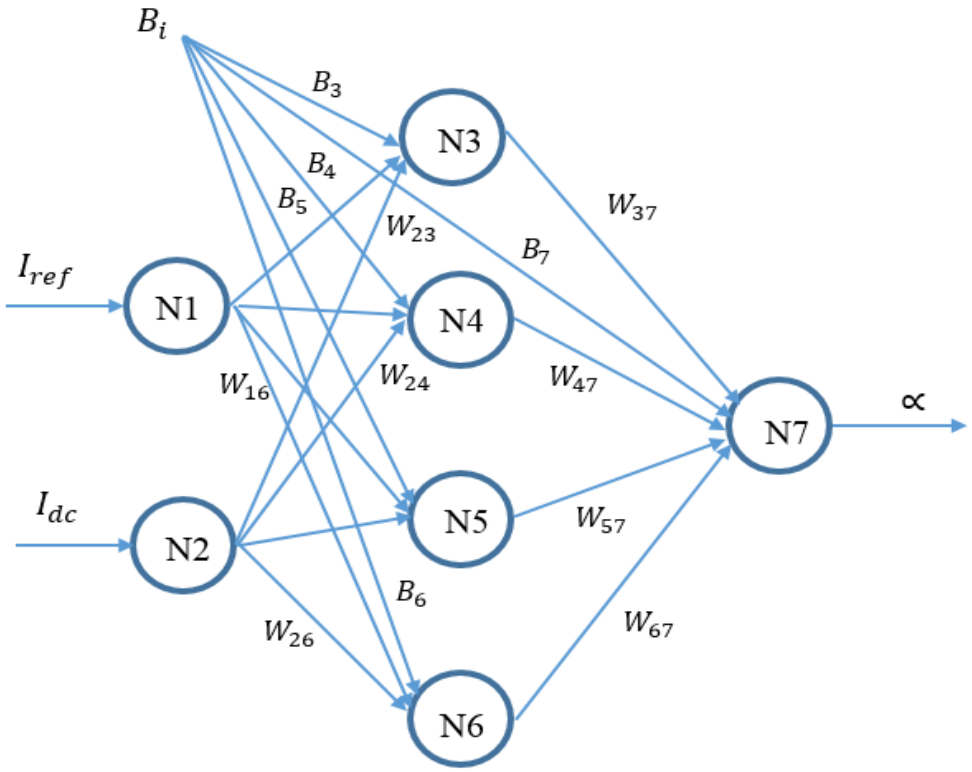

Figure 2.19: The typical Gaussian basis function neural network

The error between I_{dc} and I_{ref} is used to adjust the weight of the ANN according to the delta rule. The speed of the controller and the system stability will depend on the learning rate η and the momentum μ used in adjusting the weights of the ANN.

The proposed ANN controller consists of the following three layers.

1. **Input layer:** In this layer, they are only two neurons, one of them is fed with a constant reference current I_{ref} and the other neuron is I_{dc}.
2. **Hidden layer:** In this layer, there are (N) neurons. These are connected to the outputs of the input layer by weights V_i,B_i, where i =1,…,N. The outputs of these

neurons are acted upon by the sigmoid function. The (N) outputs of the neurons in the hidden layer are fed to the output layer through the weight W_i.

3. **Output layer:** This layer consists of one neuron only: the inputs to this neuron are the outputs OUTi from the hidden layer and the bias from the input layer. The weights and bias associated with these inputs are Wi and Bi, respectively. The database that used for training neural network desired current (I_{ref}) and actual current (I_{dc}) as input, Tan-sigmoidal activation function for hidden neurons, linear activation function for output neuron, number of iteration is 140 epoch, goal (error) 1e-5 and the neural network output represents the triggering angle that applied on rectifier unit.

2.17 Model of a Neuron

A basic neuron model as shown in Fig 2.20 can be described by a function that calculates the output as a function of a number of inputs to it. The basic idea behind the entire neuron model, including the activation functions illustrated below, has been adopted from (Anderson, 2003).

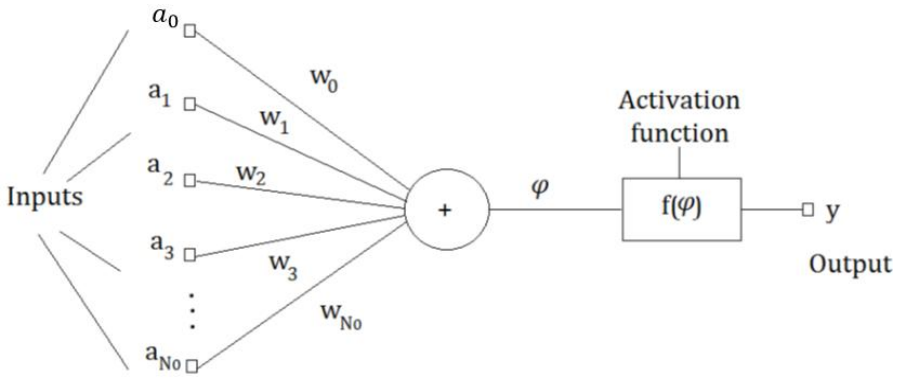

Figure 2.20: Mathematical Model of a Neuron.

The output of the neuron is given by

$$f(\varphi) = f(\sum_{i=0}^{N_0} w_i a_i) \quad 2.10$$

Where: $w_0 a_0$ is the threshold value (polarization), f(φ) is the neuron activation function, φ is the summation output signal and y is the neuron output.

$$\varphi = \boldsymbol{W^T A} \quad 2.11$$

Where: $$\boldsymbol{W} = [w_0 w_1 \ldots w_{N_0}], \ \boldsymbol{A} = [a_0 a_1 \ldots a_{N_0}]^{\boldsymbol{T}} \quad 2.12$$

The activation function acts as a squashing function, such that the output of a neuron in a neural network is between certain values (usually 0 and 1, or -1 and 1). An activation function decides how powerful the output from the neuron should be, based on the sum of its inputs. Depending upon the application's requirements, the most appropriate activation function is chosen. The activation function f (φ) can be in different forms. A few of which are illustrated below:

- **Threshold (or Step) Function**

This takes on a value of 0 if the summed input is less than a certain threshold value (φ), and the value 1 if the summed input is greater than or equal to the threshold value.

$$f(\varphi) = \begin{cases} 1, & \text{if } \varphi \geq 0 \\ 0, & \text{if } \varphi < 0 \end{cases}$$

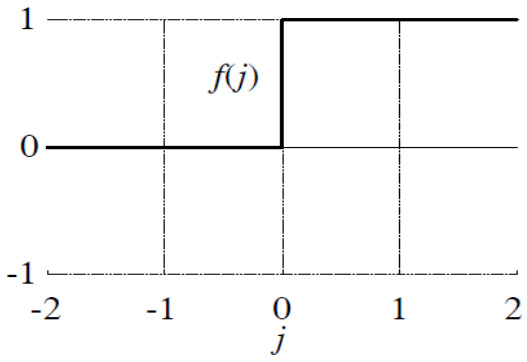

Figure 2.21: Step activation function

- **Piece wise linear function**

This function again can take on the values of 0 or -1, but can also take on values between that depending on the amplification factor in a certain region of linear operation.

$$f(\varphi) = \begin{cases} 1, & \text{for } \varphi > 1 \\ -1, & \text{for } \varphi < -1 \\ \varphi, & \text{for } -1 < \varphi < 1 \end{cases}$$

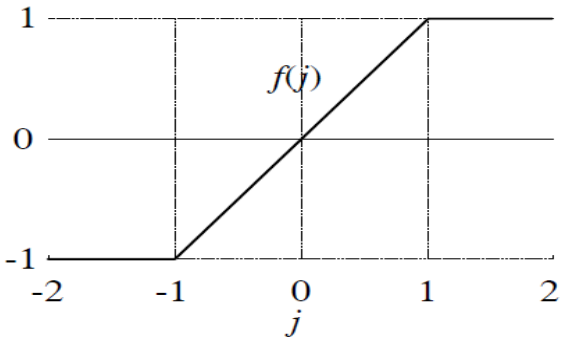

Figure 2.22: Piece wise linear activation function.

- **Sigmoid bipolar function**

This function can range between 0 and 1, but it is also sometimes useful to use the -1 to 1 range. An example of the sigmoid function is the hyperbolic tangent function

$$f(\varphi) = \tanh(\beta\varphi) = \frac{1 - e^{-2\beta\varphi}}{1 + e^{-2\beta\varphi}}$$

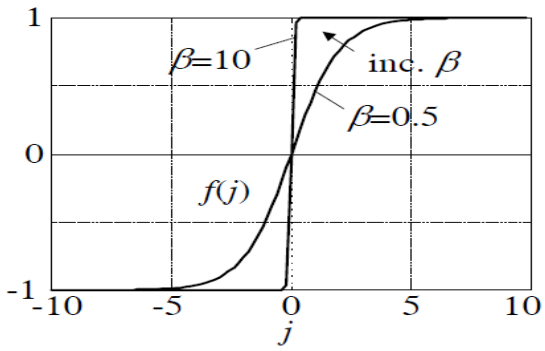

Figure 2.23: Bipolar activation function.

- **Sigmoid unipolar function**

This function can range between 0 and 1 and in this work the Sigmoid activation function has been used since the emphasis is that the neural network output should be 0 or 1 (no or yes).

$$f(\varphi) = \frac{1}{1+e^{-\beta\varphi}}$$

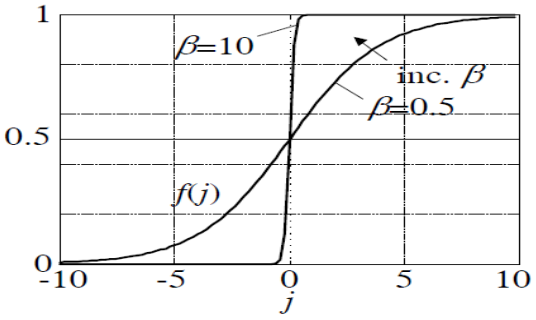

Figure 2.24: Sigmoid unipolar activation function.

Based on the way the neurons are interconnected in a model, neural networks can be broadly classified into two types namely feed-forward and feed-back networks. As the name suggests, feedback networks unlike feed-forward networks have a feedback connection fed back into the network along with the inputs. Due to their simplicity and the existence of a well-defined learning algorithm, only feed-forward networks have been used in this dissertation for the simulation and hence the application is presented in the upcoming sections.

2.17.1 The Feed-forward Networks

Feed-forward networks are the simplest neural networks where there is no feedback connection involved in the network and hence the information travel is unidirectional (El-Sharkawi, Niebur, 1996). A feed-forward network with $a_{\mathrm{N}0}$ input and y_{NR} output signals is shown in Fig 3.14. The computation process in the ith layer can be described by the following (2.13)

$$\boldsymbol{p}^{(i)} = f^{(i)}\left(\boldsymbol{w}^{(i)}\boldsymbol{g}^{(i-1)}\right) \qquad 2.13$$

Where $\boldsymbol{p}^{(i)} = \left[p_1^{(i)} p_2^{(i)} p_3^{(i)} \ \ldots \ p_{N_i}^{(i)}\right]^{\boldsymbol{T}}$ is the fault signal vector at the output of the *i*th layer.

And $\boldsymbol{W}^{(i)} = \begin{pmatrix} w_{10}^{(i)} & w_{11}^{(i)} & \ldots & w_{1N_{i-1}}^{(i)} \\ w_{20}^{(i)} & w_{21}^{(i)} & \ldots & w_{2N_{i-1}}^{(i)} \\ \vdots & \vdots & \ddots & \vdots \\ w_{N_i 0}^{(i)} & w_{N_i 1}^{(i)} & \ldots & w_{N_i N_{i-1}}^{(i)} \end{pmatrix}$ is the weighing matrix between the (*i*-1)th and the *i*th layer.

$$\boldsymbol{g}^{(i-1)} = \begin{cases} A & for\ i = 1 \\ \begin{bmatrix} 1 \\ \boldsymbol{p}^{(i-1)} \end{bmatrix} & for\ i = 2,3,\ldots,R \end{cases} \qquad 2.14$$

A is the vector containing the input signals, $\boldsymbol{f}^{(i)}$ is the activation function of the neurons in the *i*th layer and *p* is the number of processing layers. All the neurons in a particular layer are assumed to be similar in all aspects and the number of hidden layers can be more than one and is usually determined by the purpose of the neural network. The output of the processed neural network is represented by the output vector:

$$\boldsymbol{y} = \boldsymbol{p}^{(\boldsymbol{R})} = [\mathrm{y}_1 \mathrm{y}_2 \mathrm{y}_3 \ \ldots \mathrm{y}_{\mathrm{N_R}}]^T \qquad 2.15$$

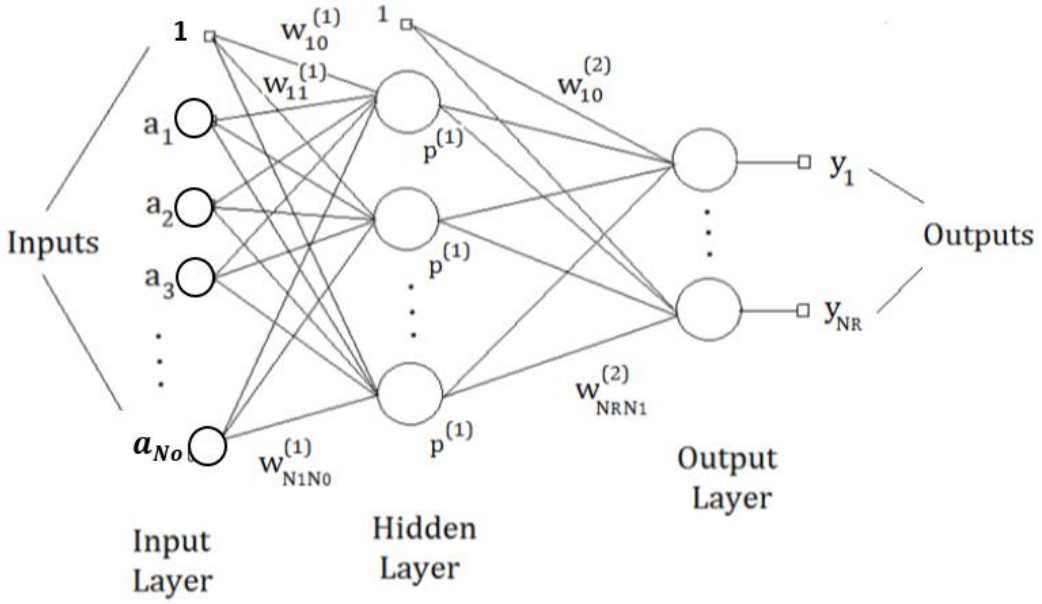

Figure 2.25: Structure of a two-layered feed-forward network.

2.17.2 The Training Process for the HVDC Neural Network Controller

Two important steps in the application of neural networks for any purpose are training and testing. The first of the two steps namely training of the chosen neural networks is dealt with in this section. Training is the process by which the neural network learns from the inputs and updates its weights accordingly. In order to train the neural network, a set of data called the training data-set is needed which is a set of input output pairs fed into the neural network.

Thereby, the neural network is taught what the output should be, when that particular input is fed into it. The ANN slowly learns the training set and slowly develops an ability to generalize upon this data and will eventually be able to produce an output when a new data is provided to it. During the training process, the neural network's weights are updated with the prime goal of minimizing the performance function. This performance function can be user defined, but usually

feed-forward networks employ Mean Square Error as the performance function and the same is adopted throughout this work.

As aforementioned, The input to the suggested ANN controller is the current reference I_{ref} and measured dc current I_{dc} and its output is the firing angle. The error between I_{dc} and I_{ref} is used to adjust the weight of the ANN according to the delta rule. The speed of the controller and the system stability will depend on the learning rate η and the momentum μ used in adjusting the weights of the ANN.

2.18 HVDC Control and Protection

The rectifier is equipped with a current controller to maintain the HVDC system current constant. The HVDC system current at the rectifier end is measured with the proper transducer and pass through the appropriate filters. After filtering, the measured current is compared to the reference current to produce the error signal. The error signal from the rectifier side, then passes through the conventional PI controller to produce firing angle order. The firing circuit which is synchronized with the AC system through phase locked loop uses the firing angle order to produce the necessary equidistant pulses for the rectifier valves.

Similarly, the inverter is provided with a current controller to maintain the HVDC system current constant and a gamma controller for maintaining a constant extinction angle. The HVDC system current at the inverter end is measured with the proper transducer and pass through the appropriate filters. After filtering, the measured current is compared to the reference current to produce an error signal. The error signal from the inverter side, then passes through the conventional PI controller to produce firing angle order. For gamma controller the gamma value is measured using zero crossing information from the commutation bus voltages and the valve

switching times. The gamma error is applied to another conventional PI controller, which produce the firing angle order for the inverter. The firing angle orders of the current and gamma controller are compared and the minimum is used to produce the firing pulses for the inerter valves.

The reference current for the current controllers are obtained from the master controller output through the voltage dependent current order limiter (VDCOL) which can reduce the reference value of direct current (I_{dref}) in case of the large decline in direct voltage, so as to suppress the over current and maintain the system voltage. In normal state, there is asmall margin(I_{dmarg}) between the direct current references of the two current controllers. Since I_{dref} f of inverter will be smaller than I_{dref} of rectifier, the output of the current controller configured in the inverter side will be regulated to its maximum, and thus the current controller will not be selected among the two controllers (current and gamma). Therefore, the gamma controller will decide the inverter's firing angle.

HVDC protection functions are implemented to protect the rectifier and the inverter. The HVDC fault protection circuit at the rectifier detects and force the delay angle into the inverter region so as to quench the fault current. The commutation failure prevention, control circuit of the inverter detects various AC faults and reduces the utmost delay angle limit in order to decrease the risk of commutation failure. The low AC voltage detection circuit at the rectifier and the inverter serves to categorize between an AC fault and a DC fault.

2.19 HVDC-VSC Power Flow Model

The HVDC was considered to consist of two VSC stations, one operating as a rectifier and the other as an inverter. The two converters are connected either back-to-back (B-T-B) or joined

together by a DC cable, depending on the application. For the purpose of fundamental frequency analysis, each converter station was represented by a complex voltage source behind the transformer's reactance (impedance Z) linked together by active power constraint equation. Hence, a schematic representation and equivalent circuit shown in Figures3.15 and 3.16 are used to derive the mathematical model of the HVDC-VSC in rectangular form for inclusion in the power flow Newton-Raphson method. The complex voltage sources representing the two VSC stations in the HVDC-VSC link are:

$$V_{VR1} = |V_{VR1}|\angle\delta_{VR1} = |V_{VR1}|(\cos\delta_{VR1} + j\sin\delta_{VR1}) = e_{VR1} + jf_{VR1} \quad 2.16$$

$$V_{VR2} = |V_{VR2}|\angle\delta_{VR2} = |V_{VR2}|(\cos\delta_{VR2} + j\sin\delta_{VR2}) = e_{VR2} + jf_{VR2} \quad 2.17$$

The voltage sources have the following voltage magnitudes and phase angle limits:

$$0 \le V_{VR1} \le V_{VR1max}\,; 0 \le \delta_{VR1} \le 2\pi; 0 \le V_{VR2} \le V_{VR2max}\,; 0 \le \delta_{VR2} \le 2\pi$$

The constraining power equation for the back-to-back HVDC-VSC, i.e.$R_{DC} = 0$ is given by

$$Re\{V_{VR1}I_{VR1}^* + V_{VR2}I_{VR2}^* + P_{DC,loss}\} = 0 \quad 2.18$$

and for the case when both VSC stations are linked by a DC cable, i.e.$R_{DC} > 0$, then

$$Re\{V_{VR1}I_{VR1}^* + V_{VR2}I_{VR2}^*\} = 0 \quad 2.19$$

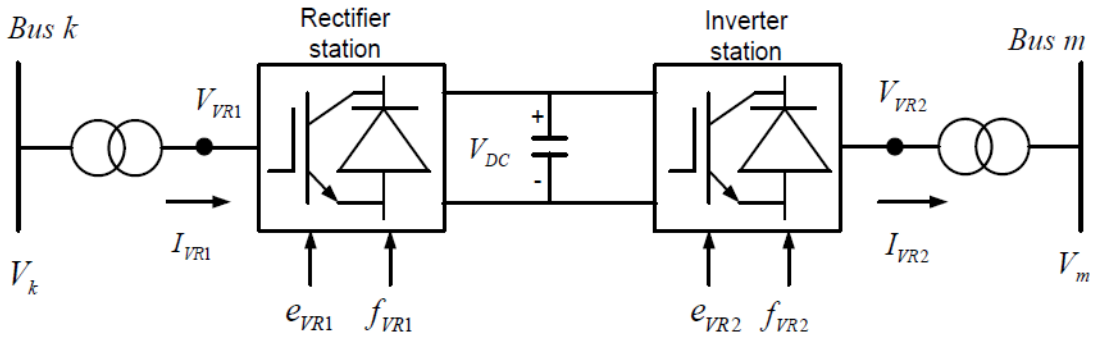

Figure 2.26: HVDC based VSC system (Nnachi, Munda, Nicolae and Mabwe, 2013)

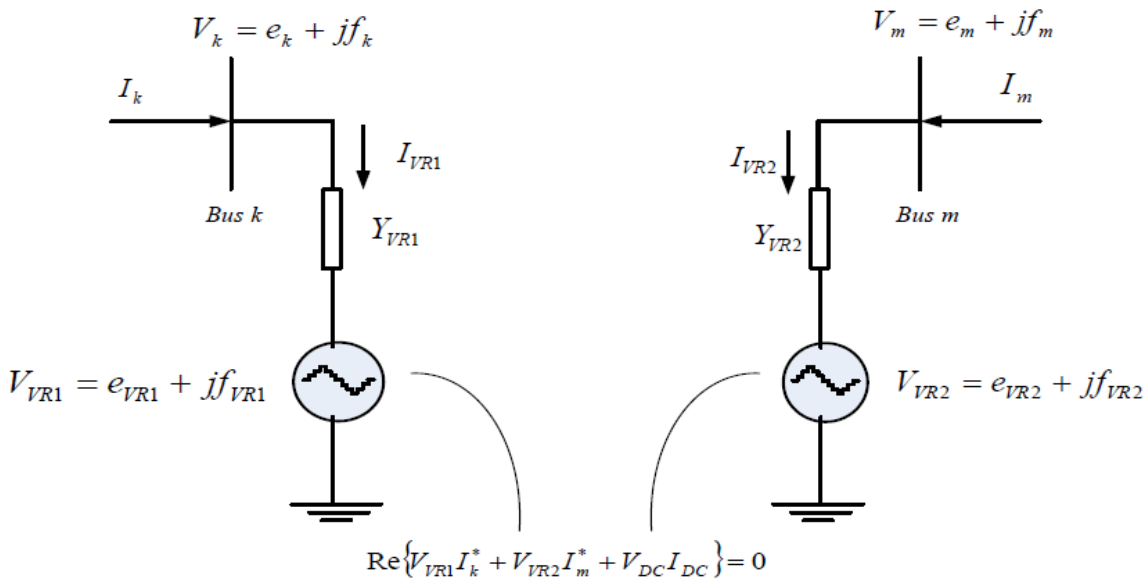

Figure 2.27: HVDC based VSC equivalent circuit (Nnachi, Munda, Nicolae and Mabwe, 2013)

The power flows from the station connected at bus k (rectifier) to the station connected at bus m (inverter), the power injected at bus *k* are

$$P_k = G_{VR1}\{e_k^2 + f_k^2 - (e_{VR1} + f_{VR1})\} + B_{VR1}(f_{VR1}e_k + e_{VR1}f_k) \quad 2.20$$

$$Q_k = G_{VR1}(f_{VR1}e_k + e_{VR1}f_k) + B_{VR1}\{-(e_k^2 + f_k^2) + e_{VR1}e_k + f_{VR1}f_k\} \quad 2.21$$

The power flows into the rectifier are described by the following equations:

$$P_{VR1} = -G_{VR1}\{-(e_{VR1}^2 + f_{VR1}^2) + e_{VR1}e_k + f_{VR1}f_k\} + B_{VR1}(e_{VR1}f_k - f_{VR1}e_k) \quad 2.22$$

$$Q_{VR1} = G_{VR1}(e_{VR1}f_k - f_{VR1}e_k) + B_{VR1}\{-(e_{VR1}^2 + f_{VR1}^2) + e_{VR1}e_k + f_{VR1}f_k\} \quad 2.23$$

The power equations for the node *m* and for the inverter are simply obtained by exchanging the subscripts k and $V_{VR1}$for m and V_{VR2}, respectively. In case of full HVDC-VSC, the relevant power equation is:

$$P_{HVDC} = P_{VR1} + P_{VR2} + P_{DC} = 0 \quad 2.24$$

2.19.1 Linearized System (HVDC-VSC) of Equations

A Newton power flow algorithm with simultaneous solution of power flow constraints and power flow control constraints of the HVDC-VSC may be represented by

$$[f(X)] = [J][\Delta X] \tag{2.25}$$

Where

$$[f(X)] = [\Delta P_k \Delta Q_k \Delta P_m \Delta Q_m \Delta P_{VR1} \Delta Q_{VR1} \Delta P_{HVDC} \Delta |V_m|^2]^T$$

$$[\Delta X] = [\Delta e_k \Delta f_k \Delta e_m \Delta f_m \Delta e_{VR1} \Delta f_{VR1} \Delta e_{VR2} \Delta f_{VR2}]^T$$

$$[J] = \begin{bmatrix} \frac{\partial P_k}{\partial e_k} & \frac{\partial P_k}{\partial f_k} & \frac{\partial P_k}{\partial e_m} & \frac{\partial P_k}{\partial f_m} & \frac{\partial P_k}{\partial e_{VR1}} & \frac{\partial P_k}{\partial f_{VR1}} & 0 & 0 \\ \frac{\partial Q_k}{\partial e_k} & \frac{\partial Q_k}{\partial f_k} & \frac{\partial Q_k}{\partial e_m} & \frac{\partial Q_k}{\partial f_m} & \frac{\partial Q_k}{\partial e_{VR1}} & \frac{\partial Q_k}{\partial f_{VR1}} & 0 & 0 \\ \frac{\partial P_m}{\partial e_k} & \frac{\partial P_m}{\partial f_k} & \frac{\partial P_m}{\partial e_m} & \frac{\partial P_m}{\partial f_m} & 0 & 0 & \frac{\partial P_m}{\partial e_{VR2}} & \frac{\partial P_m}{\partial f_{VR2}} \\ \frac{\partial Q_m}{\partial e_k} & \frac{\partial Q_m}{\partial f_k} & \frac{\partial Q_m}{\partial e_m} & \frac{\partial Q_m}{\partial f_m} & 0 & 0 & \frac{\partial Q_m}{\partial e_{VR2}} & \frac{\partial Q_m}{\partial f_{VR2}} \\ \frac{\partial P_{VR1}}{\partial e_k} & \frac{\partial P_{VR1}}{\partial f_k} & \frac{\partial P_{VR1}}{\partial e_m} & \frac{\partial P_{VR1}}{\partial f_m} & \frac{\partial P_{VR1}}{\partial e_{VR1}} & \frac{\partial P_{VR1}}{\partial f_{VR1}} & 0 & 0 \\ \frac{\partial Q_{VR1}}{\partial e_k} & \frac{\partial Q_{VR1}}{\partial f_k} & \frac{\partial Q_{VR1}}{\partial e_m} & \frac{\partial Q_{VR1}}{\partial f_m} & \frac{\partial Q_{VR1}}{\partial e_{VR1}} & \frac{\partial Q_{VR1}}{\partial f_{VR1}} & 0 & 0 \\ \frac{\partial P_{HVDC}}{\partial e_k} & \frac{\partial P_{HV\,DC}}{\partial f_k} & \frac{\partial P_{HVDC}}{\partial e_m} & \frac{\partial P_{HVDC}}{\partial f_m} & \frac{\partial P_{HVDC}}{\partial e_{VR1}} & \frac{\partial P_{HVDC}}{\partial f_{VR1}} & \frac{\partial P_{HVDC}}{\partial e_{VR2}} & \frac{\partial P_{HVDC}}{\partial f_{VR2}} \\ 0 & 0 & \frac{\partial |V_m|^2}{\partial e_m} & \frac{\partial |V_m|^2}{\partial f_m} & 0 & 0 & 0 & 0 \end{bmatrix} \tag{2.26}$$

2.20 Summary of Related Literature Review

A lot of works done by other authors as regards to transient stability improvement of power transmission network using FACTS devices such as UPFC, STATCOM, HVDC etc. have been exhaustively reviewed. The review showed that VSC-HVDC modulation could lead to substantial improvement in transient stability. But it could be noted that the critical clearing times

CCT obtained in past works were substantial and therefore there are still room for further improvement. Hence, in this work efforts would be made to reduce the CCT of fault. Another limitation of some past works is that they have used the conventional PI controller which is not smart enough compared to the intelligent controller proposed in this work.

Another issue/gap observed, is that the VSC-HVDC design was not implemented on any 330kV transmission network by some works and secondly the authors failed to demonstrate the performance of their VSC HVDC model on any practical transmission network. Also, their proposed method of enhancing the rotor angle stability was not applied or implemented on a multi-generator power transmission network like Nigerian 330kV grid. Hence, in this work the Nigerian 330kV transmission network will be used for the implementations.

All this will be achieved in this dissertation by modelling an ANN based VSC-HVDC link and incorporating same in the Nigerian 330kV grid for implementation of transient stability improvement of the network through the help of CCTs of the generators, within the network, when subjected to a balanced three-phase fault. This, unfortunately, has not been done by none of the authors whose works have been reviewed above.

CHAPTER THREE

RESEARCH METHODOLOGY

3.1 Methodology

MATLAB/PSAT software was employed as the tool for the simulations. The existing Nigerian 330kV transmission system was modeled in PSAT environment and the system load flow was performed. The eigenvalue analysis of the system buses was performed to determine the critical buses. A balanced three-phase fault was then applied to some of these critical buses and lines of the transmission network to establish the existing/current transient stability situation of the grid through the observation of the dynamic responses of the generators in the Nigeria 330-kV grid/network when the fault was applied. To this effect, VSC-HVDC was installed along to those critical lines. The inverter and the converter parameters of the HVDC were controlled by the conventional proportional integral (PI) method and artificial neural network. The generalized swing equation for a multi-machine power system was also used. The flowchart is shown in Figure 3.0.

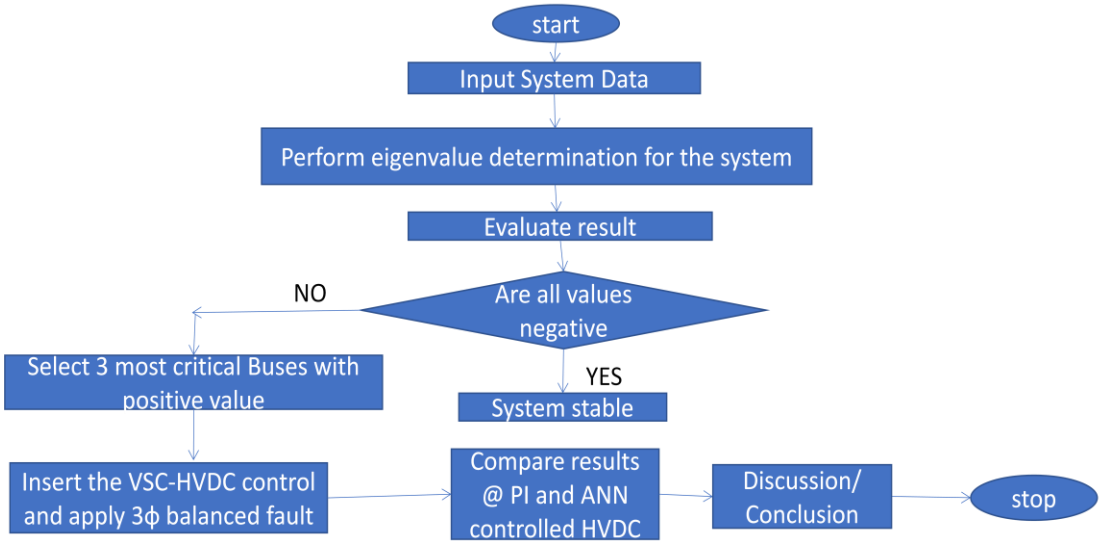

Figure 3.0: Flowchart for determination of Transient stability using Eigenvalue method

3.2 Controller for the VSC-HVDC Transmissions

The Model of HVDC Controller is shown in Figure 3.1. The ANN controller is connected in parallel with PI controller as shown in Figure 3.1.

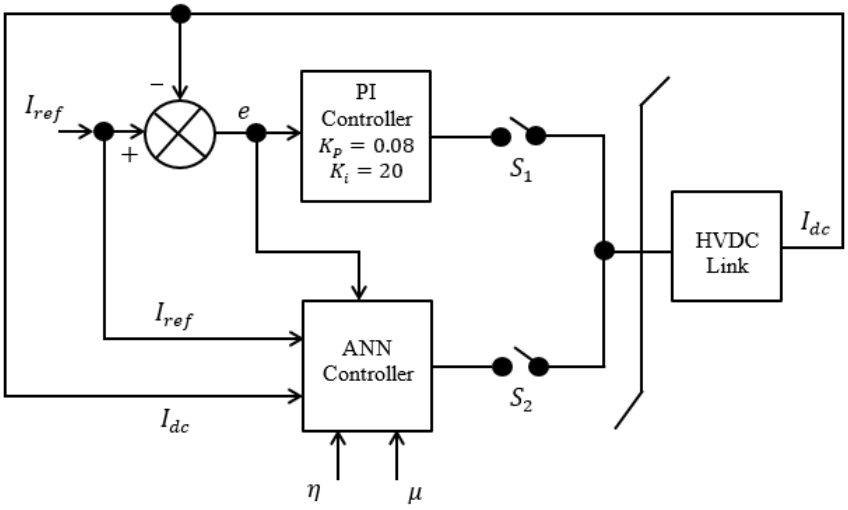

Figure 3.1: A schematic diagram of an HVDC system generic controller

Table 3.0: Training data-set for the Artificial Neural Network controller

I_{ref}	I_{dc}		
	Makurdi – Jos	Ajaokuta – Benin	Ikeja-West – Benin
5.205	4.959	5.887	5.766
5.370	5.989	5.101	5.853
5.120	5.766	5.327	5.996
5.830	5.853	5.375	5.988
5.470	4.996	5.943	5.097
5.650	5.988	4.973	5.943
5.330	5.007	5.042	5.423
5.804	5.020	5.200	4.971
5.210	5.966	5.434	5.053
5.190	5.971	5.423	5.825
5.130	5.030	5.091	5.973

5.350	5.182	5.577	5.976
5.970	5.973	5.036	5.972
5.460	5.970	5.445	5.985
5.560	5.972	5.167	5.327
5.302	4.985	5.259	5.375
5.010	5.076	5.332	5.799
5.480	5.385	4.837	5.198
5.660	5.498	5.197	5.094
5.930	5.100	5.104	5.242
5.110	5.003	5.009	5.697
5.030	5.918	5.057	5.297
5.625	5.090	5.188	5.176
5.340	5.198	5.210	5.385
5.910	5.276	5.032	5.699
5.080	5.285	5.737	5.698
5.290	5.197	5.360	5.930
5.940	5.297	5.452	5.850
5.350	5.797	5.678	5.027
5.801	5.398	4.795	5.350
5.101	5.8087	5.324	5.179
5.640	5.438	5.370	5.919
5.560	5.549	5.470	5.090

Table 3.0 shows the neural network controller training data set. The entire input data set (shown in Table 3.0) were subdivided into three; 60%, 20%, 20% for the training set, validation set and testing set respectively giving a set of three inputs and one output in each input-output pair. The output of the neural network is the firing angle. Hence, each input output pair consists of two inputs and one output.

The inputs to the ANN controller are I_{ref} and I_{dc} and its output is the firings angle$\propto$. The speed of the controller and the system stability will depend on the learning rate η and the momentum term μ used in adjusting the weights of the ANN. The ANN controller is trained on-line according to the I_{ref} and I_{dc} and by using back-propagation algorithm. The ANN learns by adjusting the weights V_n and B_n in the hidden layer and the weights W_n and B_n in the output layer.

3.3 PSAT Model of Nigerian 330kv Transmission Network

A new PSAT Model workspace was started. The needed component blocks were obtained from the PSAT Library by clicking and dragging them into the new model workspace. By arranging the component blocks, a single line network of the first Model was built in the Model workspace. Then, parameters of the component like voltage level, frequency, line impedance, reactance etc were adjusted to match the specific values of the test case network data.

The test case network was modeled to enable power flow analysis to be carried out on it. This will help to determine the critical buses/transmission lines on which the HVDC Model and its controller will be connected.

3.4 Load Flow Equation

Nodal admittance matrix can given as

$$\begin{bmatrix} I_1 \\ I_2 \\ I_3 \\ I_4 \\ \vdots \\ I_n \end{bmatrix} = \begin{bmatrix} Y_{11} & Y_{12} & Y_{13} & Y_{14} & & Y_{1n} \\ Y_{21} & Y_{22} & Y_{23} & Y_{24} & & Y_{2n} \\ Y_{31} & Y_{32} & Y_{33} & Y_{34} & \cdots & Y_{3n} \\ Y_{41} & Y_{42} & Y_{43} & Y_{44} & & Y_{4n} \\ \vdots & \vdots & \vdots & \vdots & & \vdots \\ Y_{n1} & Y_{n2} & Y_{n23} & Y_{n4} & & Y_{nn} \end{bmatrix} \begin{bmatrix} V_1 \\ V_2 \\ V_3 \\ V_4 \\ \vdots \\ V_n \end{bmatrix} \quad 3.1$$

Now define complex in a node such as k.

As $S_k = P_k + Q_k$ hence the load schedule at node k is $P_{ks} + Q_{ks}$.

Therefore the current

$$P_k = \sum_j^n Y_{kj} \left(V_k + V_j\right) \quad 3.2$$

Where Y_{kj} is the summation of all the admittances connected between node k and j, and V_k and V_j are node voltages in the respective nodes.

Since,

$$I_k = V_k \sum_{j=0}^n Y_{kj} - \sum_{j=1}^n Y_{kj} V_j \quad 3.3$$

Since from the nodal KCL admittance matrix,

$$I_k = Y_{k0} V_k + Y_{k1}(V_k - V_1) + Y_{k2}(V_k - V_2) + \cdots Y_{kn}(V_k - V_n) \quad 3.4$$

$$= (Y_{k0} + Y_{k1} + Y_{k2} \ldots Y_{kn})V_k - Y_{k1}V_1 - Y_{k1}V_1 \quad 3.5$$

The real and reactive power at bus k as

$$P_k + jQ_k = V_k + I^*_k \quad 3.6$$

Hence, $I_k = \frac{P_k + jQ_k}{I^*_k}$ 3.7

If we substitute for I_k in equation (3.3) we have

$$\frac{P_k + jQ_k}{I^*_k} = V_k \sum_{j=0}^n Y_{kj} - \sum_{j=1}^n Y_{kj} V_j \quad 3.8$$

From equation (3.8)

$$V_k = \frac{1}{Y_{kk}}\left[\frac{P_k + jQ_k}{I^*_k}\right] - \sum_{j\neq 1}^n Y_{kj} V_j \quad 3.9$$

3.5 Power Flow Analysis of Nigeria 330kV Transmission Power System

The Nigeria 330-kV transmission network used as the case study in this dissertation is shown in Figure 3.17. It consists of eleven (11) generators, twenty-nine (29) loads, comprising of forty

(40) buses and fifty-two (52) transmission lines, which cut across the six (6) Geopolitical zone (South-West, South-South, South-East, North- Central, North-West and North-East Region) of the country with long radial interconnected transmission lines.

The line diagram and data of the Nigerian transmission system were sourced from the National Control Centre of Power Holding Company of Nigeria, Osogbo, Nigeria. Power flow analysis of the Nigerian transmission system was performed in Matlab/Psat environment as shown in Figure 3.2.

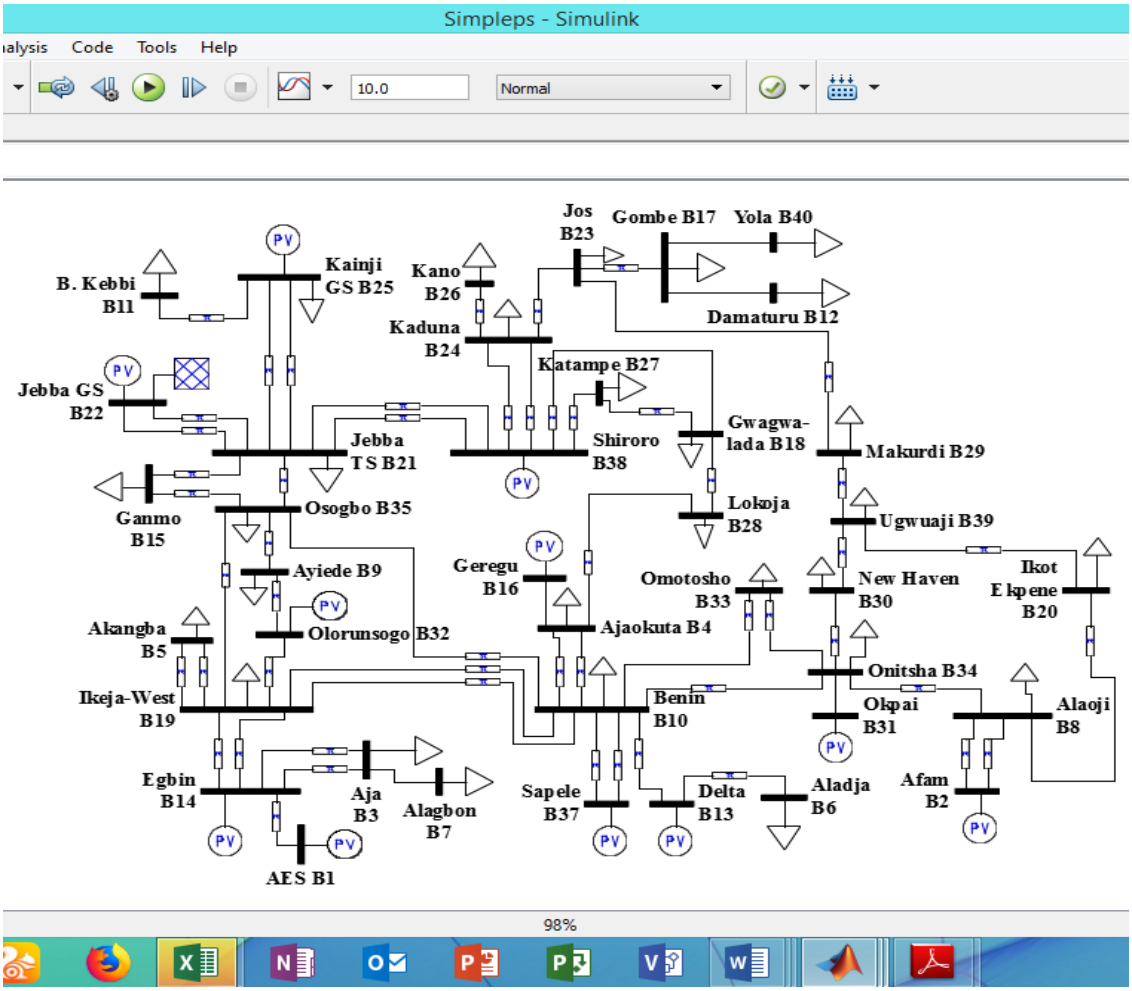

Figure 3.2: PSAT Model of the Nigeria 330kV transmission power system without VSC-HVDC

Figure 3.2 shows the PSAT modeling of the existing Nigerian 330kV transmission grid with existing system parameters as obtained from the National Control Centre. The modeling was done without the inclusion of the VSC-HVDC system. Load flow analysis was performed on the model so as to establish the current stability situation, whether there is need for its transient stability improvement or not.

3.6 Mathematical Formulation of Swing Equation for a Multi- Machine Power System

Consider a multi-machine *n*-bus power network consisting of *m* number of generators such that *n* >*m*. At any bus *I* within the system, the complex voltages (V_i), generators real power (P_{gi}) and the generator reactive power (Q_{gi}) can easily be obtained from the pre-fault load-flow analysis from which the initial machine voltages(E_i) can also be obtained. This relationship can be expressed as

$$E_i = V_i + jX_i\left[\frac{P_{gi} - j\,Q_{gi}}{V_i^*}\right] \qquad 3.10$$

Where;

X_i is the equivalent reactance at bus i. By converting each load bus into its equivalent constant admittance form, we have the load admittance as;

$$Y_{Li} = \frac{P_{Li} - j\,Q_{Li}}{|V_i|^2} \qquad 3.11$$

Where $P_{Li}$and $Q_{Li}$are the respective equivalent real and reactive powers at each load buses. The pre-fault bus admittance matrix [*bus Y*] can therefore be formed with the inclusion of generators reactance and the converted load admittance. This can be partitioned as

$$Y_{bus} = \begin{bmatrix} Y_{11} & Y_{12} \\ Y_{21} & Y_{22} \end{bmatrix} \qquad 3.12$$

Where Y_{11}, Y_{12}, Y_{21}, and Y_{22} are the sub-matrices of Y_{bus}. Out of these four sub-matrices, Y_{11}, whose dimension is $m \times m$is the main interest of this work as it contains generators buses only with the load buses eliminated. Equation (3.12) is formulated for the network conditions such as pre-fault, during fault and post-fault. The *bus Y* for the network is then formulated by eliminating all nodes except the internal generator nodes. The reduction is achieved based on the fact that injections at all load nodes are zero. The nodal equations, in compact form, can therefore be expressed as

$$\begin{bmatrix}1\\0\end{bmatrix} = \begin{bmatrix}Y_{mm} & Y_{mn}\\ Y_{nm} & Y_{nn}\end{bmatrix}\begin{bmatrix}V_m\\V_n\end{bmatrix} \quad 3.13$$

By expansion equation (3.13) can be expanded as

$$I_m = Y_{mm}V_m + Y_{mn}V_n \quad 3.14$$

and $$0 = Y_{mm}V_m + Y_{mn}V_n \quad 3.15$$

By combining equations (3.14) and (3.15) and some mathematical manipulations, the desired reduced admittance matrix can be obtained as

$$Y_{reduced} = Y_{mm} - Y_{mn}Y_{nn}^{-1}Y_{nm} \quad 3.16$$

$Y_{reduced}$ is the desired reduced matrix with dimension m x m, where m is the number of generators. The electrical power output of each machine can then be written as

$$P_{ei} = E_i^2 Y_{ii}\cos\theta_{ii} + \sum_{\substack{i=1\\ j\neq 1}}^{m} |E_i||E_j||Y_{ij}|\cos\left(\theta_{ij} - \delta_i + \delta_j\right) \quad 3.17$$

Equation (3.17) is then used to determine the system during fault $P_{ei}\,(P_{ei\,(during\,-fault\,)})$ and post-fault $P_{ei}\,(P_{ei\,(post\,-fault\,)})$ conditions.

The rotor dynamics, representing the swing equation, at any bus *i*, is given by

$$\frac{H_i}{\pi f_0}\frac{d^2\delta_i}{dt^2} + D_i\frac{d_i}{dt} = P_{mi} - P_{ei} \quad 3.18$$

All the parameters retain their usual meanings.

Consider a case when there is no damping i.e. $D_i = 0$, equation (3.18) can be re-written as

$$\frac{H_i}{\pi f_0}\frac{d^2\delta_i}{dt^2} = P_{mi} - \left(E_i^2 Y_{ii}\cos\theta_{ii} + \sum_{\substack{i=1\\ j\neq 1}}^{m} |E_i||E_j||Y_{ij}|\cos\left(\theta_{ij} - \delta_i + \delta_j\right)\right) \quad 3.19$$

The swing equation for the during-fault condition can easily be expressed as

$$\frac{H_i}{\pi f_0}\frac{d^2\delta_i}{dt^2} + D_i\frac{d_i}{dt} = P_{mi} - P_{ei\,(during\ -fault\ )} \quad 3.20$$

Similarly, the swing equation for the post fault condition can be written as

$$\frac{H_i}{\pi f_0}\frac{d^2\delta_i}{dt^2} + D_i\frac{d_i}{dt} = P_{mi} - P_{ei\,(post\ -fault\ )} \quad 3.21$$

3.7 Eigenvalue Analysis

The Eigenvalue analysis investigates the dynamic behavior of a power system under different characteristic frequencies (‘‘modes’’). In a power system, it is required that all modes are stable. Moreover, it is desired that all electromechanical oscillations are damped out as quickly as possible. The Eigen value ($\boldsymbol{\gamma}$) gives information about the proximity of the system to instability. The participation factor measures the participation of a state variable in a certain mode oscillation. The damping ratio (τ) is an indication of the ability of the system to return to stable state in the event of disturbance. For eigenvalue determination of stability, all the values must have negative real part and will lie on the left side of the S-plane. However, if any of the established eigenvalue lies on the positive right side of the S-plane, thus indicates oscillation in the system hence unstable.

The aim here is to determine the generator buses that are most marginally unstable. In order to demonstrate the effect of the HVDC on transient stability the Nigeria 330kV grid, the buses to be subjected to three phase fault should be the buses that are marginally unstable. To do this, the case study network was designed in Matlab/PSAT environment and simulation procedure and results specific to its parameters were obtained. This enabled this work to explore the peculiarity of the Nigerian power system.

The overall network/load representation comprises a large sparse nodal admittance matrix equation with a structure similar to that of the power-flow problem. The network equation is written in matrix form as:

$$\Gamma_L = Y_N V \qquad 3.22$$

Where V is the node voltage and Γ is the node current. The node admittance matrix Y_N is symmetrical, except for dissymmetry introduced by phase-shifting transformers.

This can be represented in steady state-space form as follows:

$$\boldsymbol{A}x = \dot{x} \qquad 3.23$$

To obtain the solution of equation (3.23), a scalar parameter λ called the eigenvalue is introduced such that equation (3.23) becomes;

$$\boldsymbol{A}x = \lambda x \qquad 3.24$$

Where $\boldsymbol{A} = [\boldsymbol{a_{i1}}]_{an}$ n x n square matrix, where x is n x 1 vector and λ is a number (scalar) parameter. Clearly the solution $x = 0$ for λ is usually not useful and thus is neglected.

For non-trivial solutions i.e.$x \neq 0$, the values of λ are called the eigenvalues and the characteristics values or latent roots of the matrix A and the corresponding solutions of equation

(3.24) are called eigenvectors or characteristic vectors of A. Expressed as separate equations we have;

$\boldsymbol{A}.\, x - \lambda x = 0$ 3.25

$(\boldsymbol{A} - \lambda \boldsymbol{I})x = 0$ 3.26

Notice that the unit matrix $\boldsymbol{I}$was introduced so that λ can be subtracted from matrix A. Now for equation (3.26) to have a non-trial solution, determinant of $|\boldsymbol{A} - \lambda \boldsymbol{I}|$ must be equal to zero. Hence

$$|\boldsymbol{A} - \lambda \boldsymbol{I}| = \begin{bmatrix} a_{11} - \lambda & a_{12} & \cdots & a_{1i} \\ a_{21} & a_{22} - \lambda & \cdots & a_{2i} \\ \vdots & \vdots & \cdots & \vdots \\ a_{i1} & a_{i2} & \cdots & a_{ii} - \lambda \end{bmatrix} = 0 \qquad 3.27$$

Expansion of equation (3.27) gives the characteristics equation. The n solutions of $\lambda = \lambda 1$, $\lambda 2$, $\lambda 3 \ldots . \lambda n$ are eigenvalues of A.

The output from the eigenvalue analysis on the PSAT model of the Nigeria 330kV transmission grid is extracted and tabulated in Table 3.1. To ensure that the buses to be used are marginally unstable, the buses selected are buses having eigenvalue that lie on the right side of the S-plane and having lowest value of damping ratio.

Table 3.1 Extracted output from eigenvalue analysis

Bus Number	**Bus Name**	**Eigen Value (γ)**	**Damping Ratio (τ)**	**Participation Factor (%)**
1	AES	$2.7653 \pm j8.4192$	0.6442	1.0520
2	Afam	$-1.9404 \pm j4.2813$	0.4723	0.6197
3	Aja	$-2.1746 \pm j6.7011$	0.2632	0.7139

4	Ajaokuta	$1.9640 \pm j3.1032$	0.0476	2.6122
5	Akangba	$2.0367 \pm j8.2287$	0.5941	0.6122
6	Aladja	$-3.4083 \pm j6.0053$	0.7456	2.4165
7	Alagbon	$0.2562 \pm j5.7324$	0.6745	0.4165

8	Alaoji	$-0.4528 \pm j4.2183$	0.6259	1.0817
9	Ayiede	$-2.7653 \pm j11.2419$	0.4933	0.3021
10	Benin	$2.8730 \pm j6.1437$	0.0219	3.3021
11	Brenin Kebbi	$-2.1674 \pm j5.1101$	1.3511	0.3228
12	Damaturu	$1.6064 \pm j6.8320$	0.8232	3.1297
13	Delta	$-2.0367 \pm j8.2287$	0.7624	1.1096
14	Egbin	$3.4083 \pm j7.1537$	0.8320	0.3176
l15	Ganmo	$-0.2562 \pm j5.7324$	0.8031	0.2113
16	Geregui	$-0.4528 \pm j4.2183$	0.2803	0.2113
17	Gombe	$-4.6097 \pm j7.5635$	2.3893	0.3260
18	Gwagwa	$2.3576 \pm j8.1273$	0.3048	1.0640
19	Ikeja-West	$-0.5284 \pm j3.3182$	1.1601	0.2639
20	Ikot Ekpene	$4.6097 \pm j7.3637$	0.5060	0.2680
21	Jebba TS	$-1.7356 \pm j4.9214$	0.0931	4.6422
22	Jebba GS	$-1.7653 \pm j10.4192$	0.1311	0.1422
23	Jos	$1.4011 \pm j3.1375$	0.6534	0.3252
24	Kaduna	$-2.1746 \pm j6.7011$	0.7324	1.9180

25	Kainji GS	$-1.9640 \pm j5.3208$	0.6612	1.2912
26	Kano	$2.5376 \pm j10.9419$	0.3342	1.0768
27	Katampe	$-1.7011 \pm j3.1375$	0.3442	0.0768
28	Lokoja	$-2.1746 \pm j6.7011$	0.2632	0.7139
29	Makurdi	$3.0640 \pm j5.3208$	0.0564	2.6122
30	New Haven	$2.0367 \pm j8.2287$	0.5941	0.6122
31	Okpai	$-3.4083 \pm j7.5374$	0.7456	5.4165
32	Olorunsogo	$-0.2562 \pm j4.7324$	0.2674	3.4165
33	Omotosho	$2.7297 \pm j5.5635$	0.3284	4.2720
34	Onitsha	$0.4528 \pm j4.2183$	0.6259	0.1817
35	Osogbo	$-3.8372 \pm j6.3756$	0.1842	4.3366
36	Papalanto	$-2.7653 \pm j11.2419$	0.4933	0.3021
37	Sapele	$1.7301 \pm j3.1375$	0.2193	3.3021
38	Shiroro	$0.1674 \pm j4.1170$	0.0925	6.3228
39	Ugwuaji	$-1.6064 \pm j6.8320$	0.8232	3.1297
40	Yola	$-2.0367 \pm j8.2287$	1.7624	1.1096

From the tabulation, it can be seen that the Nigeria 330kV transmission grid network is generally not stable. This is due to the fact that all the eigenvalues are not located on the left side of the S-plane. The Eigenvalues located on the left side of the S-plane are negative whereas eigenvalues located on the right side of the S-plane are positive. However, not all the buses in the power system are part of the instability. From Table 3.1, most of the eigenvalues are located on the left

side of the S-plane which means that they are stable and some eigenvalues are located on the right side of the S - plane which indicates that they are unstable. Among all the buses whose eigenvalues are located on the right side of the S-plane, the most unstable buses would be selected for application of three phase fault for the evaluation of the system transient stability improvement using ANN controlled VSC-HVDC. The buses located on the right side of the S-plane are unstable buses but since three buses are to be selected, the damping ratio is used as the criterion for the selection. The lower the damping ratio, the more unstable the bus would be.

From the Table 3.1, the buses selected are Makurdi – bus 29, Ajaokuta – bus 4 and Benin - bus 10. The eigenvalues of these buses are $3.0640 \pm j5.3208$, $1.9640 \pm j3.1032$ and $2.8730 \pm j6.1437$ with damping ratios of 0.0564, 0.0476 and 0.0219 respectively. The eigenvalues of these buses are located on the right side of the S-plane and they are the buses with the lowest damping ratio. These selected buses 29, 4 and 10 were now subjected to a three phase faults one after the other whereas the loads at buses were held constant at the demand values.

3.8 Installation of VSC-HVDC to the Nigeria 40 Bus 330kv Transmission Network for Transient Stability Improvement during Occurrence of a Three-Phase Fault

Figures 3.3 shows the PSAT Model of the Nigeria 330kV transmission power system with VSC-HVDC transmission line installed along side with Makurdi – Jos, transmission lines respectively. The choice of position for the location of the VSC-HVDC was determined through eigenvalue analysis as its eigenvalue was located on the right side of the S-plane and also is among the three buses that have the lowest damping ratio (as aforementioned). Here, Load flow analysis was performed on the model with bus 29 (Makurdi) subjected to a three phase faults whereas the

loads at other buses were held constant at the demand values. This is as to establish the stability situation, whether there is improvement in the transient stability improvement.

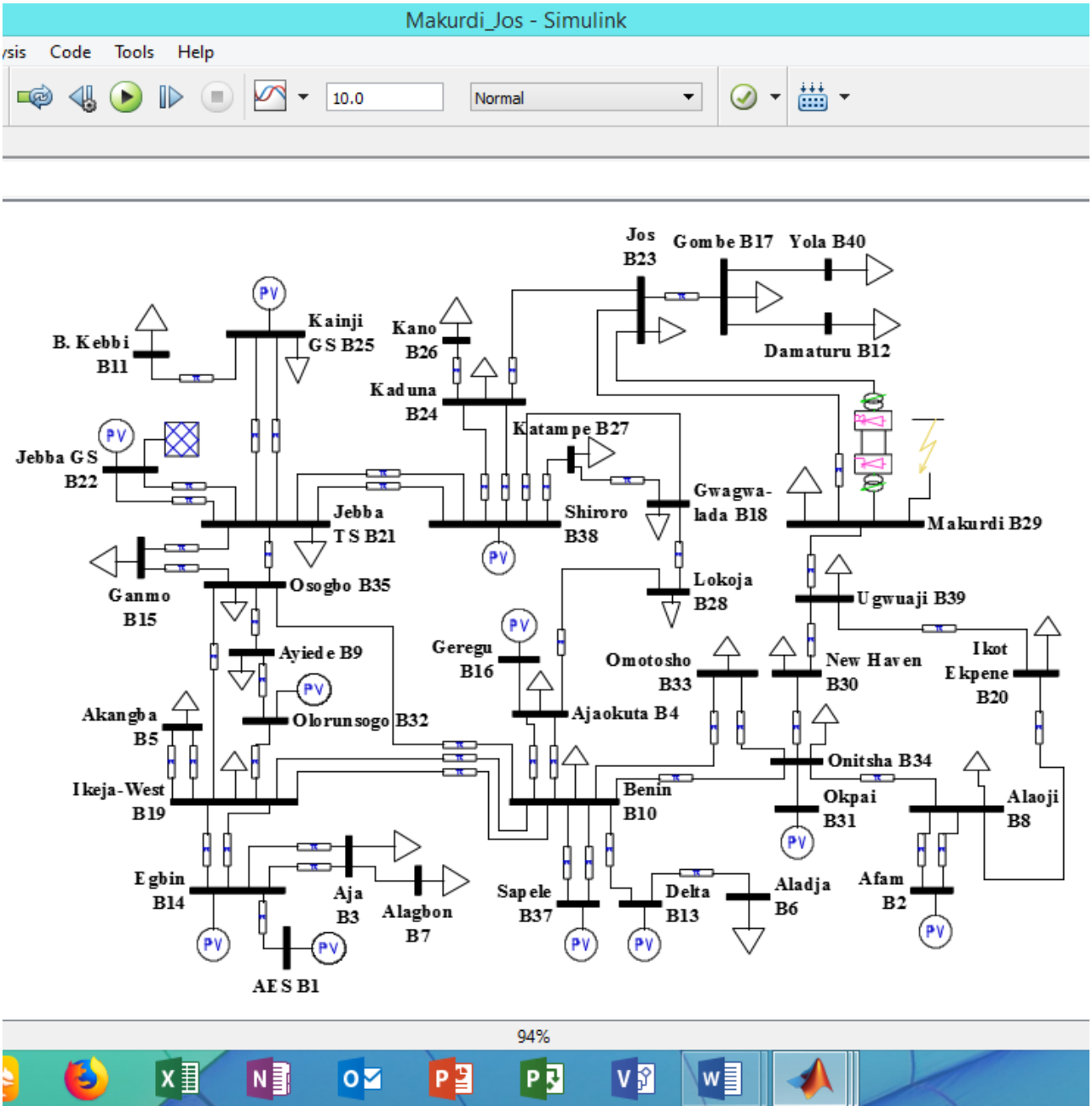

Figure 3.3: PSAT Model of the Nigeria 330kV transmission power system with VSC-HVDC installed along side with Makurdi – Jos Transmission Line

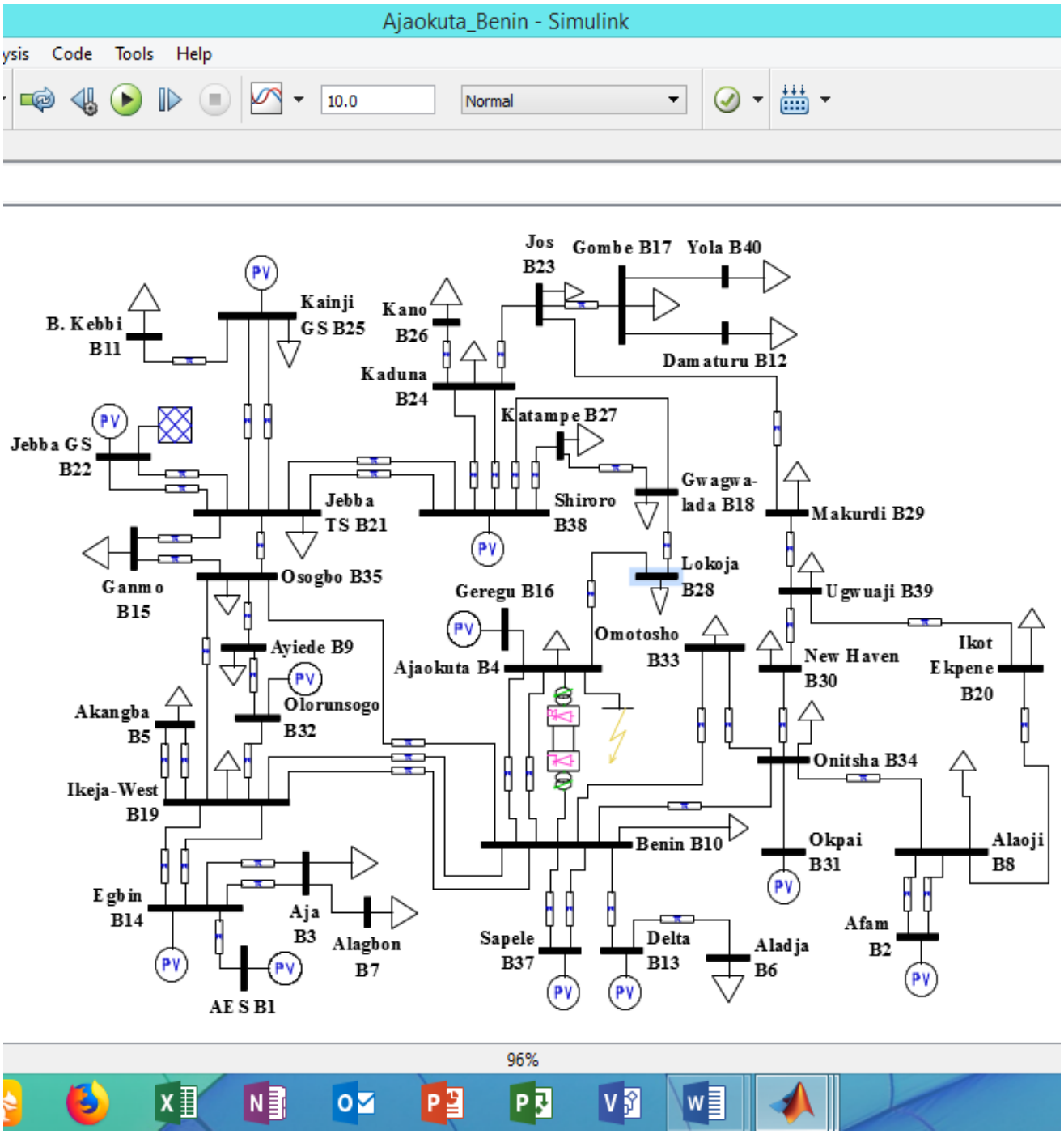

Figure 3.4: PSAT Model of the Nigeria 330kV transmission power system with VSC-HVDC installed along side with Ajaokuta – Benin Transmission Line

Figures 3.5 shows the PSAT Model of the Nigeria 330kV transmission power system with VSC-HVDC transmission line installed along side with Ajaokuta – Benin, transmission lines respectively. The choice of position for the location of the VSC-HVDC was determined through eigenvalue analysis as its eigenvalue was located on the right side of the S-plane and also is among the three buses that have the lowest damping ratio (as aforementioned). Here, Load flow analysis was performed on the model with bus 4 (Ajaokuta) subjected to a three phase faults whereas the loads at other buses were held constant at the demand values. This is as to establish the stability situation, whether there is improvement in the transient stability improvement.

Figures 3.6 shows the PSAT Model of the Nigeria 330kV transmission power system with VSC-HVDC transmission line installed along side with Benin – Ikeja West, transmission lines respectively. The choice of position for the location of the VSC-HVDC was determined through eigenvalue analysis as its eigenvalue was located on the right side of the S-plane and also is among the three buses that have the lowest damping ratio (as aforementioned). Here, Load flow analysis was performed on the model with bus 10 (Benin) subjected to a three phase faults whereas the loads at other buses were held constant at the demand values. This is as to establish the stability situation, whether there is improvement in the transient stability improvement.

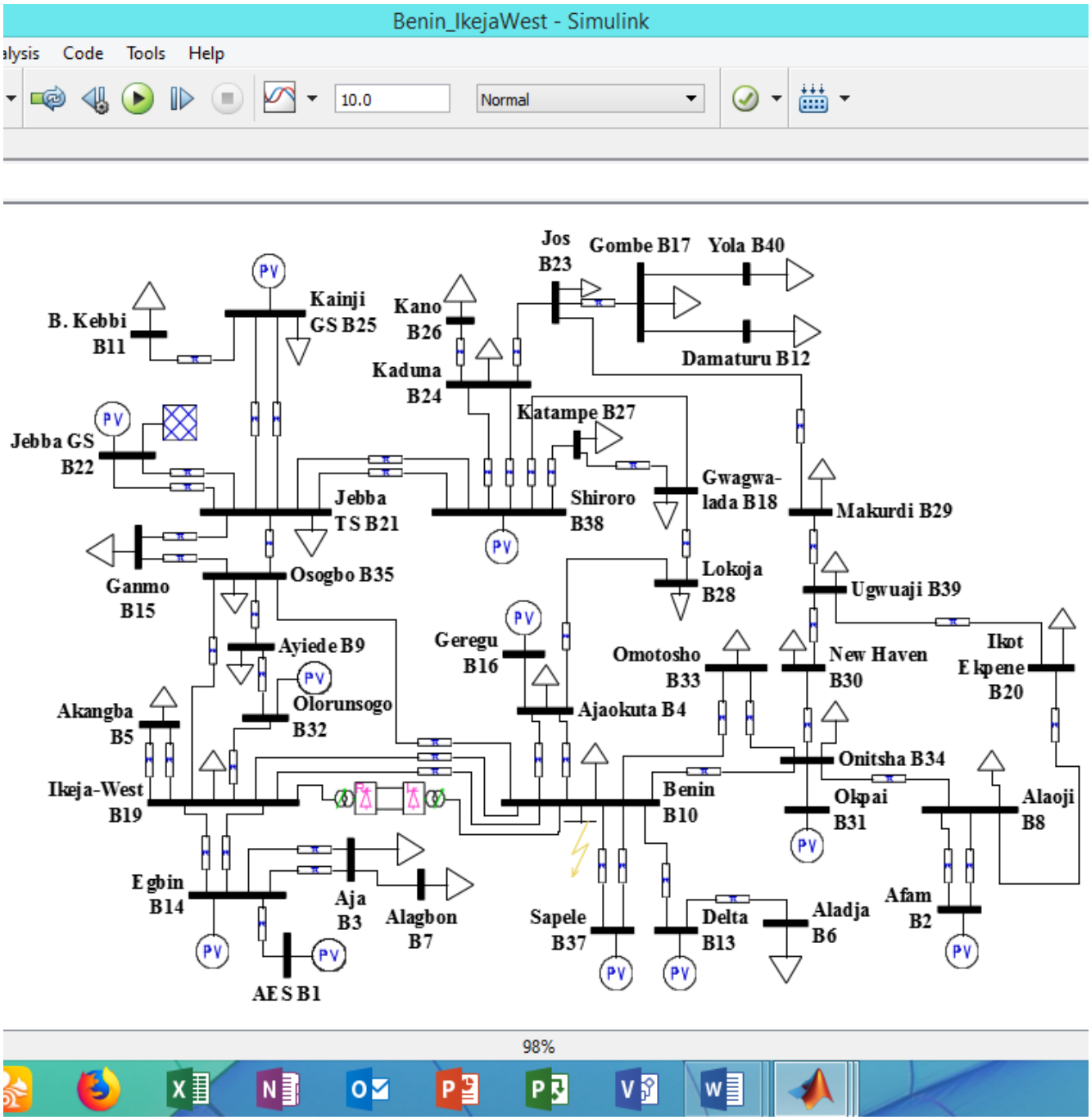

Figure 3.5: PSAT Model of the Nigeria 330kV transmission power system with VSC-HVDC installed along side with Ikeja West- Benin Transmission Line

CHAPTER FOUR

RESULTS AND DISCUSSION

The result shows clearly that there exist three most critical buses which are Makurdi, Ajaokuta and Benin buses and critical transmission lines (which include Jos - Makurdi Transmission line, Ajaokuta - Benin and Ikeja West – Benin Transmission line) within the network. The performed load flow analysis also revealed that the system losses synchronism when the balanced three-phase fault was applied to these identified critical buses and lines.

4.1 Power Flow Analysis of the Nigeria 40 Bus 330kV Transmission Network

The voltage profile of the Nigerian 40-bus 330kV transmission system are shown in Table 4.1 as obtained from the power flow analysis of the network in PSAT environment. It can be observed from Table 4.1 and Figure 4.1 that the voltage magnitude at buses 5 (Akangba), 7 (Alagbon), 17 (Gombe), 18 (Gwagwalada), 26 (Kano), 32 (Olorunsogbo), 33 (Omotosho) and 38 (Shiroro) are lower than the acceptable voltage limit of ±10% for the Nigerian 330kV transmission system. This confirms results of earlier studies on the system as reported in (Ignatius and Emmanuel, 2017). Disproportionate power flows in some of the system transmission lines as alighted in Table 4.2.

Table 4.1 The Load Flow Result of System Bus (Voltage Profile)

Bus No	Bus Name	Voltage [p.u.]	Phase Angle [rad]
1	AES	1.000000	0.016368
2	Afam	1.000000	-0.00533
3	Aja	0.998480	0.006284
4	Ajaokuta	0.989621	-0.00676
5	Akangba	0.805418	-0.10014
6	Aladja	0.996952	-0.00231
7	Alagbon	0.842001	-0.03763
8	Alaoji	1	-0.00962
9	Ayiede	0.996654	0.001761
10	Benin	0.995594	-0.00382
11	B. Kebbi	0.955445	-0.04433
12	Damaturu	0.996001	0.001354
13	Delta	1.000000	0.000672
14	Egbin	1.000000	0.007773
15	Ganmo	0.995887	-0.00372
16	Geregu	0.989101	-0.00231
17	Gombe	0.766327	-0.04365
18	Gwagwa-lada	0.853375	-0.03592
19	Ikeja-West	0.996943	0.001354
20	Ikot Ekpene	0.988973	-0.01895
21	Jebba TS	1.000000	0
22	Jebba GS	1.000000	0.00215
23	Jos	0.966434	-0.04046
24	Kaduna	0.971423	-0.03687
25	Kainji GS	1.000000	0.007816
26	Kano	0.825577	-0.20071
27	Katampe	0.973536	-0.03586
28	Lokoja	0.970445	-0.03763
29	Makurdi	0.972167	-0.03443
30	New Haven	0.985259	-0.01984
31	Okpai	0.998001	-0.03763
32	Olorunsogo	0.835771	0.61537
33	Omotosho	0.772546	-0.72907

34	Onitsha	0.992507	-0.01132
35	Osogbo	0.994828	-0.00446
36	Papalanto	0.963277	-0.04365
37	Sapele	1.000000	-0.00019
38	Shiroro	0.818990	-0.90286
39	Ugwuaji	0.981078	-0.02538
40	Yola	0.995245	-0.04763

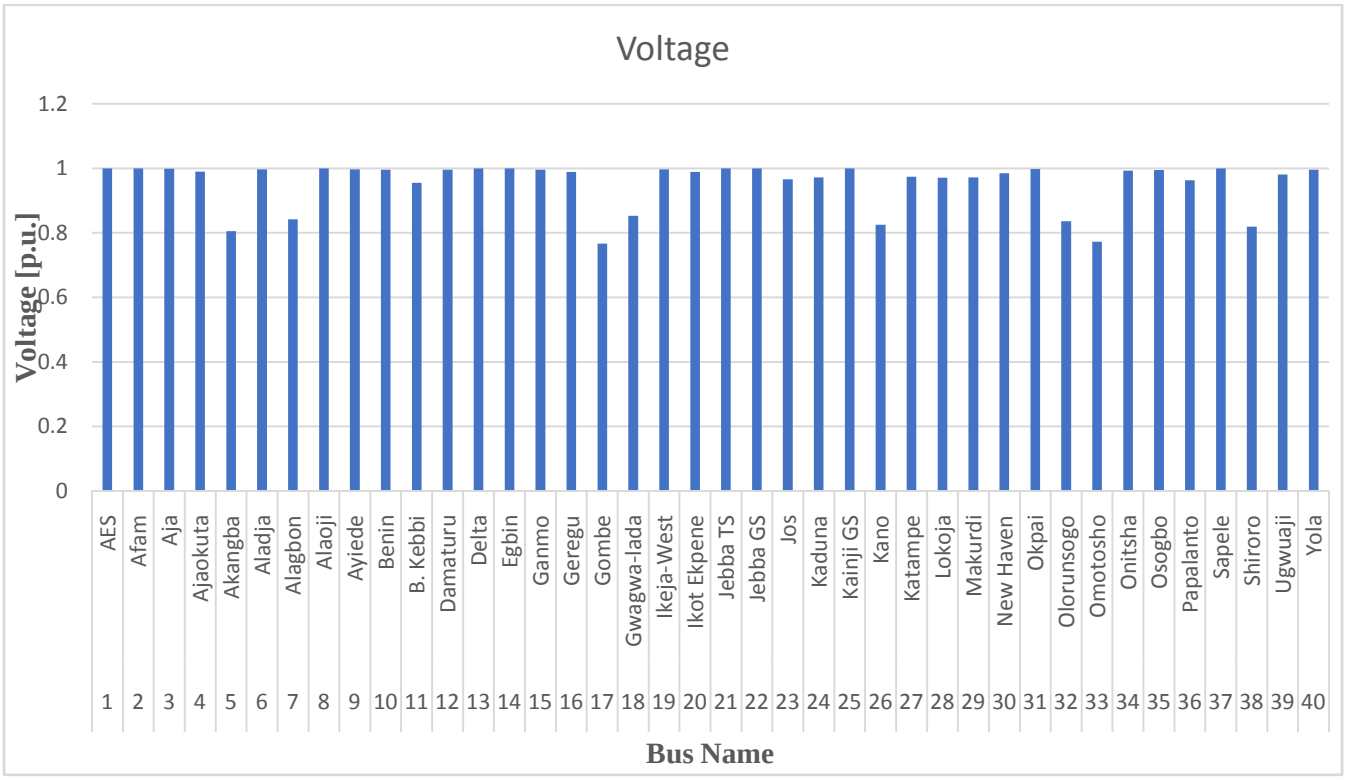

Figure 4.1 Nigeria 330kV Transmission Line Bus Voltage Profile

The system has a high total active power loss of 0.056655p.u. and reactive power loss of 0.594828p.u. In order to alleviate the power system problems of voltage limit violations, and disproportionate power flows and high active and reactive power loss and along with the main aim of improving the system transient stability during occurrence of a three-phase faults on some strategic buses in the system, the VSC-HVDCs were incorporated in the system along with those

disadvantaged transmission lines. The VSC-HVDC is controlled by artificial neural network (ANN). Table 4.2 shows the result of Nigeria 330kV Transmission Line Flows. From the Table it can be observed that the total active and reactive power losses are 5.6655p.u. and 4.94828p.u. respectively which shows that there is high energy loss in the system.

Table 4.2: Nigeria 330kV Transmission Line Flows

From Bus	To Bus	Line	P Flow [p.u.]	Q Flow [p.u.]	P Loss [p.u.]	Q Loss [p.u.]
Kainji GS B25	Jebba TS B21	1	0.158613	0.03512	1.05E-05	0.001291
Kainji GS B25	B. Kebbi B11	2	0.642774	0.535677	0.002774	0.055677
Katampe B27	Shiroro B38	3	-0.68393	-0.51016	0.000304	0.037857
Kano B26	Kaduna B24	4	-0.64	-0.48	0.000285	0.035401
Jos B23	Kaduna B24	5	-0.19092	-0.15877	2.64E-05	0.003278
Gombe B17	Jos B23	6	-0.64	-0.48	0.000564	0.002775
Jebba TS B21	Ganmo B15	7	1.32013	0.536563	0.001651	0.009751
Jebba TS B21	Osogbo B35	8	0.204288	0.094002	2.01E-05	0.002491
Osogbo B35	Ayiede B9	9	-0.08003	-0.05968	4E-06	0.000488
Osogbo B35	Ikeja-West B19	10	-0.06311	-0.05801	2.95E-06	0.000357
Ikeja-West B19	Olorunsogo B32	11	-0.87844	-0.53265	0.00086	0.004623
Ikeja-West B19	Akangba B5	12	0.320131	0.239898	0.000131	-0.0001
Kainji GS B25	Jebba TS B21	13	0.158613	0.03512	1.05E-05	0.001291
Ikeja-West B19	Akangba B5	14	0.320131	0.239898	0.000131	-0.0001
Egbin B14	Ikeja-West B19	15	1.27881	0.477797	0.00151	0.008833
Egbin B14	Ikeja-West B19	16	1.27881	0.477797	0.00151	0.008833
Aja B3	Egbin B14	17	-0.32	-0.24	0.00013	-0.00012
Aja B3	Egbin B14	18	-0.32	-0.24	0.00013	-0.00012
AES B1	Egbin B14	19	1.6	-0.24026	0.00212	0.012785
Benin B10	Ikeja-West	20	-1.0439	-0.22111	0.000932	0.005095

	B19					
Benin B10	Ikeja-West B19	21	-1.0439	-0.22111	0.000932	0.005095
Benin B10	Osogbo B35	22	-0.38535	0.225605	0.000163	0.000113
Benin B10	Ajaokuta B4	23	0.594552	0.462326	0.000465	0.002069
Jebba TS B21	Jebba GS B22	24	-1.54638	-0.09096	0.00195	0.011686
Benin B10	Ajaokuta B4	25	0.594552	0.462326	0.000465	0.002069

Sapele B37	Benin B10	26	0.8	0.935483	0.001228	0.007007
Sapele B37	Benin B10	27	0.8	0.935483	0.001228	0.007007
Onitsha B34	New Haven B30	28	1.84712	1.249318	0.004125	0.025812
Onitsha B34	Benin B10	29	-1.91611	-0.8637	0.003663	0.022803
Afam B2	Alaoji B8	30	1.2	1.387589	0.002727	0.016727
Afam B2	Alaoji B8	31	1.2	1.387589	0.002727	0.016727
Alaoji B8	Onitsha B34	32	-0.0664	0.67315	0.000377	0.001507
Delta B13	Benin B10	33	0.959479	0.911517	0.001419	0.008248
Aladja	Delta B13	34	-0.64	-0.48	0.000521	0.002423
Jebba TS B21	Jebba GS B22	35	-1.54638	-0.09096	0.00195	0.011686
Alaoji B8	Ikot Ekpene B20	36	1.820943	1.588575	0.00481	0.030246
New Haven B30	Ugwuaji B39	37	1.202995	0.743506	0.001687	0.010019
Ugwuaji B39	Makurdi B29	38	1.735302	1.318862	0.004047	0.025333
Makurdi B29	Jos B23	39	1.091254	0.813529	0.001606	0.009524
Ikot Ekpene B20	Ugwuaji B39	40	1.176133	1.078329	0.00214	0.012954
Olorunsogo B32	Ayiede B9	41	0.720696	0.543497	0.00066	0.003326
Gwagwa-lada B18	Katampe B27	42	-0.04392	-0.03106	2.45E-06	-0.00089
Lokoja B28	Ajaokuta B4	43	-0.54797	-0.41574	0.000199	0.024777
Gwagwa-lada B18	Lokoja B28	44	0.09203	0.064914	5.3E-06	0.000651
Onitsha B34	Omotosho B33	45	-0.63778	-0.19397	0.000368	0.001451
Shiroro B38	Jebba TS B21	46	-0.62231	0.432556	0.000466	0.002062
Benin B10	Omotosho B33	47	1.279876	0.685679	0.001727	0.010254

Osogbo B35	Ganmo B15	48	-0.6781	-0.0453	0.000379	0.00151
Shiroro B38	Jebba TS B21	49	-0.62231	0.432556	0.000466	0.002062
Kaduna B24	Shiroro B38	50	-0.73561	-0.57872	0.000369	0.045905
Kaduna B24	Shiroro B38	51	-0.73561	-0.57872	0.000369	0.045905
Gwagwa-lada B18	Shiroro B38	52	-0.68811	-0.51386	0.000308	0.038368
TOTAL			16.69666	13.07483	5.6655	4.94828

4.2 Response of the Nigeria 40 Bus 330kV Transmission Network to Occurrence of a Three-Phase Fault

The results obtained from the simulation are presented in this section. The simulation results are carried out on the MATLAB/PSAT environment. The demonstration for the transient stability analysis on the Nigeria 330-kV grid network, in this work, considered three scenarios as aforementioned. These scenarios are created based on the eigenvalues and the damping ratio of the buses. The buses selected are buses having eigenvalue that lies on the right side of the S-plane and having lowest value of damping ratio which ensure that they are marginally stable. The buses are Makurdi, Ajaokuta and Benin buses as explained in Chapter three. A three phase fault was created on the transmission lines connected to these three buses (very close to the buses) one after the other which forms the three scenarios.

A 3-phase fault was created at each of the three locations and the swing equations are solved to obtain the network conditions for both during-fault and post-fault using numerical solver ode45. The numerical solver, ode45, which is a built-in MATLAB/PSATS function, is employed in solving the *m*-number of swing equations within the system.

4.2.1 Scenario One: Three Phase Fault at Makurdi Bus

In this scenario, a three-phase fault was created on Makurdi bus (Bus 29) with line Makurdi – Jos (29-23) removed. That is the three-phase fault was cleared by the circuit breakers (CBs) at both ends opening to remove the faulted line from the system. Figures 4.2 and 4.3 show the dynamics responses of the generators for CCT of 300ms.

Figures 4.2 and 4.3 show the plot of the power angle curves and the frequency responses of the eleven generators in the system during a transient three-phase fault on Makurdi to Benin transmission line. It can be observed that generators at Opkai and Afam buses were most critically disturbed and failed to recover after the fault was cleared at 0.3seconds. These two generators in the system lost synchronism and became unstable as shown in Figures 4.2 and 4.3.

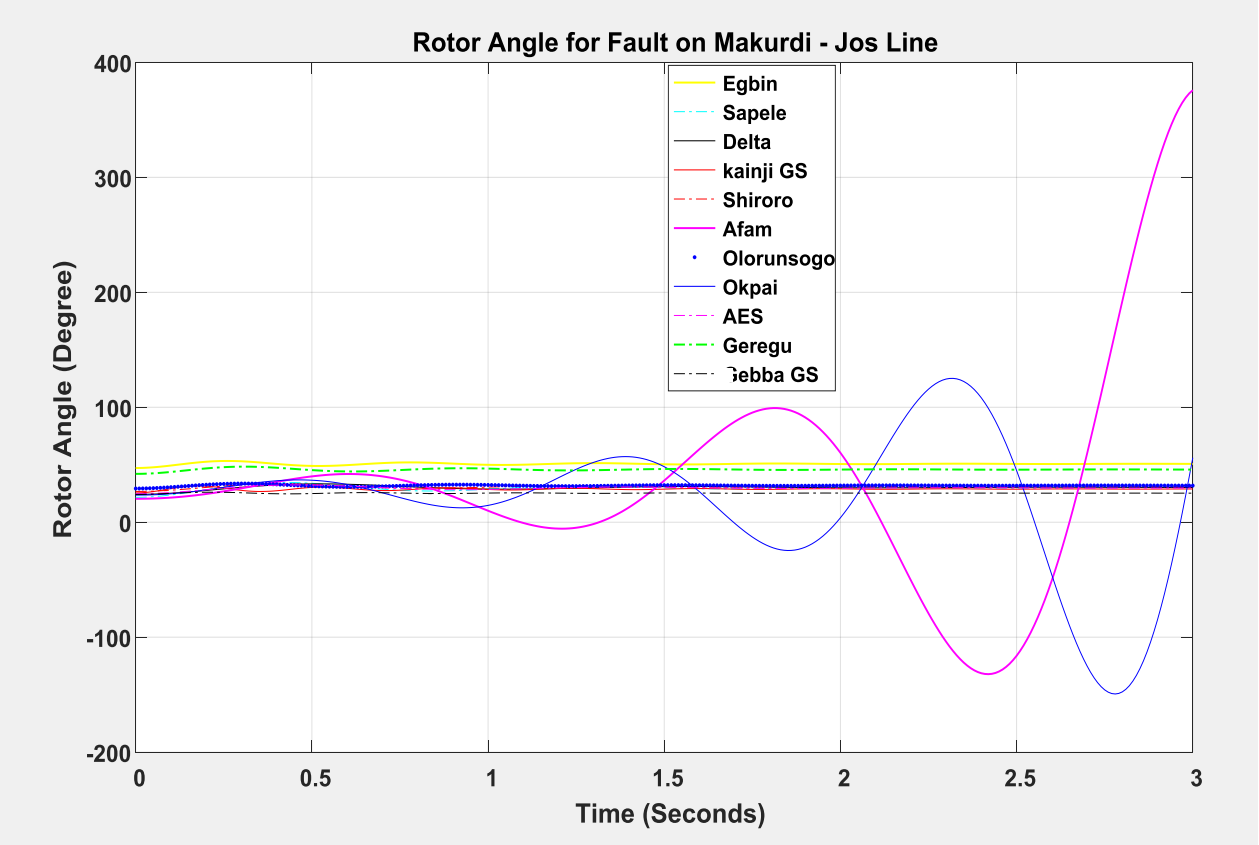

Figure 4.2: Rotor Angle response of the generators for fault clearing time of 0.3sec without any VSC-HVDC

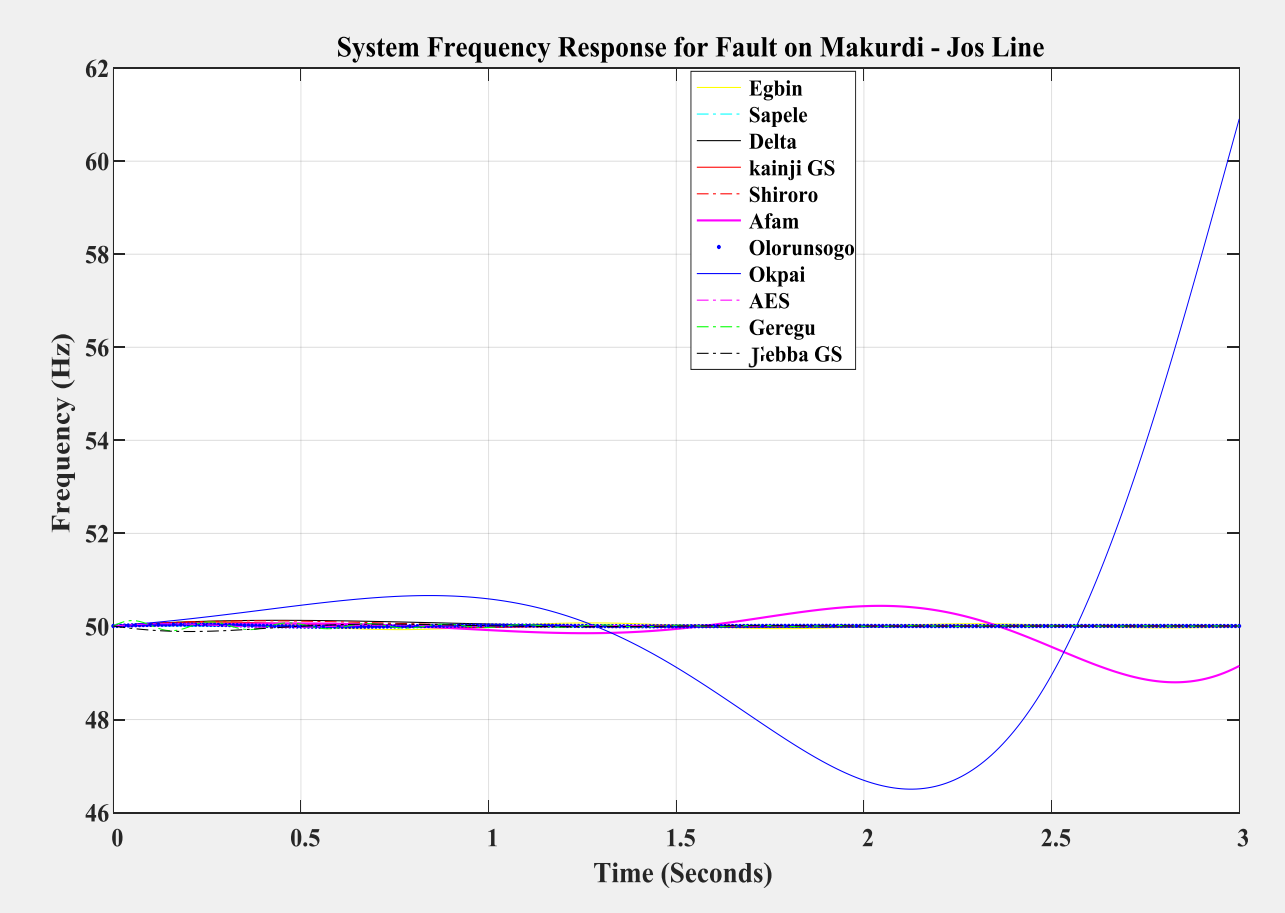

Figure 4.3: Frequency response of the system generators for fault clearing time of 0.3sec without any VSC-HVDC

The effect on the bus voltage magnitude for the three phase fault on Bus 29 was also examined. The voltage profile results of the Nigerian 40-bus 330kV transmission system after the occurrence of the fault are shown in Table 4.3 as obtained from the power flow analysis of the network in PSAT environment. It can be observed from Table 4.3 and Figure 4.4 that there are serious voltage violations at buses 5 (Akangba), 7 (Alagbon), 13 (Delta), 14 (Egbin), 26 (Kano),

32 (Olorunsogbo), 33 (Omotosho) and 37 (Sapele). The voltage magnitudes at these buses are lower than the acceptable voltage limit of ±10% for the Nigerian 330kV transmission system.

Table 4.3: The Load Flow Result of System Bus (Voltage Profile) during Occurrence of the Three Phase Fault

Bus No	Bus Name	Voltage [p.u.]	Phase Angle [rad]
1	AES	1.000000	0.016368
2	Afam	1.000000	-0.00533
3	Aja	0.980480	0.006284
4	Ajaokuta	0.974396	-0.00676
5	Akangba	0.800057	-0.10014
6	Aladja	0.990952	-0.00231
7	Alagbon	0.842001	-0.03763
8	Alaoji	1	-0.00962
9	Ayiede	0.996654	0.001761
10	Benin	0.995594	0.00382
11	B. Kebbi	0.955445	-0.04433
12	Damaturu	0.996001	0.001354
13	Delta	0.800500	-0.200672
14	Egbin	0.704520	-0.083373
15	Ganmo	0.995887	0.00372
16	Geregu	0.989101	-0.00231
17	Gombe	0.766327	-0.04365
18	Gwagwa-lada	0.853375	-0.03592
19	Ikeja-West	0.996943	0.001354
20	Ikot Ekpene	0.988973	-0.01895
21	Jebba TS	1.000000	0
22	Jebba GS	1.000000	0.00215
23	Jos	0.966434	-0.04046
24	Kaduna	0.971423	-0.03687
25	Kainji GS	1.000000	0.00781
26	Kano	0.825577	-0.20071
27	Katampe	0.973536	0.03586
28	Lokoja	0.970445	-0.03763
29	Makurdi	0.972167	-0.03443

30	New Haven	0.985259	-0.01984

31	Okpai	0.998001	-0.03763
32	Olorunsogo	0.778346	-0.47321
33	Omotosho	0.772546	-0.72907
34	Onitsha	0.992507	-0.01132
35	Osogbo	0.994828	-0.00446
36	Papalanto	0.963277	-0.04365
37	Sapele	0.704592	-0.53658
38	Shiroro	0.818990	-0.90286
39	Ugwuaji	0.981078	0.02538
40	Yola	0.995245	-0.04763

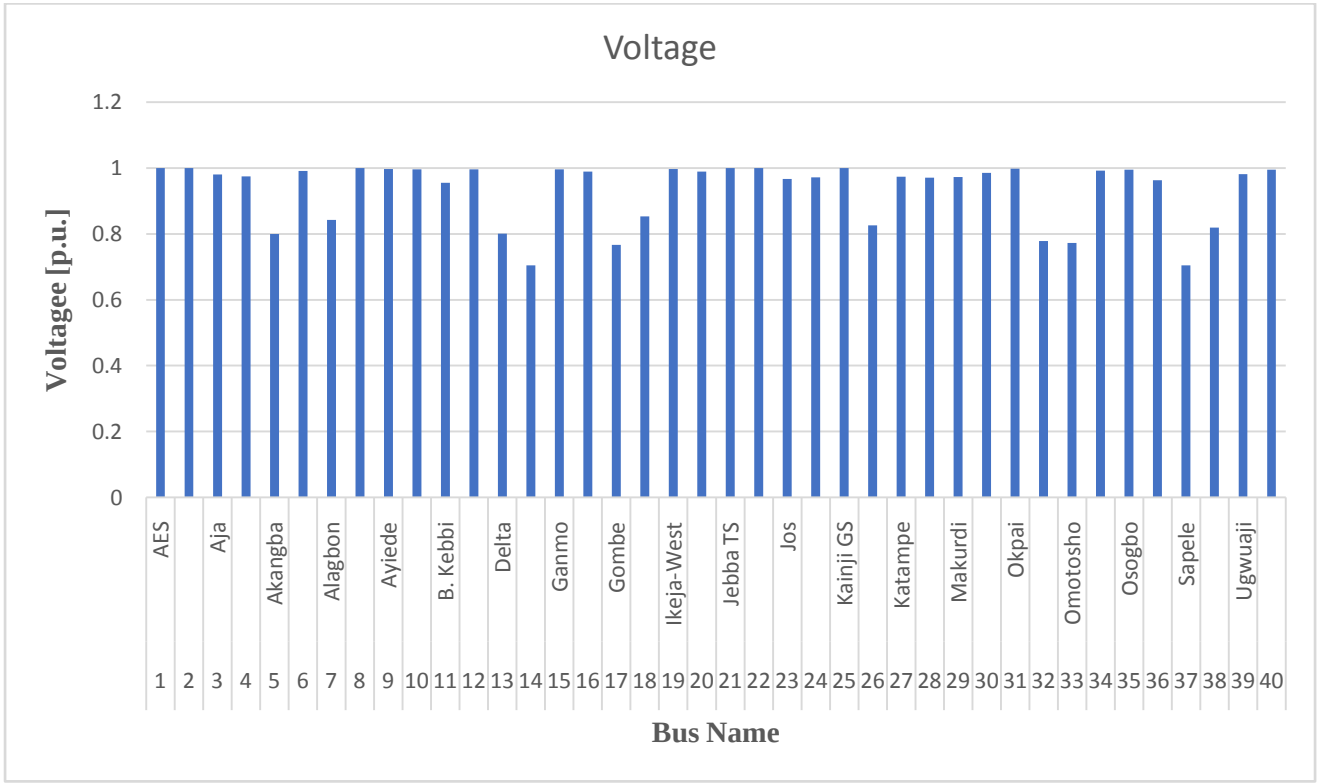

Figure 4.4 Nigeria 330kV Transmission Line Bus Voltage Profile During Occurrence of a Three Phase Fault on Makurdi Bus

4.2.2 Scenario Two: Three Phase Fault at Ajaokuta Bus

In this scenario, a three-phase fault was created on Ajaokuta bus (Bus 4) with line Ajaokuta – Benin (4-10) removed. Figures 4.5 and 4.6 show the dynamics responses of the generators for CCT of 300ms. Figures 4.5 and 4.6 show the plot of the power angle curves and the frequency responses of the eleven generators in the system during a transient three-phase fault on Ajaokuta to Benin transmission line. It can be observed that generators at Geregu, Sapele, Delta, Okpai and Afam buses were most critically disturbed and failed to recover after the fault was cleared at 0.3 seconds. These five generators in the system lost synchronism and became unstable as shown in Figures 4.5 and 4.6.

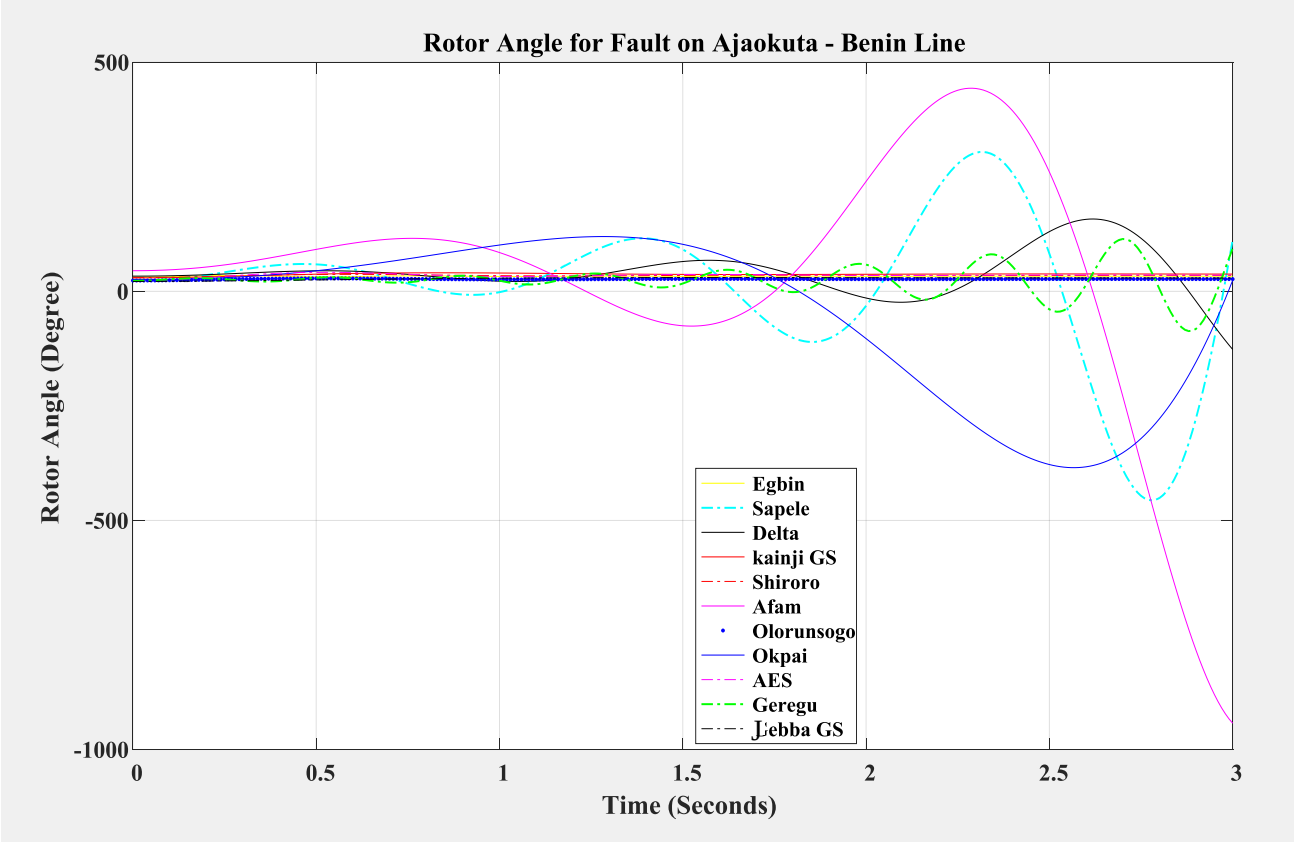

Figure 4.5: Rotor Angle response of the generators for fault clearing time of 0.3sec without any VSC-HVDC

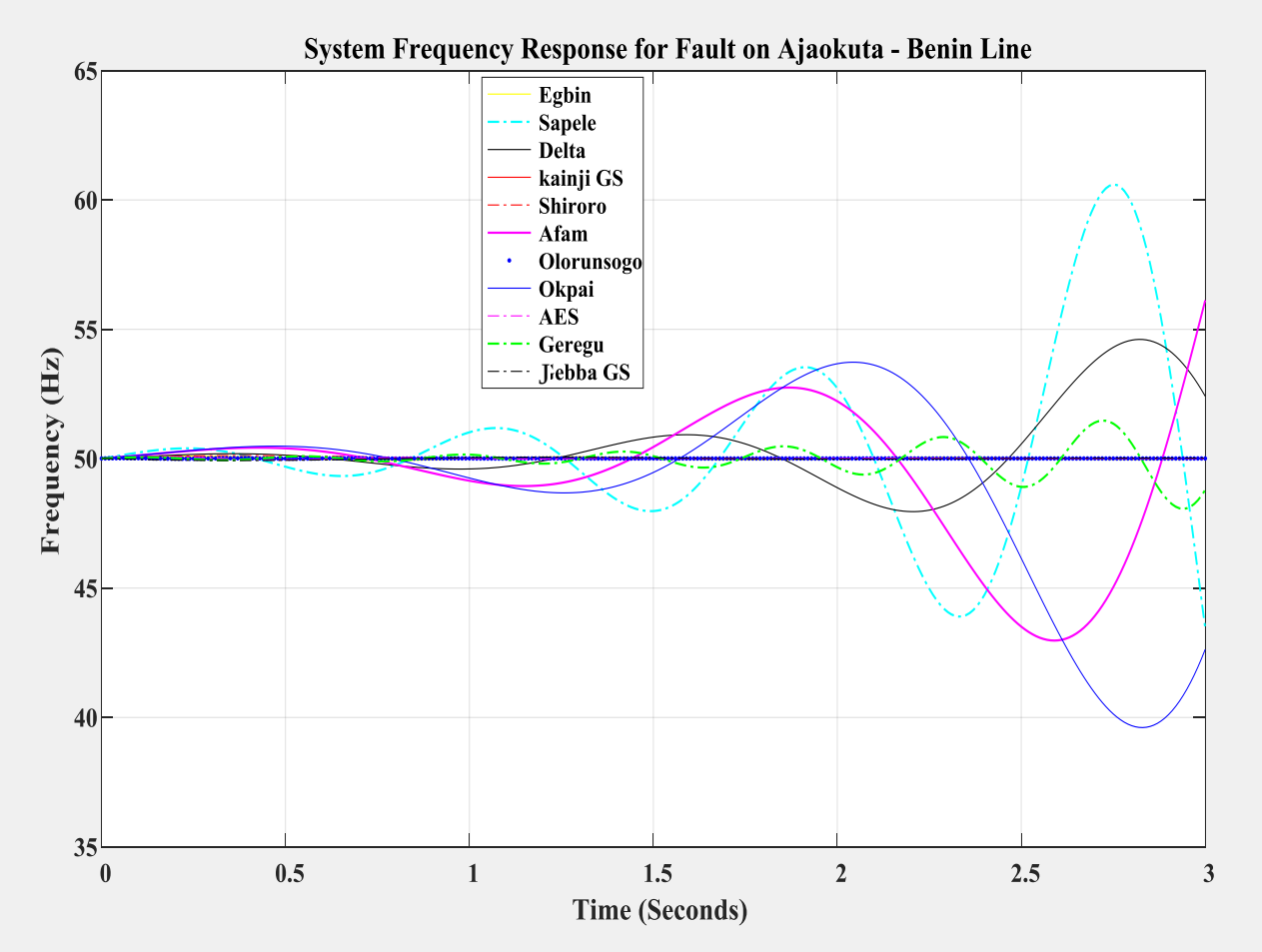

Figure 4.6: Frequency response of the system generators for fault clearing time of 0.3sec without any VSC-HVDC

The voltage profile results of the Nigerian 40-bus 330kV transmission system after the occurrence of the fault are shown in Table 4.4 as obtained from the power flow analysis of the network in PSAT environment. It can be observed from Table 4.4 and Figure 4.7 that there are serious voltage violations at buses 1 (AES), 2 (Afam), 13 (Delta), 16 (Geregu), 31 (Okpai), 32 (Olorunsogbo) and 37 (Sapele). The voltage magnitudes at these buses are lower than the acceptable voltage limit of ±10% for the Nigerian 330kV transmission system.

Table 4.4: The Load Flow Result of System Bus (Voltage Profile) during Occurrence of a Three Phase Fault on Ajaokuta Bus

Bus No	Bus Name	Voltage [p.u.]	Phase Angle [rad]
1	AES	0.773990	0.02390
2	Afam	0.822780	-0.00125
3	Aja	0.998480	0.006284
4	Ajaokuta	0.989621	-0.00676
5	Akangba	0.805418	-0.10014
6	Aladja	0.996952	-0.00231
7	Alagbon	0.842001	-0.03763
8	Alaoji	1.000000	-0.00962
9	Ayiede	0.996654	0.001761
10	Benin	0.995594	-0.00382
11	B. Kebbi	0.955445	-0.04433
12	Damaturu	0.996001	0.001354
13	Delta	0.821045	0.000607
14	Egbin	1.000000	0.007773
15	Ganmo	0.995887	-0.00372
16	Geregu	0.798931	-0.00382
17	Gombe	0.766327	-0.04365
18	Gwagwa-lada	0.853375	-0.03592
19	Ikeja-West	0.996943	0.001354
20	Ikot Ekpene	0.988973	-0.01895
21	Jebba TS	1.000000	0
22	Jebba GS	1.000000	0.00215
23	Jos	0.966434	-0.04046
24	Kaduna	0.971423	-0.03687
25	Kainji GS	1.000000	0.007816
26	Kano	0.825577	-0.20071
27	Katampe	0.973536	-0.03586
28	Lokoja	0.970445	-0.03763
29	Makurdi	0.972167	-0.03443
30	New Haven	0.985259	-0.01984

Table 4.4 Cont'd: The Load Flow Result of System Bus (Voltage Profile) during Occurrence of a Three Phase Fault on Ajaokuta Bus

31	Okpai	0.816998	-0.00953
32	Olorunsogo	0.783557	0.04615
33	Omotosho	0.772546	-0.72907
34	Onitsha	0.992507	-0.01132
35	Osogbo	0.994828	-0.00446
36	Papalanto	0.963277	-0.04365
37	Sapele	0.873953	-0.00113
38	Shiroro	0.818990	-0.90286
39	Ugwuaji	0.981078	-0.02538
40	Yola	0.995245	-0.04763

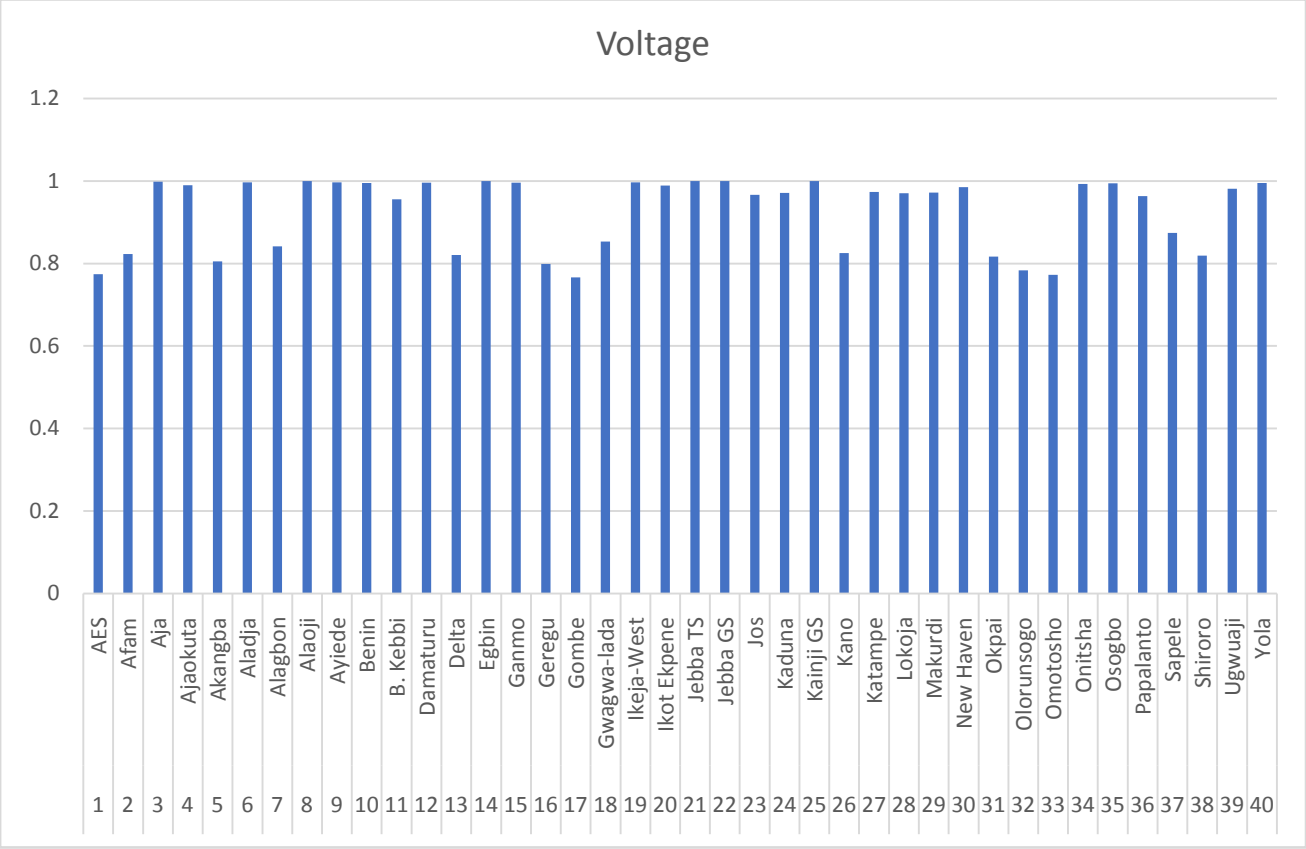

Figure 4.7 Nigeria 330kV Transmission Line Bus Voltage Profile During Occurrence of a Three Phase Fault on Ajaokuta Bus

4.2.3 Scenario Three: Three Phase Fault at Benin Bus

A three-phase fault was created on Benin bus (Bus 10) with line Benin – Ikeja West (10- 19) removed by the circuit breakers (CBs) at both ends opening to remove the faulted line from the system. Figures 4.8 and 4.9 show the dynamics responses of the generators for CCT of 300ms. Figures 4.8 and 4.9 show the plot of the power angle curves and the frequency responses of the eleven generators in the system during a transient three-phase fault on Benin to Ikeja West transmission line. It can be observed that virtually all generators in the system at were critically disturbed and all failed to recover after the fault was cleared at 0.3seconds. So, the system lost synchronism and became unstable as shown in Figures 4.8 and 4.9.

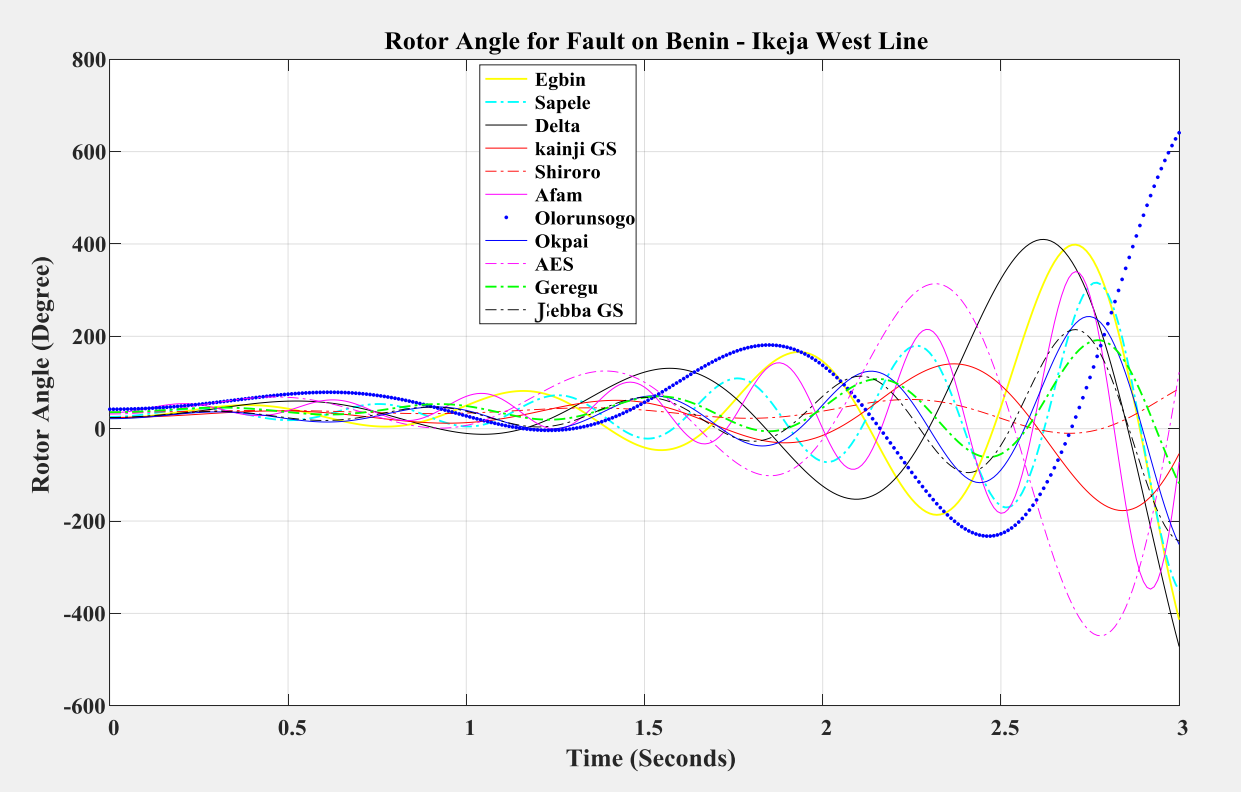

Figure 4.8: Rotor Angle response of the generators for fault clearing time of 0.3sec without any VSC-HVDC

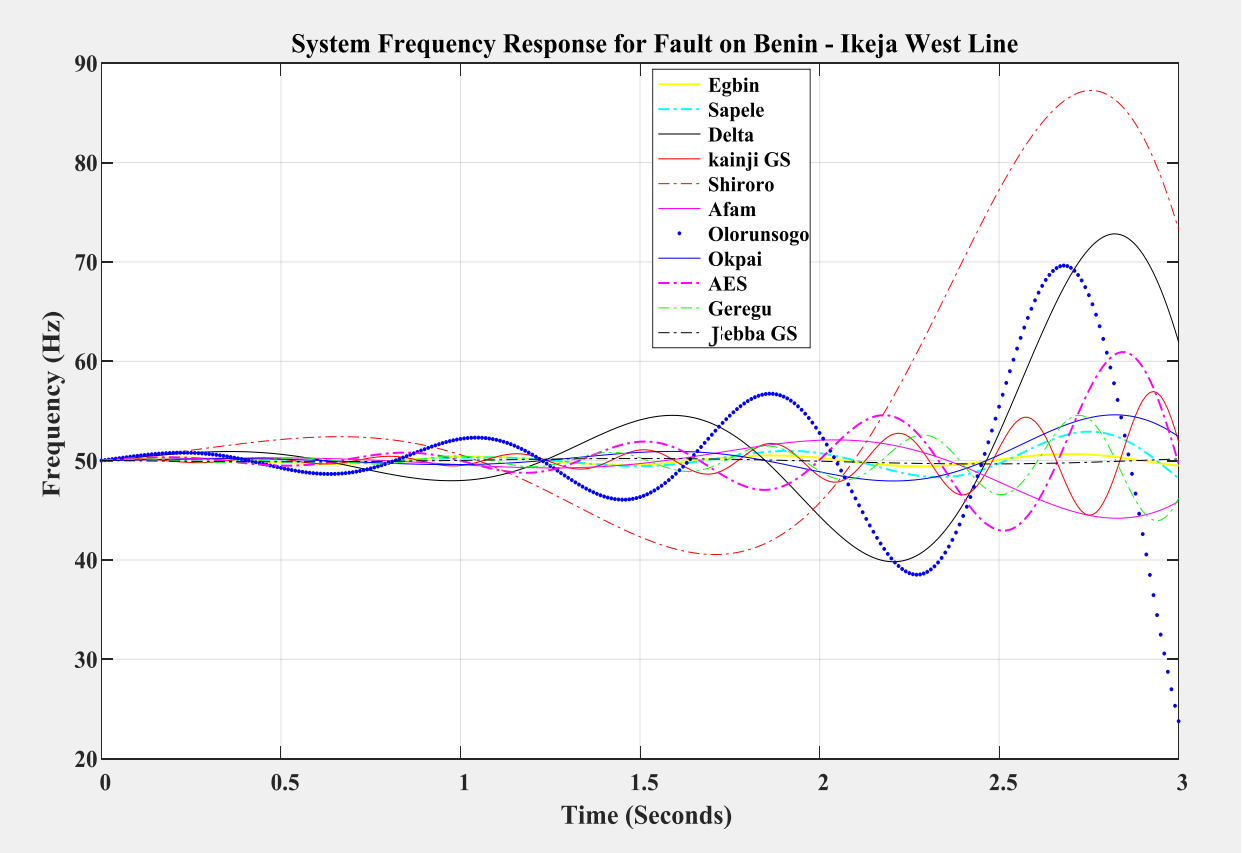

Figure 4.9: Frequency response of the system generators for fault clearing time of 0.3 sec without any VSC-HVDC

4.3 Response of the Nigeria 330kV Transmission Grid to Occurrence of a Three-Phase Fault with HVDC Installed in the Unstable Buses

Here, a VSC-HVDC is being controlled by the convectional PI method and not by the artificial neural network. As aforementioned, the simulation results are carried out on the MATLAB/PSAT environment. The idea is to see the effect of the HVDC, acting as a typical FACTS device, on the transient stability of the system during occurrence of a three-phase transient fault and also on the bus voltage violations.

Again, the demonstration for the transient stability improvement on the Nigeria 330-kV grid network, in this section, considered three scenarios used in the previous section. A 3-phase fault was created at each of the three locations and the swing equations are solved to obtain the network conditions for both during-fault and post-fault using numerical solver ode45. The numerical solver, ode45, which is a built-in MATLAB function, is employed in solving the *m*-number of swing equations within the system.

4.3.1 Scenario One: Three Phase Fault at Makurdi Bus

In this scenario, a VSC-HDVC was now installed in complementary or addition to Makurdi – Jos transmission line. As before, a three-phase fault was created on Makurdi bus (Bus 29) with line Makurdi – Jos (29-23) removed. That is the three-phase fault was cleared by the circuit breakers (CBs) at both ends opening to remove the faulted line from the system. Figures 4.10 and 4.11 show the dynamics responses of the generators for CCT of 300ms.

Figures 4.10 and 4.11 show the plot of the power angle curves and the frequency responses of the eleven generators in the system during a transient three-phase fault on Makurdi to Jos transmission line. It can be observed that those four generators at Opkai and Afam buses which were most critically disturbed and failed to recover after the fault was cleared at 0.3 seconds during a fault occurrence without VSC-HVDC, are now being held stable. This is attributed to the fact that the VSC-HVDC was able to inject enough power in the two buses (Bus 29 - 23).

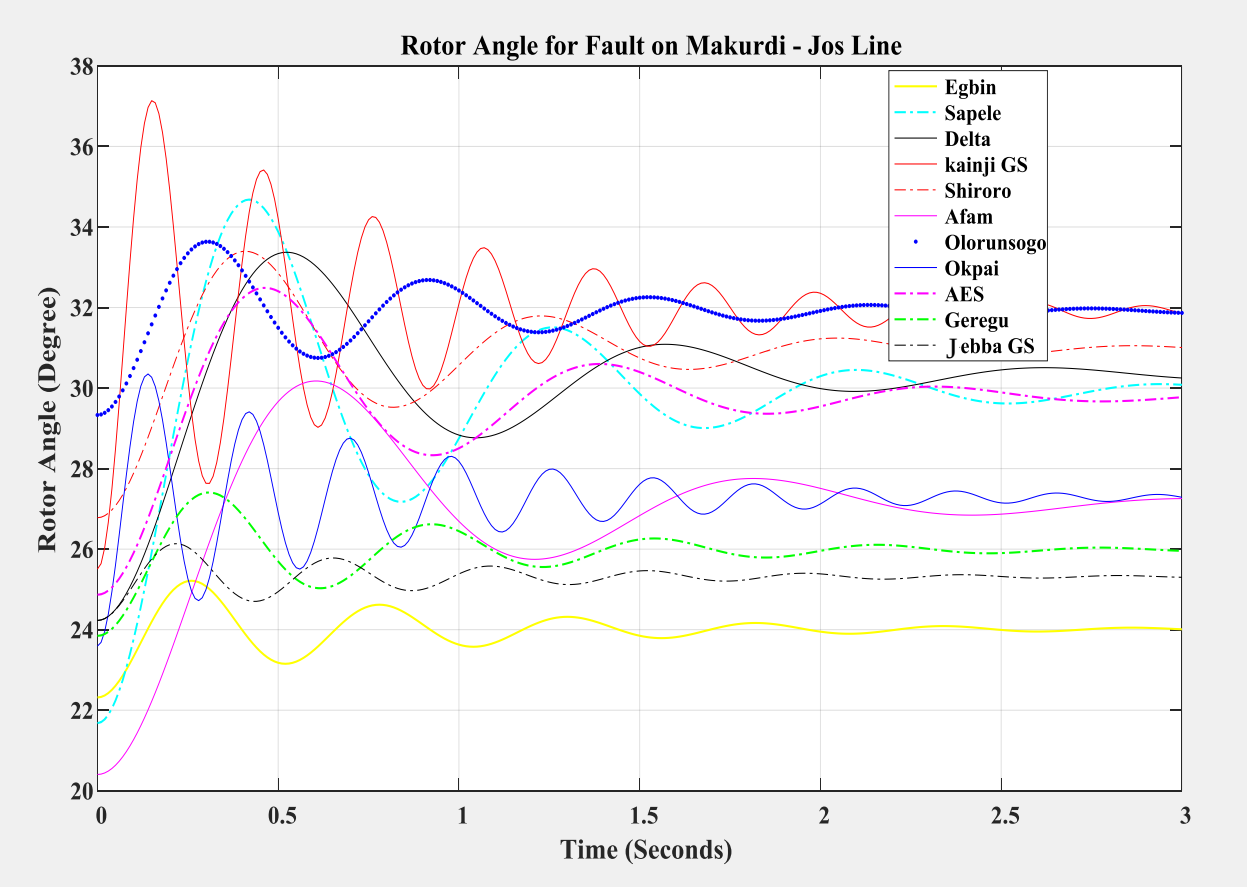

Figure 4.10: Rotor Angle response of the generators for fault clearing time of 0.3 sec (with only VSC-HVDC)

Hence, with the HVDC in the system the transient stability of the system has been improved as can be seen from the plot of the frequency and the power angle of the system generators in Figures 4.11 and 4.10 respectively.

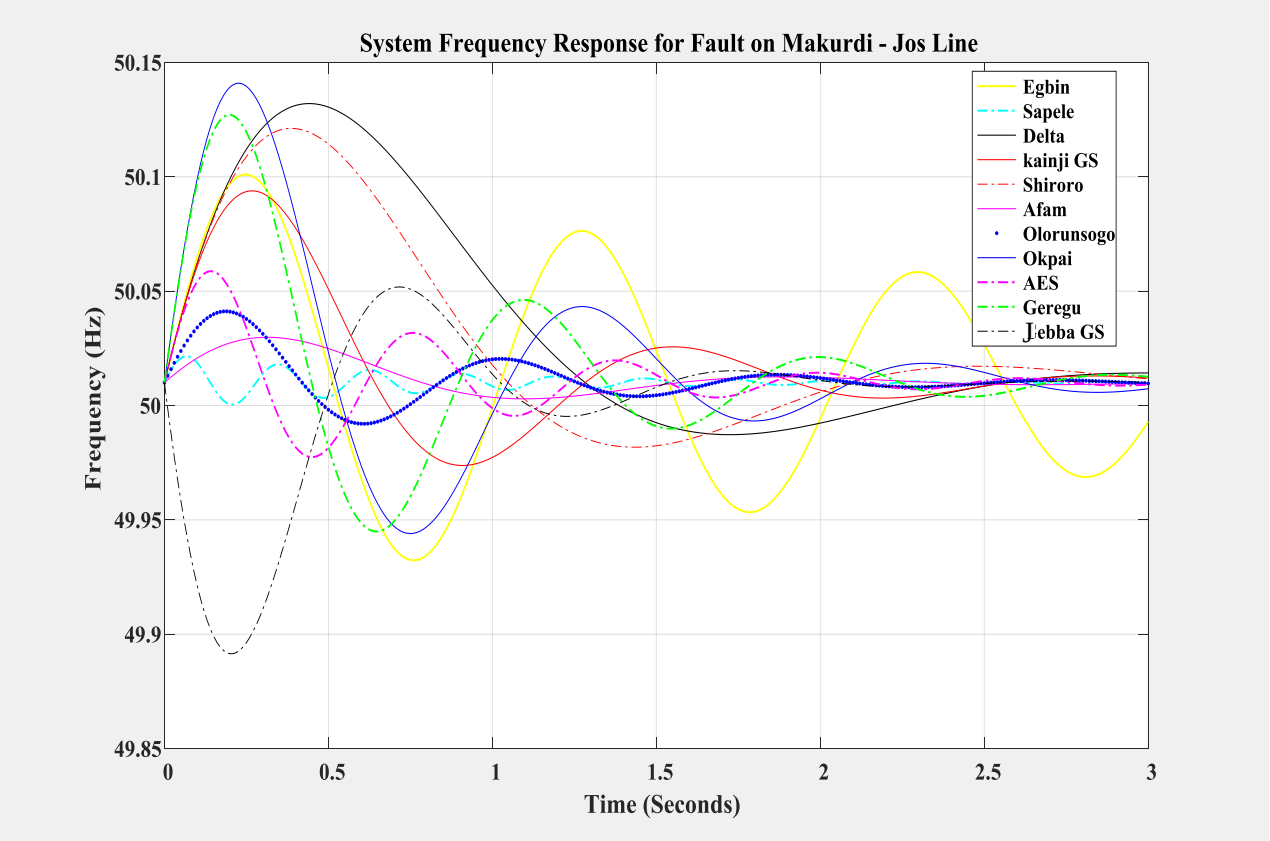

Figure 4.11: Frequency response of the system generators for fault clearing time of 0.3 sec (with only VSC-HVDC)

The voltage profile results of the Nigerian 40-bus 330kV transmission system with VSC-HVDC installed between Makurdi to Jos bus after the occurrence of the fault are shown in Table 4.5 as obtained from the power flow analysis of the network in PSAT environment. It can be observed from Table 4.5 and Figure 4.12 that the voltage violations at buses 5 (Akangba), 7 (Alagbon), 13 (Delta), 14 (Egbin), 32 (Olorunsogbo), 33 (Omotosho) and 37 (Sapele) as obtained previously have been corrected except for bus 26. The voltage magnitudes at these buses are now within the acceptable voltage limit of ±10% for the Nigerian 330kV transmission system. This is as result of the reactive power capability of the HVDC.

Table 4.5: The Load Flow Result of System Bus (Voltage Profile) during Occurrence of a Three Phase Fault on Makurdi Bus with VSC-HVDC Installed

Bus No	Bus Name	Voltage [p.u.]	Phase Angle [rad]
1	AES	1.000000	0.016368
2	Afam	1.000000	-0.00533
3	Aja	0.998480	0.006284
4	Ajaokuta	0.989621	-0.00676
5	Akangba	0.905418	-0.10014
6	Aladja	0.996952	-0.00231
7	Alagbon	0.889001	-0.03763
8	Alaoji	1.000000	-0.00962
9	Ayiede	0.996654	0.001761
10	Benin	0.995594	-0.00382
11	B. Kebbi	0.955445	-0.04433
12	Damaturu	0.996001	0.001354
13	Delta	0.958990	0.006702
14	Egbin	0.979887	0.071775
15	Ganmo	0.995887	-0.00372
16	Geregu	0.989101	-0.00231
17	Gombe	0.966327	-0.04365
18	Gwagwa-lada	0.853375	-0.03592
19	Ikeja-West	0.996943	0.001354
20	Ikot Ekpene	0.988973	-0.01895
21	Jebba TS	1.000000	0.00040
22	Jebba GS	1.000000	0.00215
23	Jos	0.966434	-0.04046
24	Kaduna	0.971423	-0.03687
25	Kainji GS	1.000000	0.007816
26	Kano	0.825577	-0.20071
27	Katampe	0.973536	-0.03586
28	Lokoja	0.970445	-0.03763
29	Makurdi	0.972167	-0.03443
30	New Haven	0.985259	-0.01984
31	Okpai	0.998001	-0.03763
32	Olorunsogo	0.971031	0.04615
33	Omotosho	0.907546	-0.72907
34	Onitsha	0.892507	-0.01132

Table 4.5 Cont'd: The Load Flow Result of System Bus (Voltage Profile) during Occurrence of a Three Phase Fault on Makurdi Bus with VSC-HVDC Installed

35	Osogbo	0.994828	-0.00446
36	Papalanto	0.963277	-0.04365
37	Sapele	0.968700	-0.00190
38	Shiroro	0.918990	-0.90286
39	Ugwuaji	0.981078	-0.02538
40	Yola	0.995245	-0.04763

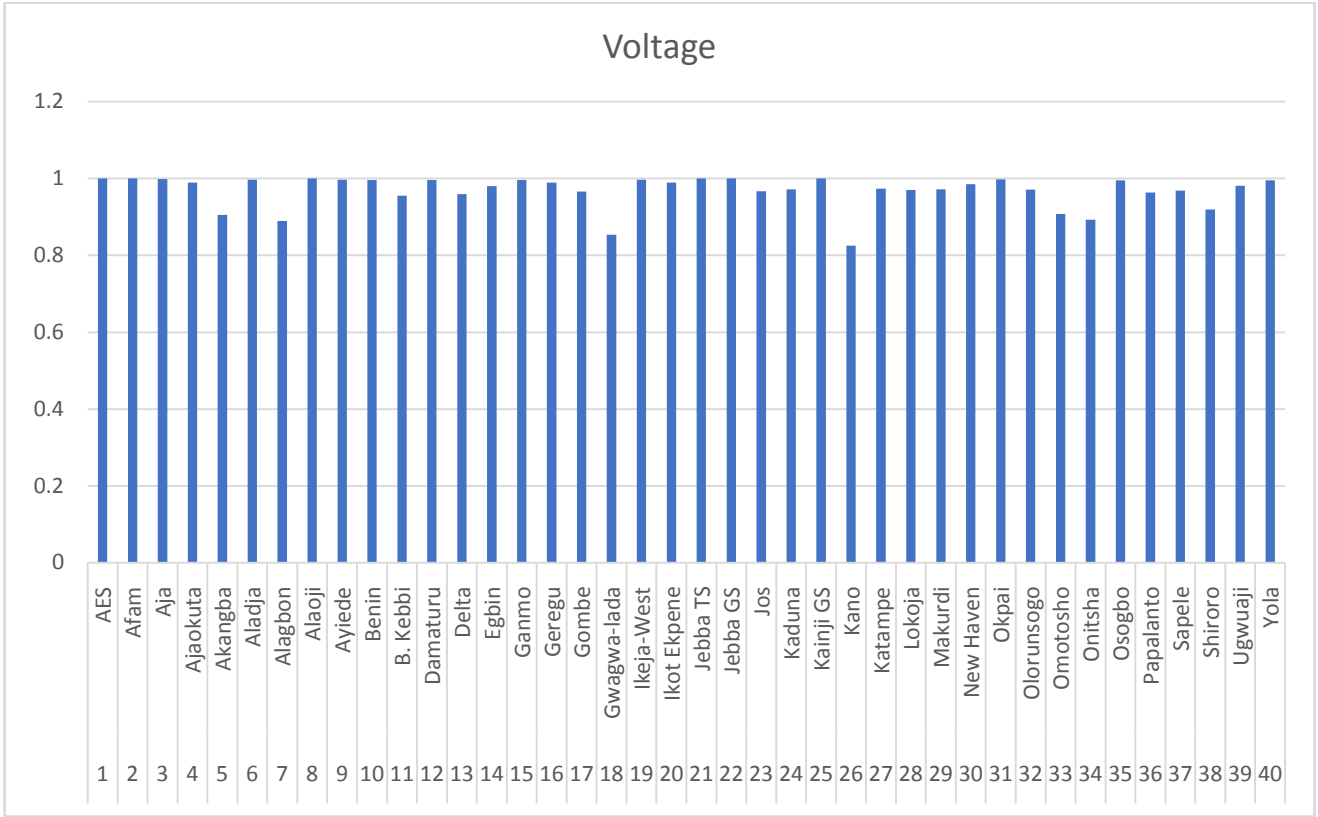

Figure 4.12: Nigeria 330kV Transmission Line Bus Voltage Profile During Occurrence of a Three Phase Fault on Makurdi Bus with VSC-HVDC Installed

4.3.2 Scenario Two: Three Phase Fault at Ajaokuta Bus

In this case, a VSC-HDVC was now installed in complementary or addition to Ajaokuta – Benin transmission line. As before, a three-phase fault was created on Ajaokuta bus (Bus 4) with line Ajaokuta – Benin (4 - 10) removed, by the circuit breakers (CBs) at both ends opening to remove the faulted line from the system. Figures 4.13 and 4.14 show the dynamics responses of the generators for CCT of 300ms.

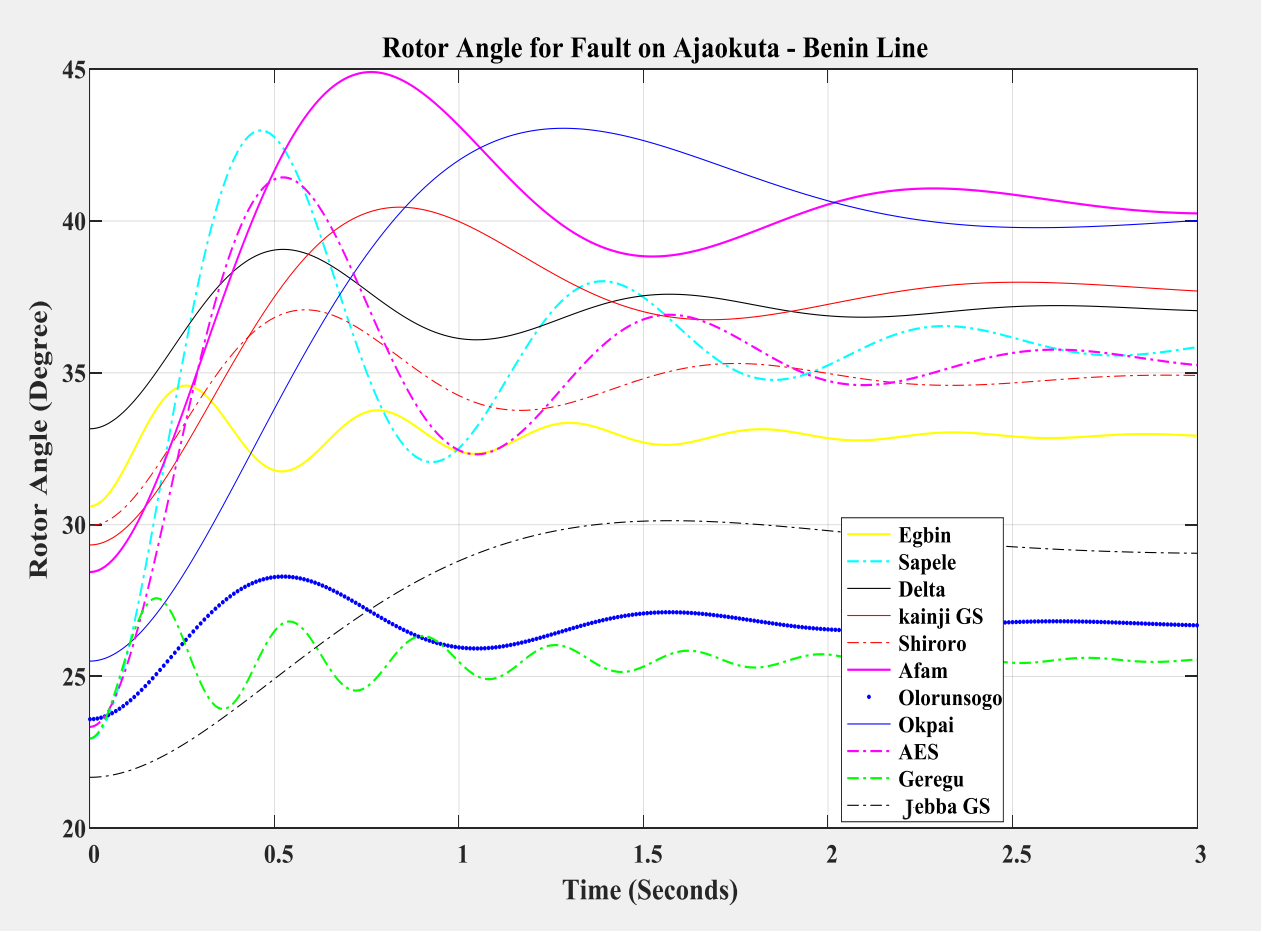

Figure 4.13: Rotor Angle response of the generators for fault clearing time of 0.3 sec with only VSC-HVDC

Figures 4.13 and 4.14 show the plot of the power angle curves and the frequency responses of the eleven generators in the system during a transient three-phase fault on Ajaokuta to Benin

transmission line. It can be observed that those generators at Geregu, Sapele, Delta, Okpai and Afam buses which were most critically disturbed and failed to recover after the was cleared at 0.3seconds during a fault occurrence without VSC-HVDC, are now being held stable. Which again, is attributed to the fact that the VSC-HVDC was able to inject enough power in the two buses (Bus 4 - 10). Hence, with the HVDC in the system the transient stability of the system has been improved as can be seen from the plot of the frequency and the rotor angle of the system generators in Figures 4.13 and 4.14 respectively.

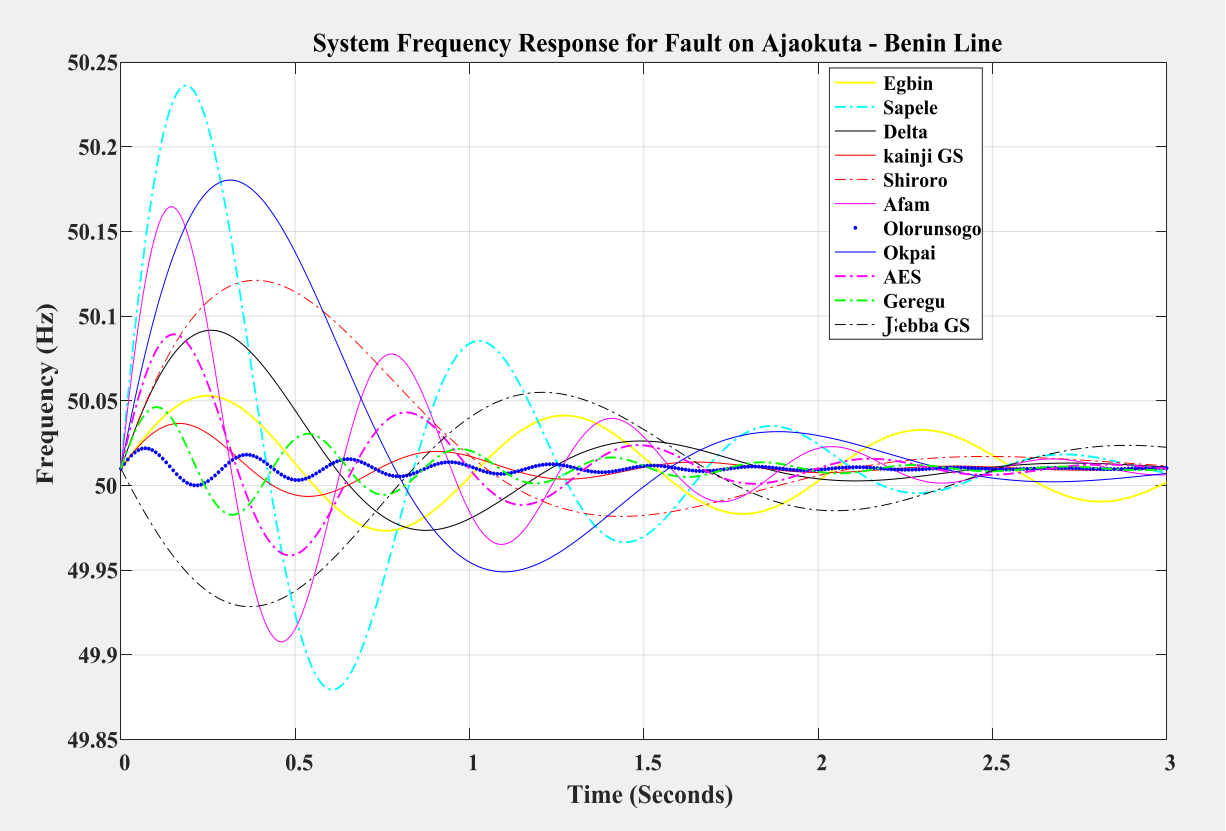

Figure 4.14: Frequency response of the system generators for fault clearing time of 0.3 sec with only VSC-HVDC

The voltage profile results of the Nigerian 40-bus 330kV transmission system with VSC-HVDC installed between Ajaokuta to Benin bus after the occurrence of the fault are shown in Table 4.6 as obtained from the power flow analysis of the network in PSAT environment. It can be

observed from Table 4.6 and Figure 4.15 that the voltage violations at buses 1 (AES), 2 (Afam), 13 (Delta), 16 (Geregu), 31 (Okpai), 32 (Olorunsogbo) and 37 (Sapele) as obtained previously have been corrected. The voltage magnitudes at these buses are now within the acceptable voltage limit of ±10% for the Nigerian 330kV transmission system. This is as result of the reactive power capability of the HVDC.

Table 4.6: The Load Flow Result of System Bus (Voltage Profile) during Occurrence of a Three Phase Fault on Ajaokuta Bus with VSC-HVDC Installed

Bus No	Bus Name	Voltage [p.u.]	Phase Angle [rad]
1	AES	0.905738	0.02336
2	Afam	0.909903	-0.01134
3	Aja	0.998480	0.006284
4	Ajaokuta	0.989621	-0.00676
5	Akangba	0.805418	-0.10014
6	Aladja	0.996952	-0.00231
7	Alagbon	0.842001	-0.03763
8	Alaoji	1.000000	-0.00962
9	Ayiede	0.996654	0.001761
10	Benin	0.995594	-0.00382
11	B. Kebbi	0.955445	-0.04433
12	Damaturu	0.996001	0.001354
13	Delta	0.922923	0.00146
14	Egbin	1.000000	0.007773
15	Ganmo	0.995887	-0.00372
16	Geregu	0.919679	-0.00953
17	Gombe	0.766327	-0.04365

Table 4.6 Cont'd: The Load Flow Result of System Bus (Voltage Profile) during Occurrence of a Three Phase Fault on Ajaokuta Bus with VSC-HVDC Installed

18	Gwagwa-lada	0.853375	-0.03592
19	Ikeja-West	0.996943	0.001354
20	Ikot Ekpene	0.988973	-0.01895
21	Jebba TS	1.000000	0.0004
22	Jebba GS	1.000000	0.00215
23	Jos	0.966434	-0.04046
24	Kaduna	0.971423	-0.03687
25	Kainji GS	1.000000	0.007816
26	Kano	0.825577	-0.20071
27	Katampe	0.973536	-0.03586
28	Lokoja	0.970445	-0.03763
29	Makurdi	0.972167	-0.03443
30	New Haven	0.985259	-0.01984
31	Okpai	0.941849	-0.05617
32	Olorunsogo	0.919188	0.05615
33	Omotosho	0.772546	-0.72907
34	Onitsha	0.992507	-0.01132
35	Osogbo	0.994828	-0.00446
36	Papalanto	0.963277	-0.04365
37	Sapele	0.960770	-0.00380
38	Shiroro	0.818990	-0.90286
39	Ugwuaji	0.981078	-0.02538
40	Yola	0.995245	-0.04763

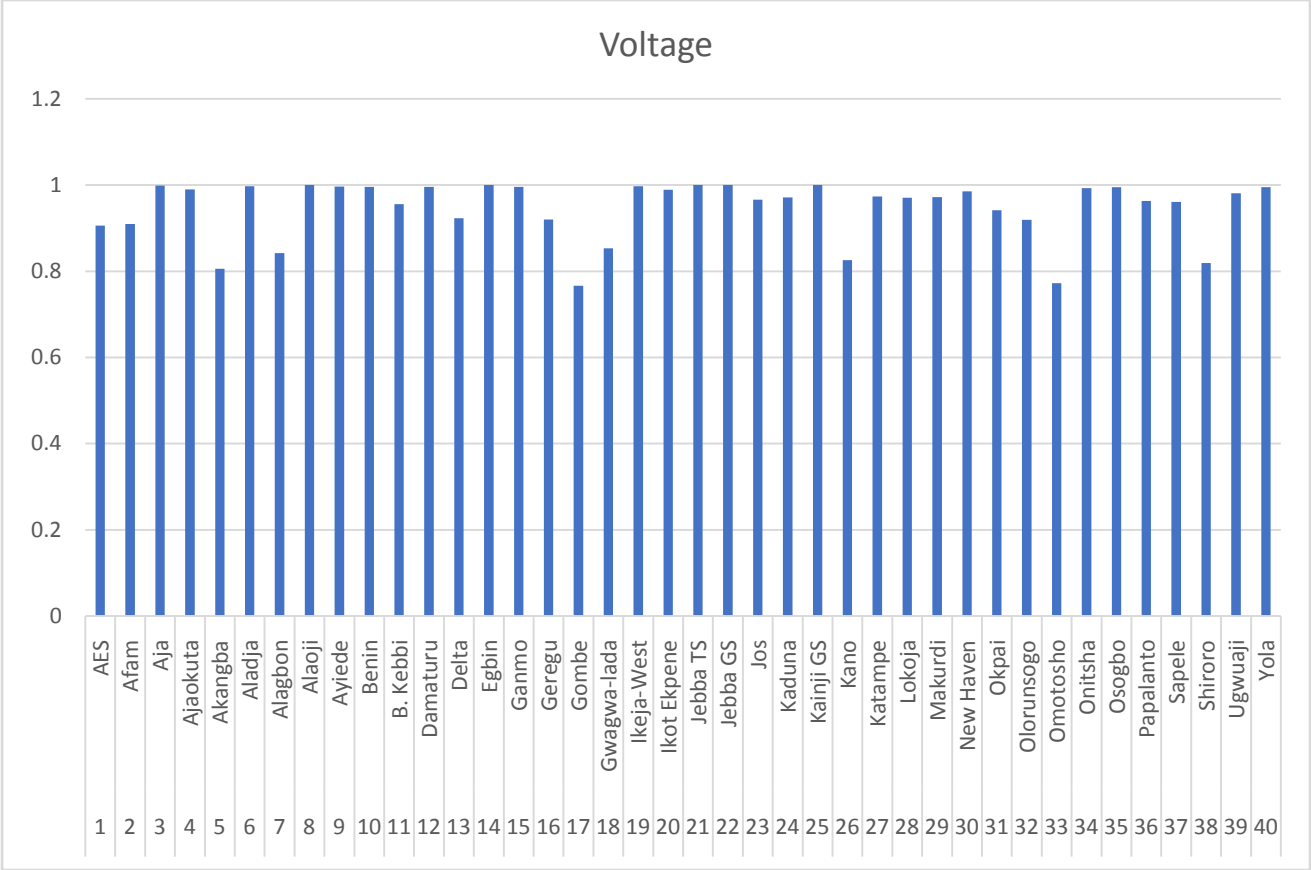

Figure 4.15: Nigeria 330kV Transmission Line Bus Voltage Profile During Occurrence of a Three Phase Fault on Ajaokuta Bus with VSC-HVDC Installed

4.3.3 Scenario Three: Three Phase Fault at Benin Bus

Here, the location of the VSC-HDVC was changed to complement Benin – Ikeja West transmission line. Again, a three-phase fault was created on Benin bus (Bus 10) with line Benin – Ikeja West (10- 19) removed, by the circuit breakers (CBs) at both ends opening to remove the faulted line from the system. Figures 4.16 and 4.17 show the dynamics responses of the generators for CCT of 300ms.

Figures 4.16 and 4.17 show the plot of the power angle curves and the frequency responses of the eleven generators in the system during a transient three-phase fault on Benin to Ikeja West transmission line. It can be observed that all the generators in the system which were critically disturbed and failed to recover after the fault was cleared at 0.3 seconds during a fault occurrence without VSC-HVDC in the system, are all stable. This again, is attributed to the fact that the VSC-HVDC was able to inject enough power in the two buses (Bus 10 - 19). Hence, with the HVDC in that position the transient stability of the system has been improved as can be seen from the plot of the frequency and the power angle of the system generators in Figures 4.16 and 4.17 respectively.

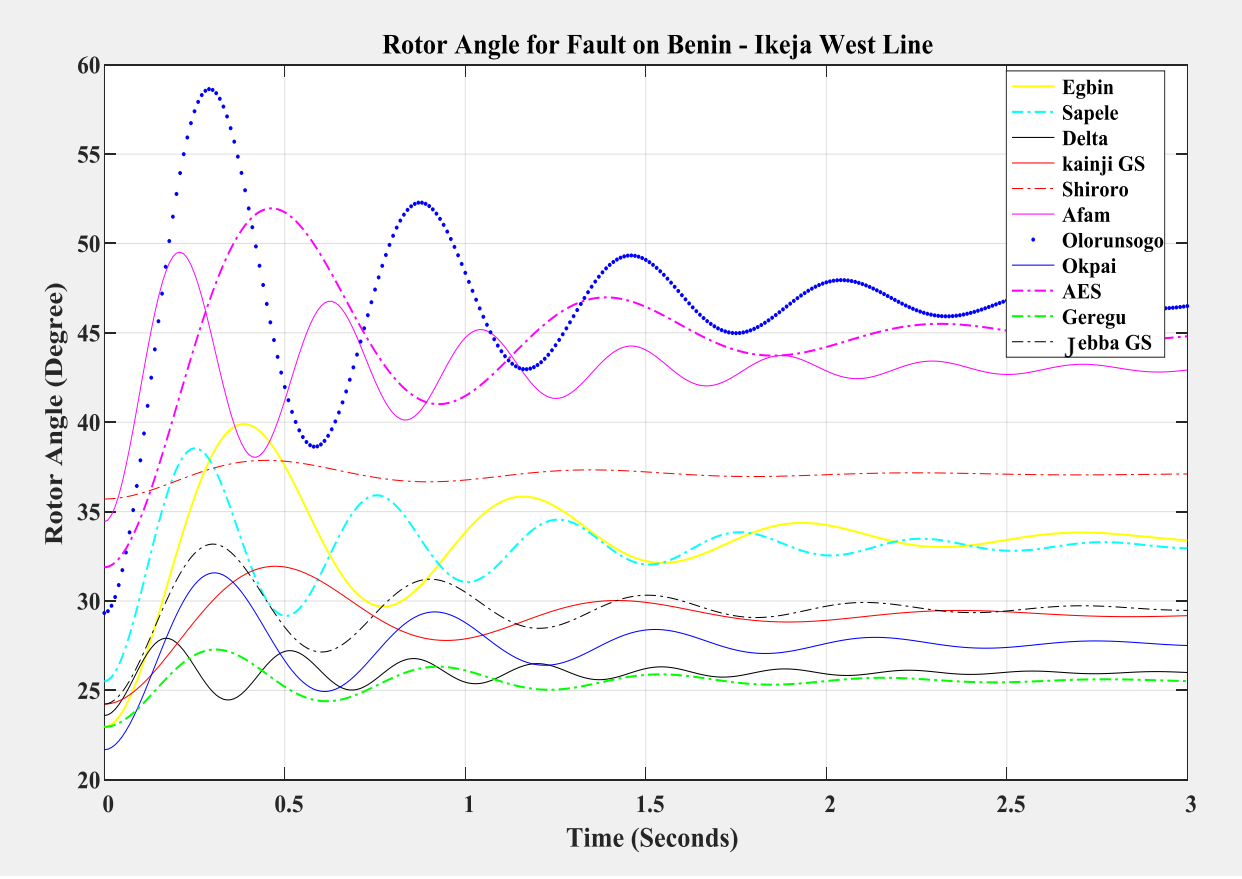

Figure 4.16: Power Angle response of the generators for fault clearing time of 0.3 sec with only VSC-HVDC

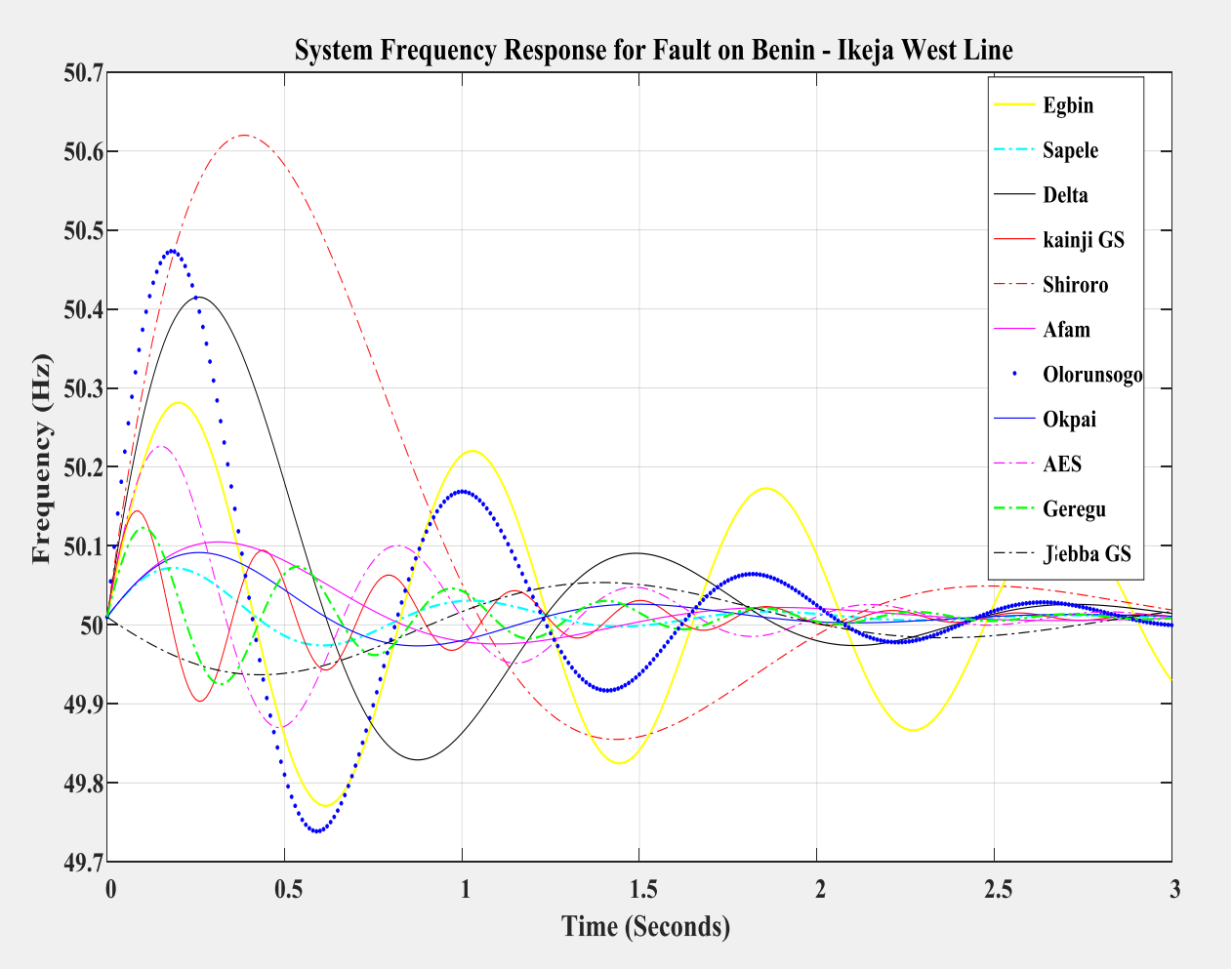

Figure 4.17: Frequency response of the system generators for fault clearing time of 0.3 sec with only VSC-HVDC

The voltage profile results of the Nigerian 40-bus 330kV transmission system with VSC-HVDC installed between Benin to Ikeja West bus after the occurrence of the fault are shown in Table 4.7 as obtained from the power flow analysis of the network in PSAT environment. It can be observed from Table 4.7 and Figure 4.18 that the voltage magnitudes at the bus voltages are now within the acceptable voltage limit of ±10% for the Nigerian 330kV transmission system. This is as result of the reactive power capability of the HVDC.

Table 4.7: The Load Flow Result of System Bus (Voltage Profile) during Occurrence of a Three Phase Fault on Benin Bus with VSC-HVDC Installed

Bus No	Bus Name	Voltage [p.u.]	Phase Angle [rad]
1	AES	0.930561	0.016368
2	Afam	0.905654	-0.00533
3	Aja	0.998480	0.006284
4	Ajaokuta	0.989621	-0.00676
5	Akangba	0.980541	-0.10014
6	Aladja	0.996952	-0.00231
7	Alagbon	0.984200	-0.03763
8	Alaoji	1.000000	-0.00962
9	Ayiede	0.936654	0.001761
10	Benin	0.995594	-0.00382
11	B. Kebbi	0.912544	-0.04433
12	Damaturu	0.996001	0.001354
13	Delta	0.934967	0.000672
14	Egbin	0.929967	0.007773
15	Ganmo	0.995887	-0.00372
16	Geregu	0.989101	-0.00231
17	Gombe	0.976632	-0.04365
18	Gwagwa-lada	0.953375	-0.03592
19	Ikeja-West	0.996943	0.001354
20	Ikot Ekpene	0.988973	-0.01895
21	Jebba TS	0.999967	0
22	Jebba GS	0.999967	0.00215
23	Jos	0.926433	-0.04046
24	Kaduna	0.971423	-0.03687
25	Kainji GS	1.000000	0.007816
26	Kano	0.982557	-0.20071
27	Katampe	0.973536	-0.03586
28	Lokoja	0.970445	-0.03763
29	Makurdi	0.972167	-0.03443
30	New Haven	0.985259	-0.01984
31	Okpai	0.998001	-0.03763
32	Olorunsogo	0.983565	0.61537
33	Omotosho	0.928672	-0.72907
34	Onitsha	0.907250	-0.01132

Table 4.7 Cont'd: The Load Flow Result of System Bus (Voltage Profile) during Occurrence of a Three Phase Fault on Benin Bus with VSC-HVDC Installed

35	Osogbo	0.994828	-0.00446
36	Papalanto	0.963279	-0.04365
37	Sapele	0.920670	-0.00019
38	Shiroro	0.998189	-0.90286
39	Ugwuaji	0.981078	-0.02538
40	Yola	0.939224	-0.04763

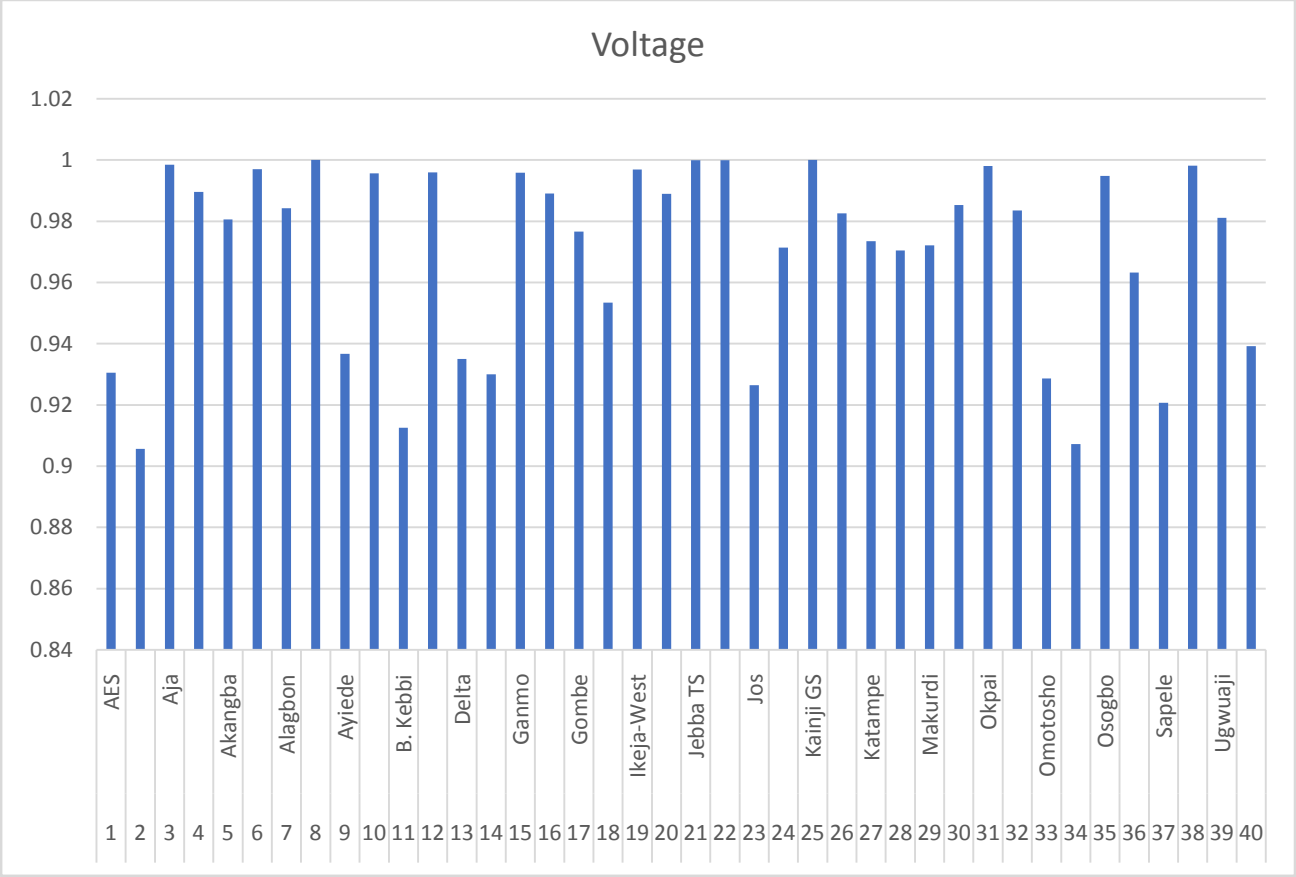

Figure 4.18: Nigeria 330kV Transmission Line Bus Voltage Profile During Occurrence of a Three Phase Fault on Benin Bus with VSC-HVDC Installed

4.4 Response of the Nigeria 330kV Transmission Grid to Occurrence of a Three-Phase Fault with ANN Controlled VSC-HVDC Installed in the Unstable Buses

Here, artificial neural network was used to regulate and control the parameters of the rectifier and the inverter of the VSC-HVDC instead of the convectional PI method. The idea is to see the effect of the HVDC, whose parameters are being controlled by neural network, on the transient stability of the system during occurrence of a three-phase transient fault and also on the bus voltage violations.

Again, the demonstration for the transient stability improvement on the Nigeria 330-kV grid network, in this section, considered three scenarios used in the previous sections. A three-phase fault was created at each of the three locations and the swing equations are solved to obtain the network conditions for both during-fault and post-fault using numerical solver ode45. The numerical solver, ode45, which is a built-in MATLAB function, is employed in solving the *m*-number of swing equations within the system. The CCTs for the three phase fault has been improved from 300ms to 200ms resulting to a 33.33% improvement.

4.4.1 Scenario One: Three Phase Fault at Makurdi Bus

In this scenario, a ANN controlled VSC-HDVC was now installed in addition to Makurdi – Jos transmission line. As before, a three-phase fault was created on Makurdi bus (Bus 29) with line Makurdi – Jos (29 - 23) removed. That is the three-phase fault was cleared by the circuit breakers (CBs) at both ends opening to remove the faulted line from the system. Figures 4.19 and 4.20 show the dynamics responses of the generators for CCT of 200ms.

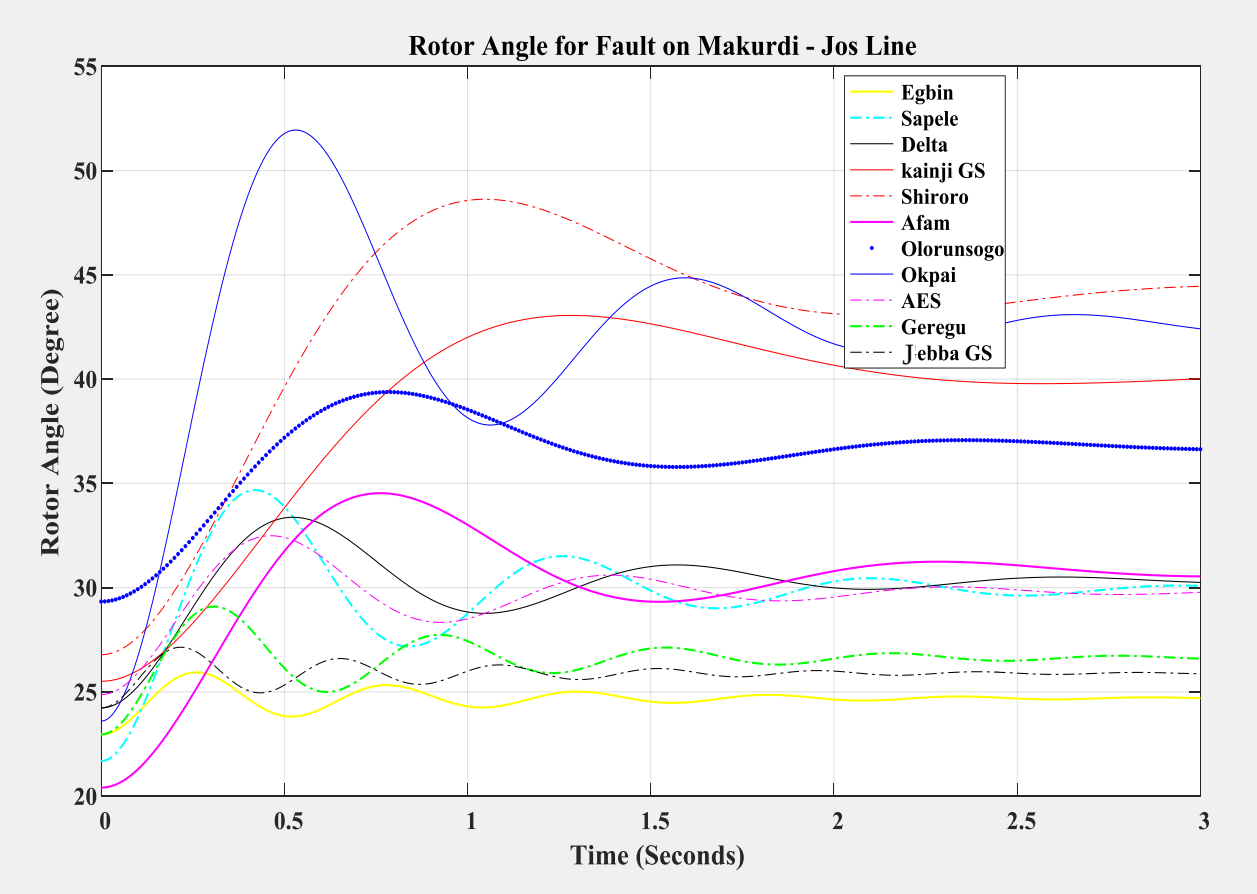

Figure 4.19: Rotor Angle response of the generators for fault clearing time of 0.2sec with ANN Controlled VSC-HVDC

Figures 4.19 and 4.20 show the plot of the power angle curves and the frequency responses of the eleven generators in the system during a transient three-phase fault on Makurdi to Jos transmission line. It can be observed that the oscillation of the generators at Opkai and Afam buses which were most critically disturbed during a fault occurrence without VSC-HVDC, along with other buses, have achieved faster damping. It can be observed that the CCT has been increased from 300 milli-seconds to 200 milli-seconds and also the oscillations were quickly damped compare to the results obtain when the VSC-HVDC was being controlled by the conventional PI method. This can be attributed to the intelligent response of the neural network

in controlling the parameters of the VSC-HVDC, which enabled to inject the needed power in the two buses (Bus 29 - 23) in time and most appropriately.

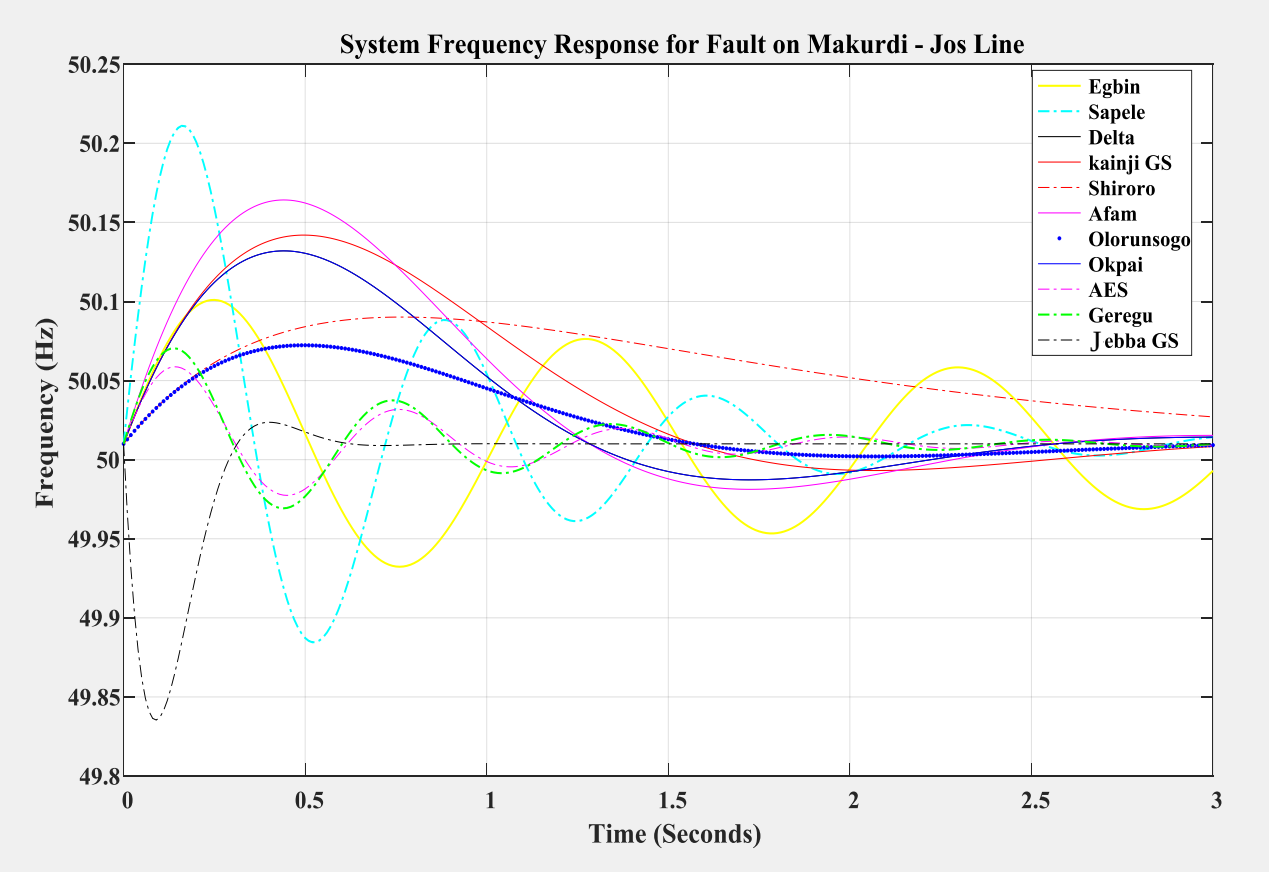

Figure 4.20: Frequency response of the system generators for fault clearing time of 0.2sec with ANN Controlled VSC-HVDC

Interestingly, it can be observed that a quick recharging of the DC-link capacitor due to a power injection created an additional damping of the post fault oscillations of the AC-side power angle and frequency oscillations, hence enhancing transient stability. Therefore, it could be said that from Figures 4.19 and 4.20, the transient stability of the system has been further improved with the intelligent HVDC in the system.

The voltage profile results of the Nigerian 40-bus 330kV transmission system with ANN Controlled VSC-HVDC installed between Makurdi to Jos bus after the occurrence of the fault are shown in Table 4.8 as obtained from the power flow analysis of the network in PSAT environment. It can be observed from Table 4.8 and Figure 4.21 that the voltage violations at buses 5, 7, 13, 14, 32, 33 and 37 which were 0.905418,0.889001,0.958990,0.979887,0.971031,0.907546 and 0.968700 as obtained previously when the VSC-HVDC was being controlled by the conventional PI method are now improved to 0.999541,0.999541, 1.001000, 0.999887, 0.989031, 0.997546 and 1.000000 respectively. This is as result of the intelligent response of the VSC-HVDC in injecting adequate reactive power timely.

Table 4.8: The Load Flow Result of System Bus (Voltage Profile) during Occurrence of a Three Phase Fault on Makurdi Bus with ANN Controlled VSC-HVDC Installed

Bus No	Bus Name	Voltage [p.u.]	Phase Angle [rad]
1	AES	1.000000	0.016368
2	Afam	1.000000	-0.00533
3	Aja	0.998480	0.006284
4	Ajaokuta	0.989621	-0.00676
5	Akangba	0.999541	-0.10014
6	Aladja	0.996952	-0.00231
7	Alagbon	0.889001	-0.03763
8	Alaoji	1.000000	-0.00962
9	Ayiede	0.996654	0.001761

Table 4.8 Cont'd: The Load Flow Result of System Bus (Voltage Profile) during Occurrence of a Three Phase Fault on Makurdi Bus with ANN Controlled VSC-HVDC Installed

10	Benin	0.995594	-0.00382
11	B. Kebbi	0.955445	-0.04433
12	Damaturu	0.996001	0.001354
13	Delta	1.001000	0.006702
14	Egbin	0.999887	0.071775
15	Ganmo	0.995887	-0.00372
16	Geregu	0.989101	-0.00231
17	Gombe	0.966327	-0.04365
18	Gwagwa-lada	0.853375	-0.03592
19	Ikeja-West	0.996943	0.001354
20	Ikot Ekpene	0.988973	-0.01895
21	Jebba TS	1.000000	0.00040
22	Jebba GS	1.000000	0.00215
23	Jos	0.966434	-0.04046
24	Kaduna	0.971423	-0.03687
25	Kainji GS	1.000000	0.007816
26	Kano	0.825577	-0.20071
27	Katampe	0.973536	-0.03586
28	Lokoja	0.970445	-0.03763
29	Makurdi	0.972167	-0.03443
30	New Haven	0.985259	-0.01984
31	Okpai	0.998001	-0.03763
32	Olorunsogo	0.989031	0.04615
33	Omotosho	0.997546	-0.72907
34	Onitsha	0.892507	-0.01132
35	Osogbo	0.994828	-0.00446
36	Papalanto	0.963277	-0.04365
37	Sapele	1.000000	-0.00190
38	Shiroro	0.918990	-0.90286
39	Ugwuaji	0.981078	-0.02538
40	Yola	0.995245	-0.04763

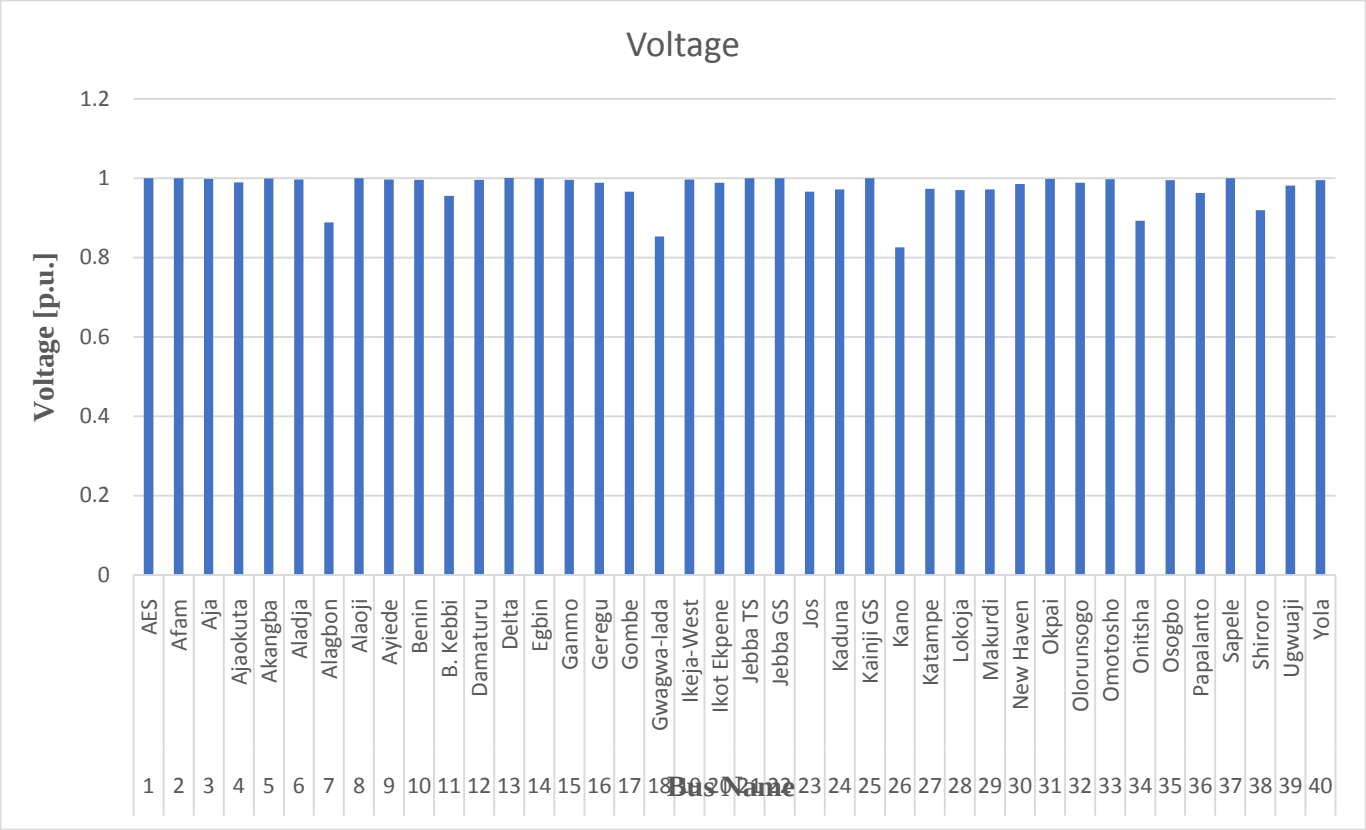

Figure 4.21: Nigeria 330kV Transmission Line Bus Voltage Profile During Occurrence of a Three Phase Fault on Makurdi Bus with ANN Controlled VSC-HVDC Installed

4.4.2 Scenario Two: Three Phase Fault at Ajaokuta Bus

Here, the position of the ANN controlled VSC-HDVC was changed to Ajaokuta – Benin transmission line. As before, a three-phase fault was created on Ajaokuta bus (Bus 4) with line Ajaokuta – Benin (4-10) removed by the CBs at both ends opening to remove the faulted line from the system. Figures 4.22 and 4.23 show the dynamics responses of the generators for CCT of 200ms.

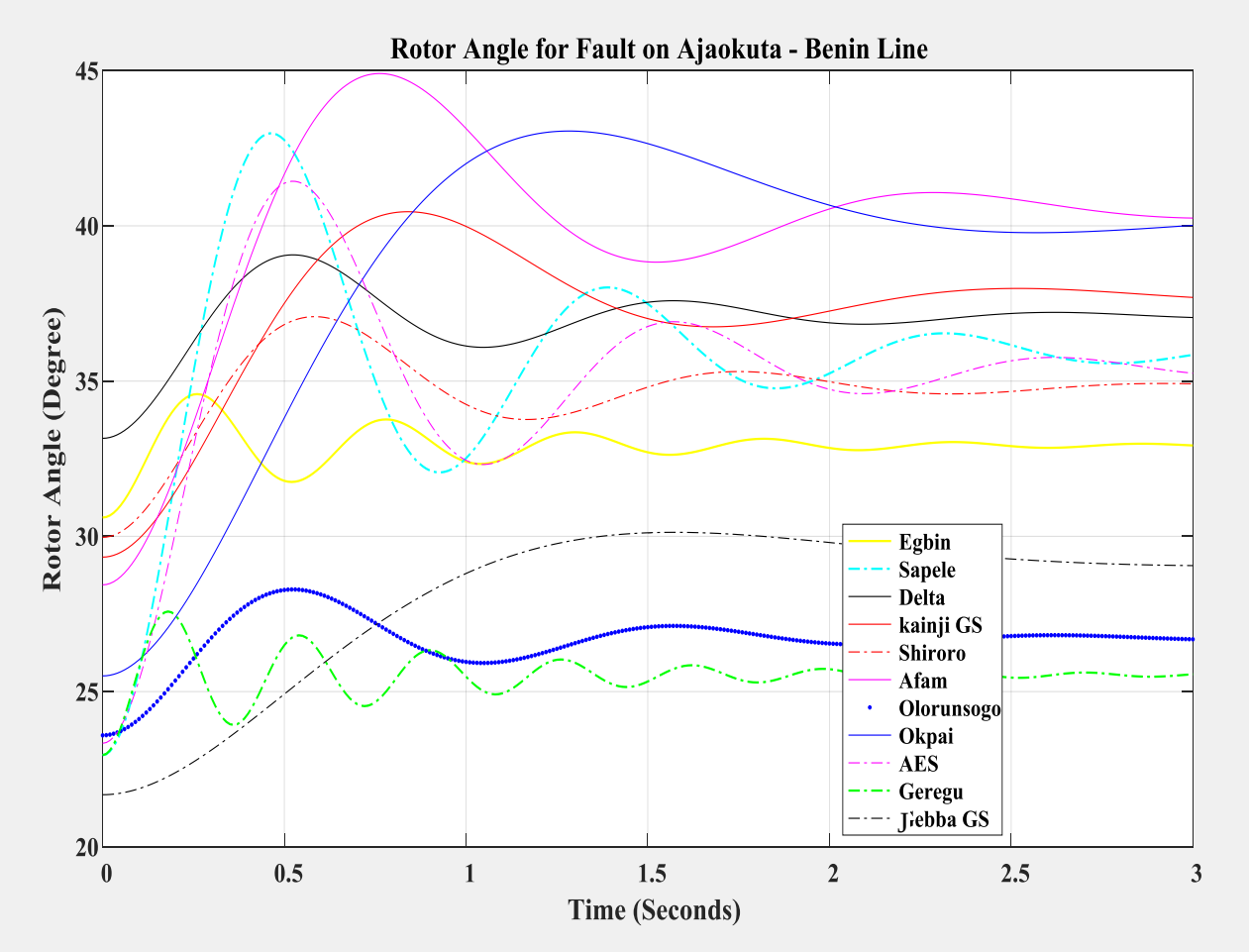

Figure 4.22: Rotor Angle response of the generators for fault clearing time of 0.2 sec with ANN Controlled VSC-HVDC

Figures 4.22 and 4.23 show the plot of the power angle curves and the frequency responses of the eleven generators in the system during a transient three-phase fault on Ajaokuta to Benin transmission line. It can be observed that the oscillation of those five generators at Geregu, Sapele, Delta, Okpai and Afam buses which were most critically disturbed during a fault occurrence without VSC-HVDC, along with other generators, have achieved faster damping. It can also be noted that the CCT has been increased from 300 milli-seconds to 200 milli-seconds

and also the oscillations were quickly damped compare to the results obtain when the VSC-HVDC was being controlled by the conventional PI method.

This, again can be attributed to the intelligent response of the neural network in controlling the parameters of the VSC-HVDC, which enabled to inject the needed power in the two buses (Bus 4 – 10) in time and most appropriately. Hence, from Figures 4.22 and 4.23, the transient stability of the system has been further improved with the intelligent HVDC in the system.

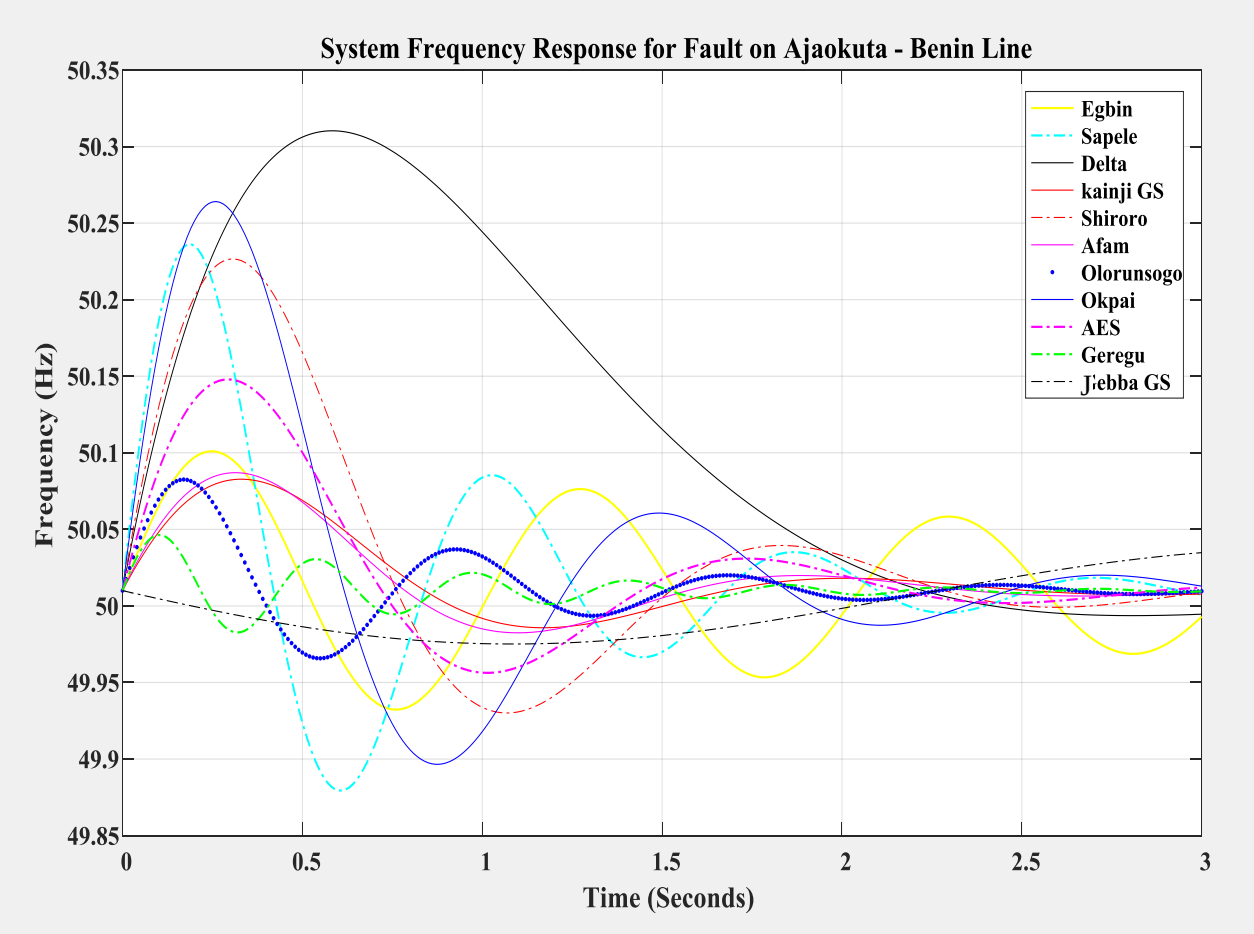

Figure 4.23: Frequency response of the system generators for fault clearing time of 0.2sec with ANN Controlled VSC-HVDC

The voltage profile results of the Nigerian 40-bus 330kV transmission system with ANN Controlled VSC-HVDC installed between Ajaokuta to Benin bus after the occurrence of the fault are shown in Table 4.9 as obtained from the power flow analysis of the network in PSAT environment. It can be observed from Table 4.9 and Figure 4.24 that the voltage violations at buses 1, 2, 13, 16, 31, 32 and 37 which were 0.905738, 0.909903, 0.922923, 0.919679, 0.941849, 0.919188 and 0.960770 as obtained previously when the VSC-HVDC was being controlled by the conventional PI method are now improved to 0.998421, 1.000000, 0.999275, 0.979914, 0.997805, 0.998835 and 1.000000 respectively. This is as result of the intelligent response of the VSC-HVDC in injecting adequate reactive power timely.

Table 4.9: The Load Flow Result of System Bus (Voltage Profile) during Occurrence of a Three Phase Fault on Ajaokuta Bus with ANN Controlled VSC-HVDC Installed

Bus No	Bus Name	Voltage [p.u.]	Phase Angle [rad]
1	AES	0.998421	0.02336
2	Afam	1.000000	-0.01134
3	Aja	0.998480	0.006284
4	Ajaokuta	0.989621	-0.00676
5	Akangba	0.805418	-0.10014
6	Aladja	0.996952	-0.00231
7	Alagbon	0.842001	-0.03763
8	Alaoji	1	-0.00962
9	Ayiede	0.996654	0.001761
10	Benin	0.995594	-0.00382
11	B. Kebbi	0.955445	-0.04433
12	Damaturu	0.996001	0.001354
13	Delta	0.999275	0.00146
14	Egbin	1.000000	0.007773
15	Ganmo	0.995887	-0.00372
16	Geregu	0.979914	-0.00953

Table 4.9 Cont'd: The Load Flow Result of System Bus (Voltage Profile) during Occurrence of a Three Phase Fault on Ajaokuta Bus with ANN Controlled VSC-HVDC Installed

17	Gombe	0.766327	-0.04365
18	Gwagwa-lada	0.853375	-0.03592
19	Ikeja-West	0.996943	0.001354
20	Ikot Ekpene	0.988973	-0.01895
21	Jebba TS	1.000000	0
22	Jebba GS	1.000000	0.00215
23	Jos	0.966434	-0.04046
24	Kaduna	0.971423	-0.03687
25	Kainji GS	1.000000	0.007816
26	Kano	0.825577	-0.20071
27	Katampe	0.973536	-0.03586
28	Lokoja	0.970445	-0.03763
29	Makurdi	0.972167	-0.03443
30	New Haven	0.985259	-0.01984
31	Okpai	0.997805	-0.05617
32	Olorunsogo	0.998835	0.05615
33	Omotosho	0.772546	-0.72907
34	Onitsha	0.992507	-0.01132
35	Osogbo	0.994828	-0.00446
36	Papalanto	0.963277	-0.04365
37	Sapele	1.000000	-0.00380
38	Shiroro	0.818990	-0.90286
39	Ugwuaji	0.981078	-0.02538
40	Yola	0.995245	-0.04763

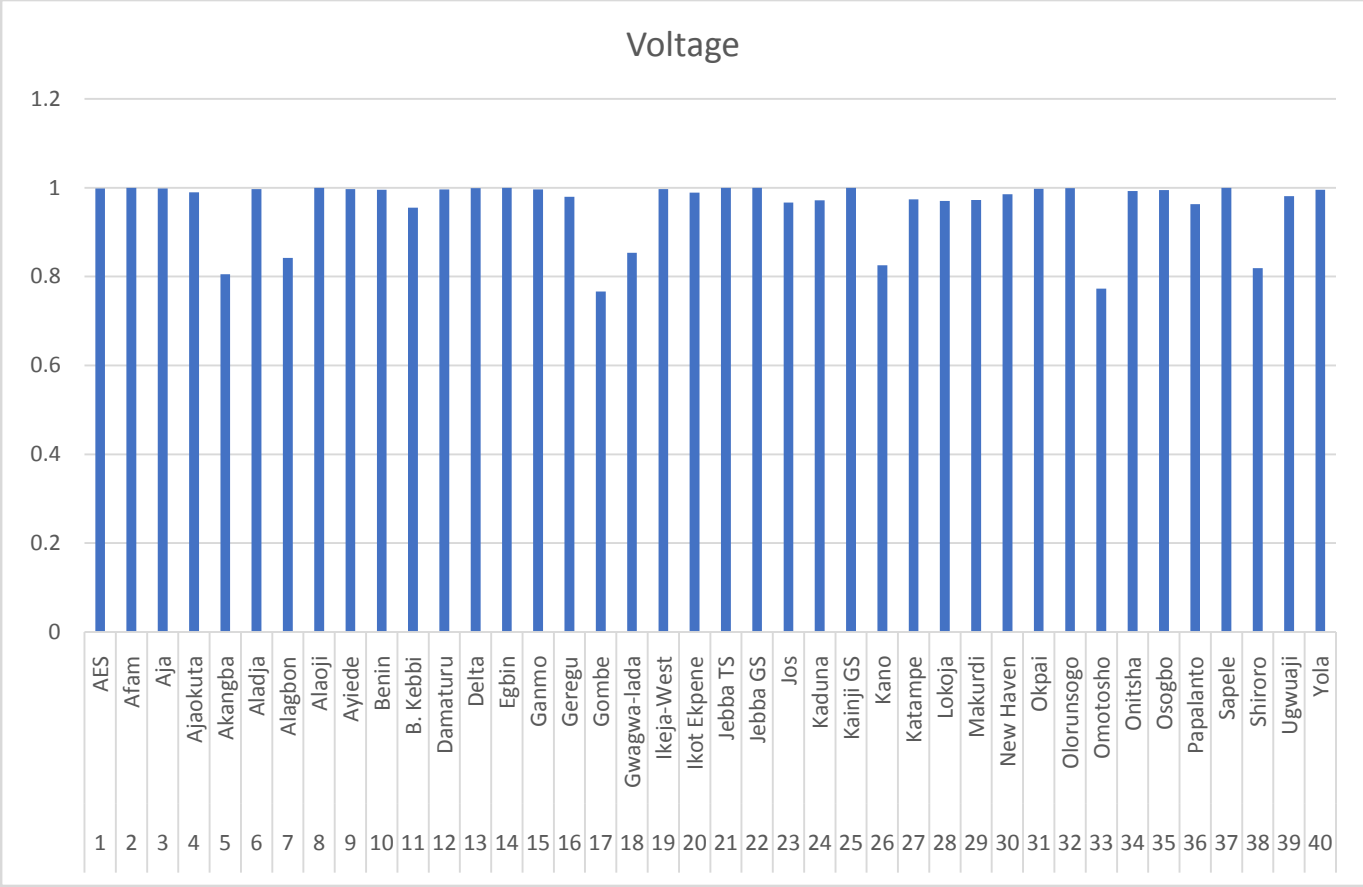

Figure 4.24: Nigeria 330kV Transmission Line Bus Voltage Profile During Occurrence of a Three Phase Fault on Ajaokuta Bus with ANN Controlled VSC-HVDC Installed

4.4.3 Scenario Three: Three Phase Fault at Benin Bus

Here, the position of the ANN controlled VSC-HDVC was changed to Benin – Ikeja West transmission line. As before, a three-phase fault was created on Benin bus (Bus 10) with line Benin – Ikeja west (10 - 19) removed by the CBs at both ends opening to remove the faulted line from the system. Figures 4.25 and 4.26 show the dynamics responses of the generators for CCT of 200ms.

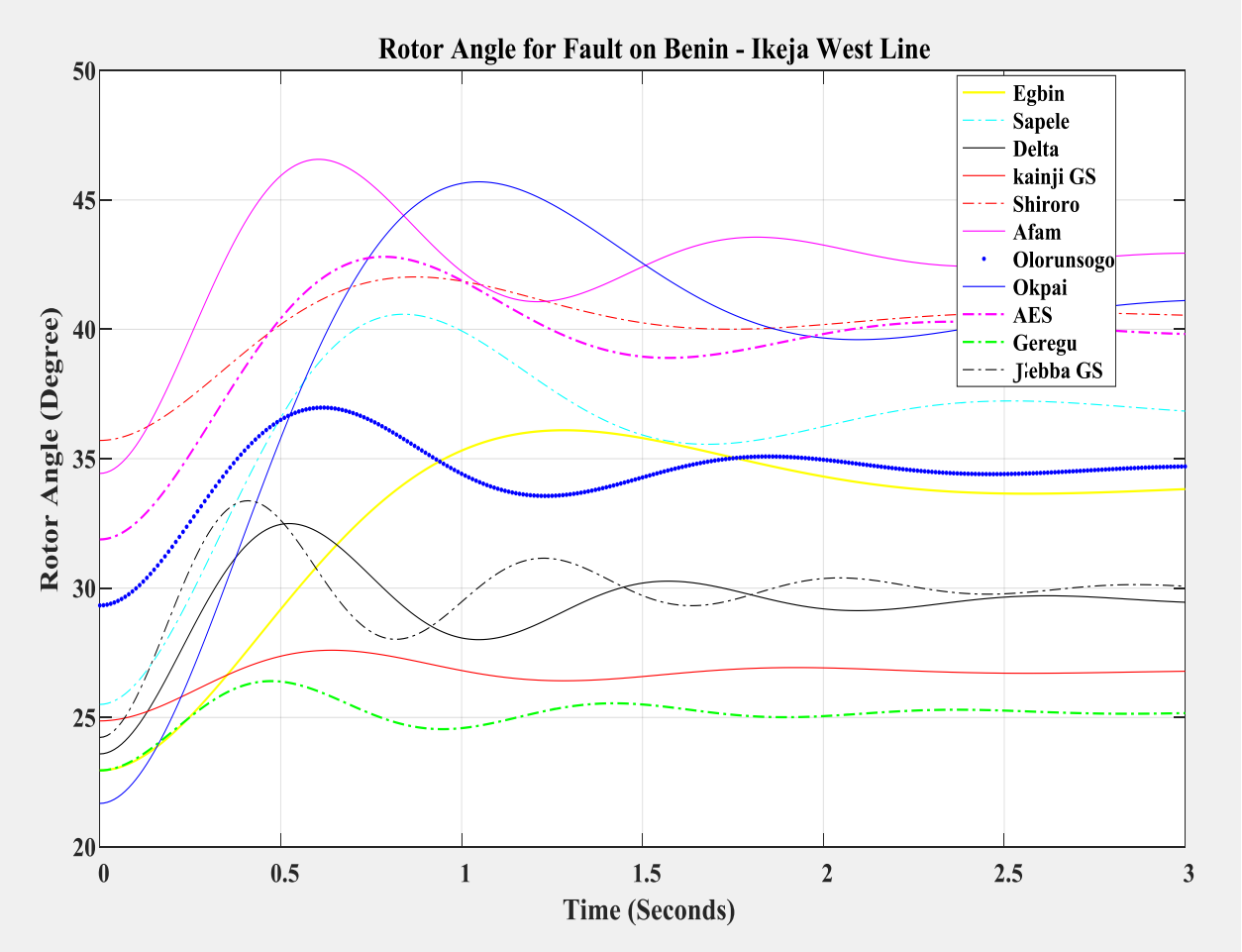

Figure 4.25: Rotor Angle response of the generators for fault clearing time of 0.2sec with ANN Controlled VSC-HVDC

Figures 4.25 and 4.26 show the plot of the power angle curves and the frequency responses of the eleven generators in the system during a transient three-phase fault on Benin to Ikeja West transmission line. It can be observed that all the generators in the system which were all critically disturbed during a fault occurrence without VSC-HVDC, have achieved faster damping. It can also be noted that the CCT has been increased from 300 milli-seconds to 200 milli-seconds and also the oscillations were quickly damped compare to the results obtain when the VSC-HVDC was being controlled by the conventional PI method.

This, again can be attributed to the intelligent response of the neural network in controlling the parameters of the VSC-HVDC, which enabled to inject the needed power in the two buses (Bus 10 – 19) in time and most appropriately. Hence, from Figures 4.25 and 4.26, the transient stability of the system has been further improved with the intelligent HVDC in the system.

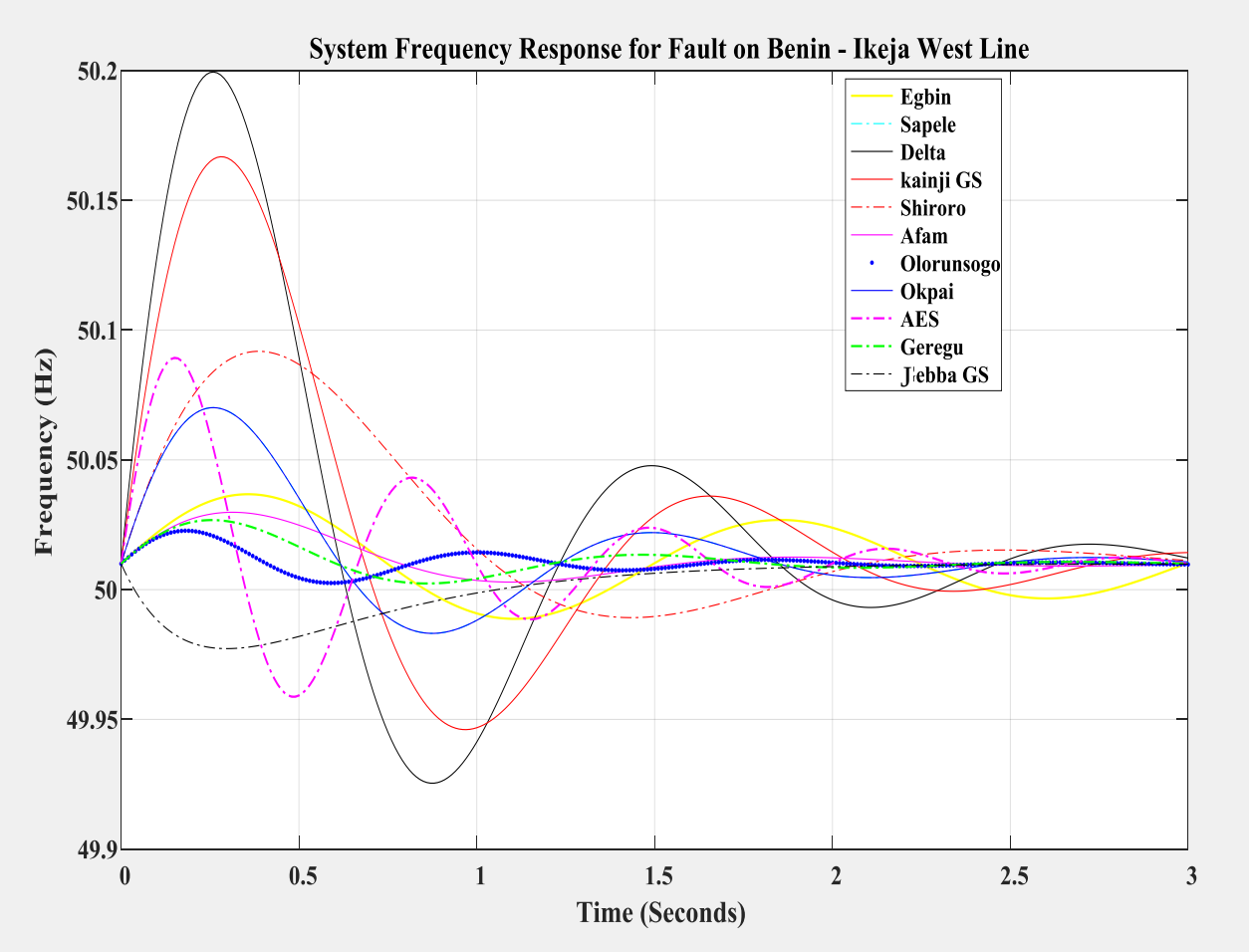

Figure 4.26: Frequency response of the system generators for fault clearing time of 0.2sec with ANN Controlled VSC-HVDC

The voltage profile results of the Nigerian 40-bus 330kV transmission system with ANN Controlled VSC-HVDC installed between Benin to Ikeja West bus after the occurrence of the fault are shown in Table 4.10 as obtained from the power flow analysis of the network in PSAT

environment. It can be observed from Table 4.10 and Figure 4.27 that the voltage violations at buses 1, 2, 13, and 37 which were 0.930561,0.905654,0.922923 and 0.920670 as obtained previously when the VSC-HVDC was being controlled by the conventional PI method are now all improved to 1.000000p.u. each while the voltages at buses 16, 31, 32 remained the same. This is as result of the intelligent response of the VSC-HVDC in injecting adequate reactive power timely.

Table 4.10: The Load Flow Result of System Bus (Voltage Profile) during Occurrence of a Three Phase Fault on Benin Bus with ANN Controlled VSC-HVDC Installed

Bus No	Bus Name	Voltage [p.u.]	Phase Angle [rad]
1	AES	1.000000	0.016368
2	Afam	1.000000	-0.00533
3	Aja	0.998480	0.006284
4	Ajaokuta	0.989621	-0.00676
5	Akangba	0.980541	-0.10014
6	Aladja	0.996952	-0.00231
7	Alagbon	0.984200	-0.03763
8	Alaoji	1.000000	-0.00962
9	Ayiede	0.996654	0.001761
10	Benin	0.995594	-0.00382
11	B. Kebbi	0.955445	-0.04433
12	Damaturu	0.996001	0.001354
13	Delta	1.000000	0.000672
14	Egbin	1.000000	0.007773
15	Ganmo	0.995887	-0.00372
16	Geregu	0.989101	-0.00231
17	Gombe	0.976632	-0.04365
18	Gwagwa-lada	0.953375	-0.03592

Table 4.10 contd: The Load Flow Result of System Bus (Voltage Profile) during Occurrence of a Three Phase Fault on Benin Bus with ANN Controlled VSC-HVDC Installed

19	Ikeja-West	0.996943	0.001354
20	Ikot Ekpene	0.988973	-0.01895
21	Jebba TS	1.000000	0.00456
22	Jebba GS	1.000000	0.00215
23	Jos	0.966434	-0.04046
24	Kaduna	0.971423	-0.03687
25	Kainji GS	1.000000	0.007816
26	Kano	0.982557	-0.20071
27	Katampe	0.973536	-0.03586
28	Lokoja	0.970445	-0.03763
29	Makurdi	0.972167	-0.03443
30	New Haven	0.985259	-0.01984
31	Okpai	0.998001	-0.03763
32	Olorunsogo	0.983565	0.61537
33	Omotosho	0.997725	-0.72907
34	Onitsha	0.992507	-0.01132
35	Osogbo	0.994828	-0.00446
36	Papalanto	0.963279	-0.04365
37	Sapele	1.000000	-0.00019
38	Shiroro	0.998189	-0.90286
39	Ugwuaji	0.981078	-0.02538
40	Yola	0.995245	-0.04763

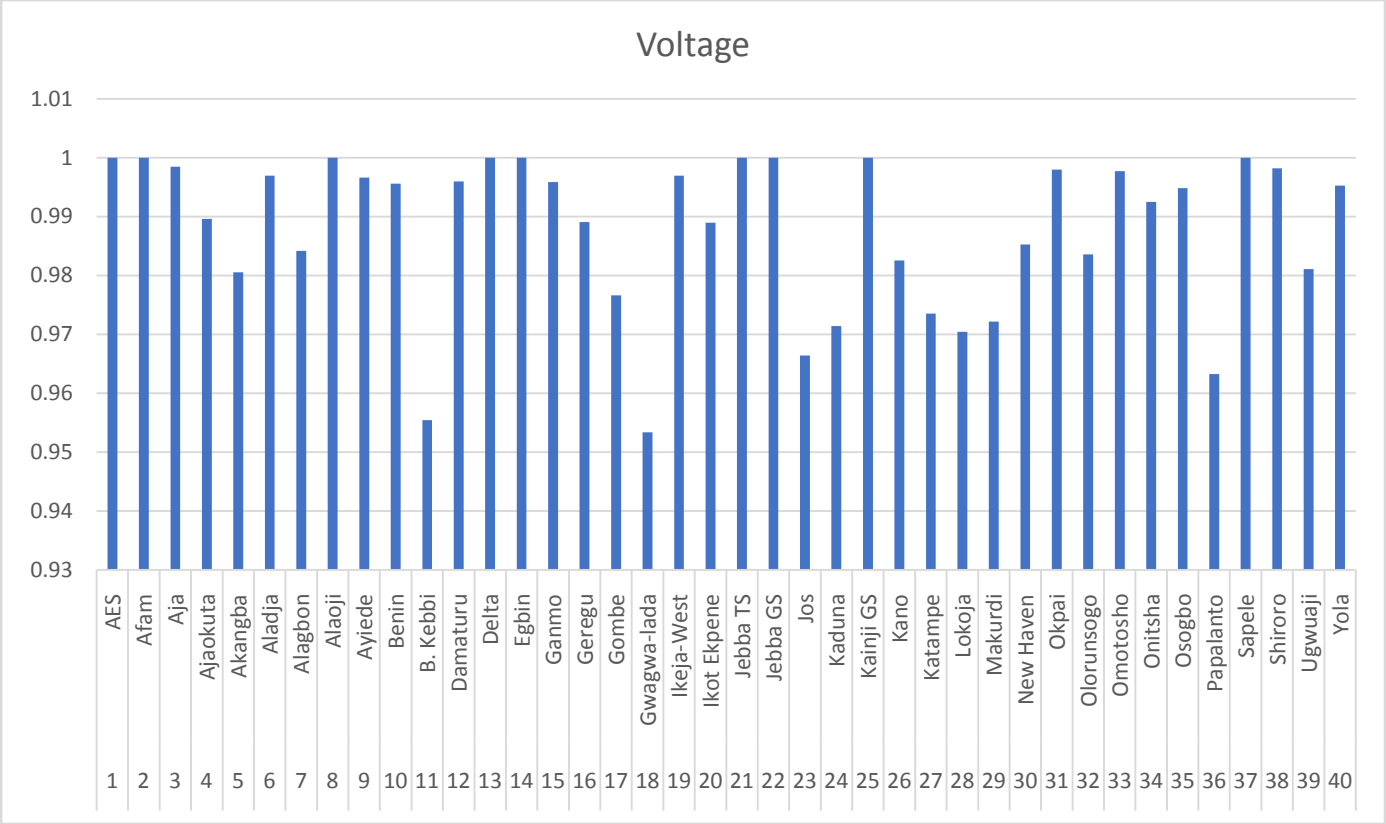

Figure 4.27: Nigeria 330kV Transmission Line Bus Voltage Profile During Occurrence of a Three Phase Fault on Benin Bus with ANN Controlled VSC-HVDC Installed

4.5: COMPARISM OF THE RESULTS

Table 4.11: The Voltage Profile Comparism Results

S/N	Case Locations	Without HVDC	With PI controlled HVDC	With ANN controlled HVDC	Remarks
1	Base 1	0.805418, 0.842001, 0.766327, 0.853375, 0.825577, 0.835771, 0.772546, 0.818990			The position in the network
2	Markudi	0.800057, 0.842001, 0.800500, 0.704520, 0.778346, 0.772546, 0.704592	0.905418, 0.889001, 0.958990, 0.979887, 0.971031, 0.907546, 0.968700	0.999541, 0.999541, 1.001000, 0.999887, 0.989031, 0.997546	Improved with the ANN
3	Ajaokuta	0.773990, 0.822780, 0.821045, 0.798931, 0.816998, 0.783557, 0.873953	0.905738, 0.909903, 0.922923, 0.919679, 0.941849, 0.919188, 0.960770	0.998421, 1.000000, 0.999275, 0.979914, 0.997805, 0.998835, 1.000000	Improved with the ANN
4	Benin	0	0.930561, 0.905654, 0.934967, 0.989101, 0.998001, 0.983565, 0.920670	1.001000, 1.001000, 1.001000, 1.001000, 1.001000, 1.001000, 1.001000,	Improved with the ANN

Table 4.12: Critical Clearing Time Comparism Results

S/N	Case Locations	Without HVDC	With PI controlled HVDC	With ANN controlled HVDC	Remarks
1	Markudi	0.3	0.3	0.2	Improved with the ANN
2	Ajaokuta	0.3	0.3	0.2	Improved with the ANN
3	Benin	0.3	0.3	0.2	Improved with the ANN

CHAPTER FIVE

CONCLUSION AND RECOMMENDATION

5.1 Conclusion

In this work, transient stability improvement of the Nigeria 330-kV grid system using intelligent VSC-HVDC has been carried out. The mathematical formulations for the analysis are presented. The location of a balanced 3-phase fault, at various nodes, was determined based on the most critical buses within the network which was determined through eigenvalue analysis and damping ratio. The dynamic responses for various fault locations are obtained. The results obtained show that the Nigeria 330-kV transmission network is presently operating on a time-bomb alert state which could lead to total blackout if a 3-phase fault occurs on some strategic buses. The result obtained shows that when a 3-phase fault of any duration occurs on Makurdi, Ajaokuta or Benin bus, the system losses synchronism immediately. Also, Jos - Makurdi and Ikeja West - Beninand Ajaokuta – Benin transmission lines have been identified as critical lines that can excite instability in the power network if removed to clear a 3-phase fault.

Hence, the need for measures that will improve transient stability like the incorporation of FACTS devices into the transmission network, use of fast acting circuit breakers, use of breaking resistors at generator buses, short circuit current limiters, etc. to avoid total system collapse, if a 3-phase fault occurs on the aforementioned critical buses or transmission lines. HVDC as a FACTS device has been used to improve the transient stability of the network. The HVDC was intelligently controlled using artificial neural network.

The inverter and the converter parameters of the HVDC were controlled by the conventional PI method and artificial neural network. The results obtained showed that greater transient stability was achieved when the HVDC was controlled with the artificial neural network as can be seen by observing the dynamic response of the generators in the Nigeria 330-kV grid network. The generalized swing equations for a multi-machine power system was presented. The entire simulation of the Nigeria 330kV transmission network was done in MATLAB/PSAT environment.

5.2 Contribution to Knowledge

The dissertation has successfully contributed to body of knowledge by demonstrating that the transient stability of the Nigeria 330kV transmission system can be significantly improved by applying an intelligent HVDC to the network.

The dissertation also demonstrated that that critical clearing time CCT of the line was improved.

The dissertation was able show that the inverter and converter parameters of the HVDC could be controlled using artificial neural network instead of the conventional PI controller.

Finally, the imminent system collapse of the Nigeria 330kV transmission network as a result of the system being on a red-alert has been mitigated by this dissertation.

5.3 Recommendation

Considering the unstable nature of Nigeria 330kV grid system as analyzed and the significant impact of the ANN HVDC link in improving the transient stability of the network, it will be wise

to recommend the installation of the VSC-HVDC transmission lines alongside with the three most critical lines (which are Makurdi – Jos, Ajaokuta - Benin and Benin – Ikeja West transmission lines respectively) having seen the magnificent improvement.

The result of the eigenvalue analysis shows that numerous buses on the Nigerian 330kV grid apart from the three chosen (Makurdi, Ajaokuta and Benin) are unstable, this dissertation work therefore recommends that researchers should also install/apply ANN controlled VSC HVDC links on those remaining unstable buses to compare their impact on the grid.

REFRENCES

Abido M. A. (2009). Power system enhancement using FACTS controllers: A review. *The Arabian Journal for Science and Engineering*, Vol.34, No.1B, pp.153–172.

Abikhanova G., Ahmetbekova A., Bayat E., Donbaeva A., Burkitbay G. (2018). International motifs and plots in the Kazakh epics in China (on the materials of the Kazakh epics in China), Opción, Año 33, No. 85. 20-43.

Adepoju G. A., Komolafe, O. A, Aborisade, D.O. (2011). Power Flow Analysis of the Nigerian Transmission System Incorporating Facts Controllers. *International Journal of Applied Science and Technology Vol. 1 No. 5; September 2011*

Agha F. N., Josiah M., Dan V. N., Augustin M. M. (2015). Transient stability analysis of VSC HVDC transmission with power injection on the DC-link. *Turkish Journal of Electrical Engineering & Computer Sciences.*

Al-Rawi N. M., Anwar A. and Abdul-Majeed A.M., (2007). Computer aided transient stability analysis. Computer Sci., 3: 149-153 DOI:10.3844/jcssp.2007.149.153

Ali M. E., Yehia S., Abou-Hashema M. El-Sayed and Amer N. A. E.(2019). HVDC over HVAC Transmission System: Fault Conditions Stability Study. International Journal of Research Studies in Electrical and Electronics Engineering(IJRSEEE) *Volume 5, Issue 1, 2019, PP 24-37 ISSN 2454-9436*

Anshika R. (2016). 3 Main Types of HVDC Links. Transmission | Electrical Engineering. http://www.engineeringenotes.com/electrical-engineering/hvdc-transmission/3-main types-of-hvdc-links-transmission-electrical-engineering/29259

Ayodele T R, Jimoh A A, Munda J L, and Agee J T, (2012). Challenges of grid integration of wind power on power system grid integrity. A review. International Journal of Renewable Energy Research, 2, 618-626

Ayodele T R, Jimoh A. A., Munda J. L., and Agee J T, (2012). The impact of wind power on power system transient stability based on probabilistic weighting method. Journal of Renewable and Sustainable Energy, 4, 1-18.

Ayodele T. R., Ogunjuyigba A. S. O. and Oladele O. O., (2016). Improving the Transient Stability of Nigerian 330kV Transmission Network using SVC, Nigeria Journal of Technology, pp. 155-166.

Babainejad, S. and R. Keypour, (2010). Analysis of transient voltage stability of a variable speed wind turbine with doubly fed induction generator affected by different electrical parameters of induction generator. Trends Applied Sci. Res., 5: 251-278.

Bompard E., Fulli G., Ardelean M. and Masera M. (2014). It's a Bird, It's a Plane, It's a... Supergrid. *IEEE power & energy magazine*, Vol.12, No.2, pp.41–50.

Chettih, S., M. Khiat and A. Chaker, (2008). Optimal distribution of the reactive power and voltages control in Algerian network using the genetic algorithm method. Inform. Technol. J., 7: 1170-1175. DOI: 10.3923/itj.2008.1170.1175

D´ıez-Maroto L. (2013). Improvement of Voltage Ride Through Capability of Synchronous Generators with Supplementary Excitation Controllers. *Master thesis, Universidad Pontificia Comillas*.

Eleschová Ž., Smitková M. and Beláň A. (2010). Evaluation of Power System Transient Stability and Definition of the Basic Criterion. International Journal of Energy, Issue 1, Vol. 4.

Ekici S., Yildirim S. and Poyraz M. (2009). A Transmission line fault locator based on Elman recurrent networks. Applied soft computing vol.9 pp.341-374.

Eriksson R. (2014). Coordinated Control of Multiterminal DC Grid Power Injections for Improved Rotor-Angle Stability Based on Lyapunov Theory. *IEEE Transactions on Power Delivery*, Vol.29, No.4, pp.1789–1797.

Eseosa O. and Odiase F. O. (2012). Efficiency Improvement of Nigeria 330kV Network using FACTS devices. International Journal of Advances in Engineering and Technology, pp. 26- 41.

Eseosa O., and Onahaebi S. O. (2015). Optimal location of IPFC in Nigeria 330kV Integrated Power Network using GA Technique. Journal of Electrical and Electronics Systems, pp. 1-8.

Fuchs A., Imhof M., Demiray T. and Morari M. (2014). Stabilization of Large Power Systems Using VSC HVDC and Model Predictive Control. *IEEE Transactions on Power Systems*, Vol.29, No.1, pp.480–488.

Hannan, M.A. and K.W. Chan, (2006). Transient analysis of FACTS and custom power devices using phasor dynamics. J. Applied Sci., 6: 1074-1081. DOI: 10.3923/jas.2006.1074.1081

Haque M. H. (2004). Improvement of First Swing Stability Limit by Utilizing Full Benefit of Shunt FACTS Devices. *IEEE Transactions on Power Systems,* Vol.19, No.4, pp.1894–1902.

Haque M. H. and Kumkratug P. (2004). Application of Lyapunov stability criterion to determine the control strategy of a STATCOM. *IEE Proc. Gener. Transm. Distrib.*, Vol.151, No.3, pp.415–420.

Haykin, S. (1994). *Neural Networks: A comprehensive foundation*. Macmillan Collage Publishing Company, Inc., New York.

Ignatius K. O., Emmanuel A. O. (2017). Transient Stability Analysis of the Nigeria 330-kV Transmission Network. American Journal of Electrical Power and Energy Systems 2017; 6(6): 79-87,http://www.sciencepublishinggroup.com/j/epes, doi: 10.11648/j.epes.20170606.11; ISSN: 2326-912X (Print); ISSN: 2326-9200 (Online)

Izuegbunem F. I., Ubah C. B. and Akwukwaegbu I. O. (2012). Dynamic security assessment of 330kV Nigeria power system. Academic Research International Journal, pp. 456- 466.

Karthikeyan K. and Dhal P. K. (2015). Transient Stability Enhancement by Optimal location and tuning of STATCOM using PSO. Smart and Grid Technologies (ELSEVEIR), pp. 340-351.

Kezunovic, M. (1997). *A survey of neural net applications to protective relaying and fault analysis.* International Journal of Engineering Intelligent Systems for Electronics, Engineering and Communications 5(4), pp. 185-192.

Kumar, M., Raghuwanshi, N. S., Singh, R., Wallender W. W., and Pruitt, W. O. (2012). Estimating Evapotranspiration using Artificial Neural Network. Journal of irrigation and Drainage Enginneering, 128, 224-233.

Kundur P. (1999). Power System Stability and Control. New York: *McGraw Hill Education.*

Lakshminarayana P., Shishir R., Mukesh K. K. and Ganga A. (2014). Power system transient stability margin estimation using artificial neural networks. Electrical and Electronics Engineering: An International Journal (ELELIJ) Vol 3, No 4.

Leonard L. and Grigsby. (2012). Electric Power Engineering Handbook. Second Edition. Power System Stability and Control. Boca Raton, USA: CRC Press - Taylor & Francis Group, 2012

Machowski J., Kacejko P., Nogal L. and Wancerz M. (2013). Power system stability enhancement by WAMS-based supplementary control of multi-terminal HVDC networks. *Control Engineering Practice*, Vol.21, No.5, pp.583–592.

Lukowicz M., Rosolowski E. (2013). Artificial neural network based dynamic compensation of current transformer errors. Proceedings of the 8th International Symposium on Short-Circuit Currents in Power Systems, Brussels, pp. 19-24.

Masaki, Y. and Junji, Y. (2010). Enhancement of Transient Stability Using Fault Current Limiter and Thyristor Controlled Breaking Resistor. IEE Xplore, 1-6.

Masood N., Hassan A. and Chowohury A. (2012). Enhancement of real power transfer capability of transmission line. Journal of Energy and Power Engineering, pp. 1114-1118.

Nwohu M. N., Isah A., Usman A. U. and Sadiq A. A. (2016). Optimal placement of thyristor controlled series compensator (TCSC) on Nigerian 330kV transmission grid to minimize real power losses. International Journal of Research Studies in Electrical and Electronics Engineering, pp. 18-26.

Nirupama S. (2016). Improving Transient Stability. http://www.engineeringenotes.com/electrical-engineering/power-system/24809

Oluseyi P. O., Adelaja T. S., and Akinbulire T. O. (2017). Analysis of the Transient Stability Limit of Nigeria's 330kV Transmission sub-network. Nigeria Journal of Technology, pp. 213-226.

Parry, M. and N. Gangatharan, (2005). Adaptive data transmission in multimedia networks. Am. J. Applied Sci., 2: 730-733. DOI: 10.3844/ajassp.2005.730.733

Pao, Y. H. (2012). *Adaptive Pattern Recognition and Neural Networks*. Reading: Wesley. p.309.

Prabha K., John P., Venkat A., Göran A., Anjan B., Claudio C., Nikos H., David H., Alex S., Carson T., Thierry V. C., and Vijay V. (2004). Definition and Classification of Power System Stability IEEE/CIGRE Joint Task Force on Stability Terms and Definitions I. EEE Transactions on Power Systems

Rani, A. and Arul, P. (2013). Transient Stability Enhancement of Multi-Machine Power System Using UPFC and SSSC. International Journal of Innovative Technology and Exploring Engineering, 3, 77-81.

Roberto R. J. P. and Charpentier R. S. (2000). High Voltage Direct Current (HVDC) Transmission Systems Technology Review Paper. Presented at Energy Week 2000, Washington, D.C, USA, March 7-8, 2000

Sachidananda D. (2019). Methods of improving stability. https://electricalshouters.com/methods-of-improving-stability/

Sagar, N., Pavan, G. and Rajalakshmi, M. (2016). Transient Stability Analysis of IEEE 59 Bus System with FCL and SVC Controller Using ETAP. Journal of Chemical and Pharmaceutical Sciences, 2016, 248-251.

Sanni S. O., Haruna J. O., Jimoh B. and Aliyu U. O. (2016). An analysis of transient stability enhancement capability of UPFC in a multi-machine power system. *FUOYE Journal of Engineering Technology, pp. 48-54.*

Sanz M., Chaudhuri B. and Strbac G. (2016). Coordinated Corrective Control for Transient Stability Enhancement in Future Great Britain Transmission System", *19th PSCC Genoa,* pp. 1–7.

Seyed A. T., Reza H. and Majid N. (2008). Comparison of different control strategies in GA-based optimized UPFC controller in electric power systems. Am. J. Eng. Applied Sci., 1: 45-52. DOI:10.3844/ajeassp.2008.45.52

Sharma P. R. and Hooda, (2012). Transient Stability Analysis of Power System using MATLAB. International Journal of Engineering Sciences and Research Technology, pp. 418-422, 2012.

Sidhu, T.S., Singh, H. and Sachdev, M.S. (2005). *Design, implementation and testing of an artificial neural network based fault direction discriminator for protecting transmission lines.* IEEE Trans. On Power Delivery, vol. 10, no., pp 697-706.

Sigrist L., Echavarren F., Rouco L. and Panciatici P. (2015). A fundamental study on the impact of HVDC lines on transient stability of power systems. *PowerTech Eindhoven*.

Singaravelu S. and Seenivasan S. (2014). Modelling and Simulation of Monopolar HVDC Transmission System Feeding a Strong AC Network with Firefly Algorithm based Optimal PI Controller.*International Journal of Computer Applications (0975 – 8887) Volume 102 – No.10.*

Sravani, T., Hari, G. and Basha, J. (2010). Improvement of Power System Stability Using SFCL in Elastic Power Grid under Voltage Unbalance Conditions. International Journal of Emerging Trends in Electrical and Electronics, 10, 80-89.

Srinvasa, J. and Amarnath, J. (2014). Enhancement of transient Stability in a deregulated Power System Using FACTS Devices. Global Journal of Researches in Engineering, 14, 1-17.

Tang G., Xu Z., Dong H. and Xu Q. (2016). Sliding Mode Robust Control Based Active-Power Modulation of Multi-Terminal HVDC Transmissions. *IEEE Transactions on Power Systems,* Vol.31, No.2, pp.1614–1623.

Tarafdar, M., Haque and Kashtiban, A. M. (2005). *Applications of Neural Networks in Power Systems; A Review*. Transactions on Engineering, Computing and Technology V6 ISSN1305-5313.

Taylor C. W., Mechenbier J. R. and Matthews C. E., (1993). Transient Excitation Boosting at Grand Coulee Third Power Plant: Power System Application and Field Tests. I*EEE Transactions on Power systems*, Vol.8, No.3, pp.1291–1298.

Van H. D. and Ghandhari M. (2010). Multi-terminal VSC HVDC for the European supergrid: Obstacles. *Renewable and Sustainable Energy Reviews*, Vol.14, No.9, pp.3156–3163.

Vasilic, S., and Kezunovic, M. (2004). Fuzzy *ART Neural Network Algorithm for Classifying the Power System Fault*s. IEEE Transactions on Power Delivery, pp 1-9.

Vittal and Vijay. (2007). Direct Stability Methods. https://circuitglobe.commm/different-types-hvdc-links.html

Zhou Y., Huang H., Xu Z., Hua W., Yang F. and Liu S. (2015). Wide area measurement system-based transient excitation boosting control to improve power system transient stability. *IET Generation, Transmission & Distribution*, Vol.9, No.9, pp.845–854.

APPENDIX

Appendix 1: The basic building blocks of an electric power system

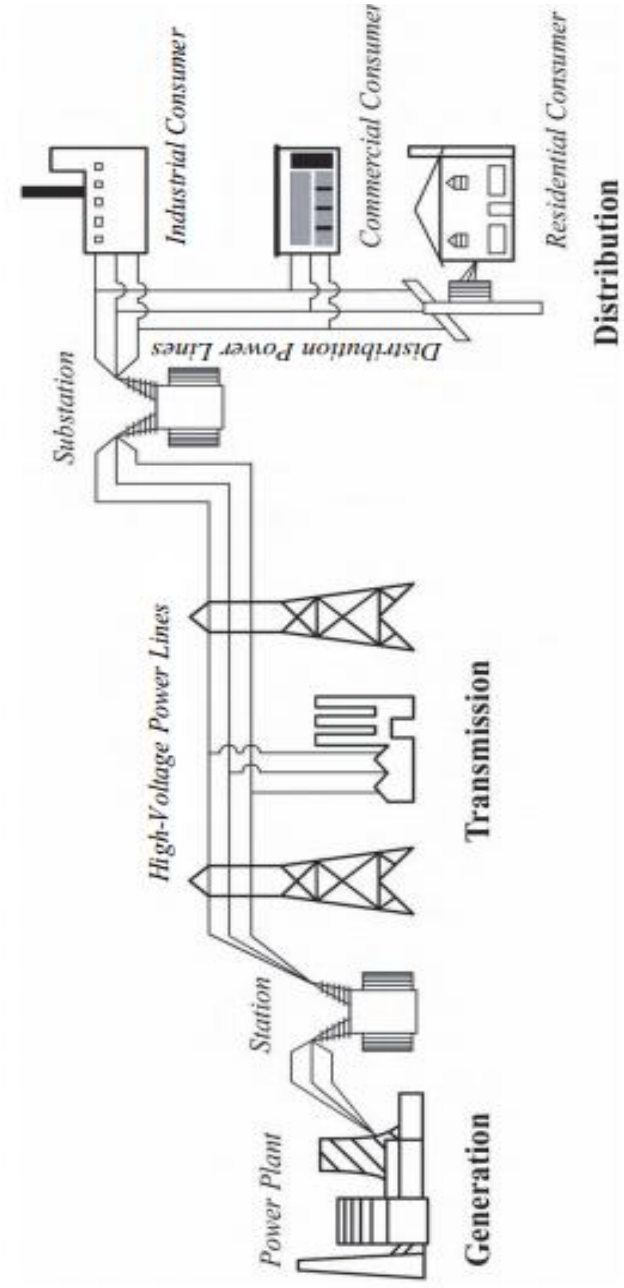

Appendix 2: Parameters of the network. (SOURCE: NCC OSOGBO)

S/N	Bus	Bus name	V[kV]	V[p.u]	phase [deg]	Pgen [MW]	Qgen [MVar]	Pload [MW]	Qload [MVar]
1	Bus1	Kebbi	330	1	0	0	0	120	40
2	Bus10	Akangba	330	1	0	0	0	204	95
3	Bus11	Egbin	334.29	1.013	0	706.7136	190.7935	0	0
4	Bus12	Shiroro	331.65	1.005	0	200	353.7643	0	0
5	Bus13	Kaduna	330	1	0	0	0	200	97
6	Bus14	Makurdi	330	1	0	0	0	180	65
7	Bus15	Jos	330	1	0	0	0	250	125
8	Bus16	Damaturu	330	1	0	0	0	130	70
9	Bus17	Yola	330	1	0	0	0	100	40
10	Bus18	Gombe	330	1	0	0	0	160	95
11	Bus19	Benin	330	1	0	0	0	157	80
12	Bus2	Kanji	331.65	1.005	0	578	-115.594	0	0
13	Bus20	Maiduguri	331.65	1.005	0	300	33.862	0	0
14	Bus21	Onitsha	330	1	0	0	0	115	42
15	Bus22	Owerri	330	1	0	0	0	180	75
16	Bus23	New Haven	330	1	0	0	0	113	56
17	Bus24	Sapele	331.65	1.005	0	400	-16.5882	0	0
18	Bus25	Delta	331.65	1.005	0	250	-0.47524	0	0
19	Bus26	Aladja	330	1	0	0	0	182	67
20	Bus27	Alaoji	330	1	0	300	-69.4982	0	0
21	Bus28	Afam	331.65	1.005	0	450	238.2384	0	0
22	Bus29	Katamkpe	330	1	0	0	0	198	94
23	Bus3	Jebba	331.65	1.005	0	278	84.55218	0	0
24	Bus30	Ugwuaji	330	1	0	0	0	116	46
25	Bus31	Omoku	330	1	0	0	0	110	67
26	Bus33	Ikot Ekpene	330	1	0	0	0	140	75
27	Bus35	Gwagwalada	330	1	0	0	0	203	102

28	Bus4	Ganmo	330	1	0	0	0	200	102
29	Bus5	Oshogbo	330	1	0	0	0	201	137
30	Bus6	Ayede	330	1	0	0	0	139	61
31	Bus7	Papalanto	331.65	1.005	0	204	-18.5558	0	0
32	Bus8	Olunrunsogo	331.65	1.005	0	260	-35.6647	0	0
33	Bus9	Ikeja West	330	1	0	0	0	429	248
34	Bus32	Olorunsogo	330	1	0	525.6	79.18	0	0
35	Bus34	Onitsha	330	1	0	0	0	326	114.5
36	Bus36	Aja	330	1	0	0	0	120	161.5
37	Bus37	Sapele	330	1	0	153	94.81	0	0
38	Bus38	Shiroro	330	1	0	108	70.51	0	0
39	Bus39	Ugwuaji	330	1	0	0	0	86	34.5
40	Bus40	Yola	330	1	0	0	0	85	26.5

Appendix 3: Transmission Line parameters (SOURCE: NCC OSOGBO)

From Bus	To Bus	Resistance (R (p.u))	Reactance (X (p.u))	Line length (KM)
Kebbi	Kanji	0.01006	0.08711	310
Jebba	Kanji	0.00311	0.02641	81
Jos	Gombe	0.00923	0.07944	265
Yola	Gombe	0.00923	0.07944	240
Damaturu	Gombe	0.00058	0.00489	160
Damaturu	Maiduguri	0.00431	0.03667	260
Maiduguri	Makurdi	0.0115	0.09988	
Jos	Makurdi	0.0086	0.07389	285
Katamkpe	Makurdi	0.00298	0.02532	
Ayede	Osogbo	0.0041	0.03486	119
Ayede	Olunrunsogo	0.00214	0.01818	
Ayede	Papalanto	0.00215	0.01822	

Jebba	Shiroro	0.00853	0.0733	244
Papalanto	Ikeja West	0.00058	0.00489	
Olunrunsogo	Ikeja West	0.00463	0.03938	
Osogbo	Ikeja West	0.0088	0.07565	235
Osogbo	Benin	0.00877	0.07535	251
Ikeja West	Akangba	0.00058	0.00489	18
Egbin	Aja	0.00018	0.00152	14
Ikeja West	Egbin	0.00222	0.01883	62
Benin	Ikeja West	0.00688	0.05883	280
Benin	Delta	0.00343	0.02913	107
Aladja	Delta	0.00115	0.00973	30
Jebba	Ganmo	0.00402	0.03416	70
Sapele	Aladja	0.00225	0.01913	93
Benin	Sapele	0.00179	0.01519	50
Benin	Onitsha	0.00487	0.04149	137
Onitsha	New Haven	0.00286	0.02429	96
Makurdi	New Haven	0.00867	0.07447	252
Onitsha	Alaoji	0.0049	0.04179	138
Alaoji	Afam	0.00058	0.00489	25
Afam	Omoku	0.00118	0.01003	
Omoku	Ikot Ekpene	0.00079	0.00669	
Afam	Ikot Ekpene	0.00286	0.02429	
Ganmo	Osogbo	0.00498	0.0424	87
Alaoji	Owerri	0.00179	0.01522	
Ugwuaji	Owerri	0.00536	0.04571	
Ugwuaji	New Haven	0.00247	0.02095	6.5
New Haven	Ikot Ekpene	0.00286	0.02429	209
Jebba	Oshogbo	0.00557	0.04749	157
Kaduna	Shiroro	0.00343	0.02913	
Shiroro	Gwagwalada	0.00058	0.00489	144

Gwagwalada	katamkpe	0.00452	0.03848	60
Kaduna	Jos	0.00695	0.05942	197

Appendix 4: Bus data

S/N	Bus	Bus name	V[kV]	V[p.u]	phase [deg]	Pgen [MW]	Qgen [MVar]	Pload [MW]	Qload [MVar]
1	Bus1	Kebbi	330	1	0	0	0	120	40
2	Bus10	Akangba	330	1	0	0	0	204	95
3	Bus11	Egbin	334.29	1.013	0	706.7136	190.7935	0	0
4	Bus12	Shiroro	331.65	1.005	0	200	353.7643	0	0
5	Bus13	Kaduna	330	1	0	0	0	200	97
6	Bus14	Makurdi	330	1	0	0	0	180	65
7	Bus15	Jos	330	1	0	0	0	250	125
8	Bus16	Damaturu	330	1	0	0	0	130	70
9	Bus17	Yola	330	1	0	0	0	100	40
10	Bus18	Gombe	330	1	0	0	0	160	95
11	Bus19	Benin	330	1	0	0	0	157	80
12	Bus2	Kanji	331.65	1.005	0	578	-115.594	0	0
13	Bus20	Maiduguri	331.65	1.005	0	300	33.862	0	0
14	Bus21	Onitsha	330	1	0	0	0	115	42
15	Bus22	Owerri	330	1	0	0	0	180	75
16	Bus23	New Haven	330	1	0	0	0	113	56
17	Bus24	Sapele	331.65	1.005	0	400	-16.5882	0	0
18	Bus25	Delta	331.65	1.005	0	250	-0.47524	0	0
19	Bus26	Aladja	330	1	0	0	0	182	67
20	Bus27	Alaoji	330	1	0	300	-69.4982	0	0
21	Bus28	Afam	331.65	1.005	0	450	238.2384	0	0
22	Bus29	Katamkpe	330	1	0	0	0	198	94

23	Bus3	Jebba	331.65	1.005	0	278	84.55218	0	0
24	Bus30	Ugwuaji	330	1	0	0	0	116	46
25	Bus31	Omoku	330	1	0	0	0	110	67
26	Bus33	Ikot Ekpene	330	1	0	0	0	140	75
27	Bus35	Gwagwalada	330	1	0	0	0	203	102
28	Bus4	Ganmo	330	1	0	0	0	200	102
29	Bus5	Oshogbo	330	1	0	0	0	201	137
30	Bus6	Ayede	330	1	0	0	0	139	61
31	Bus7	Papalanto	331.65	1.005	0	204	-18.5558	0	0
32	Bus8	Olunrunsogo	331.65	1.005	0	260	-35.6647	0	0
33	Bus9	Ikeja West	330	1	0	0	0	429	248
34	Bus32	Olorunsogo	330	1	0	525.6	79.18	0	0
35	Bus34	Onitsha	330	1	0	0	0	326	114.5
36	Bus36	Aja	330	1	0	0	0	120	161.5
37	Bus37	Sapele	330	1	0	153	94.81	0	0
38	Bus38	Shiroro	330	1	0	108	70.51	0	0
39	Bus39	Ugwuaji	330	1	0	0	0	86	34.5
40	Bus40	Yola	330	1	0	0	0	85	26.5